CHALMERS

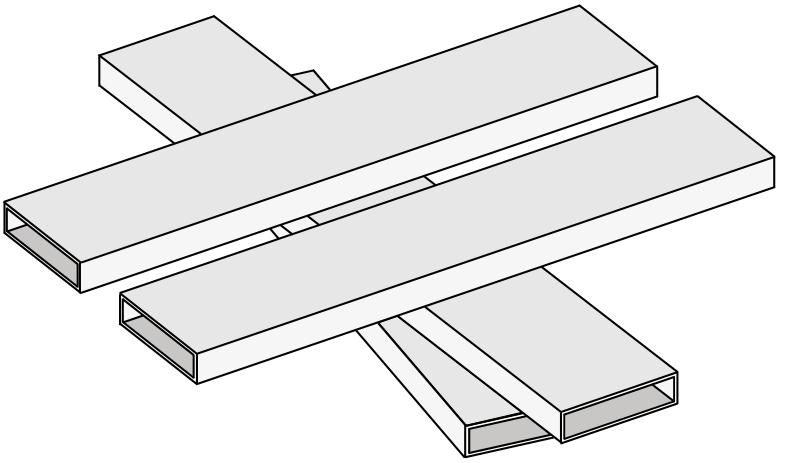

# Moment Method Analysis of Slot Coupled Waveguides

*Thesis for the Degree of Master of Science*

Carl Toft

Department of Signals and Systems

Antenna Group

Chalmers University of Technology

Gothenburg, Sweden 2014

# Moment Method Analysis of Slot Coupled Waveguides

MASTER's THESIS
as part of mandatory clauses in
fulfillment of Master's Degree from the
Chalmers University of Technology, Gothenburg, Sweden

by

**Carl Toft**
**Department of Signals and Systems**

September, 2014

Moment Method Analysis of Slot Coupled Waveguides
Carl Toft. - Gothenburg : Chalmers University of Technology, 2014.



This thesis is carried out under supervision of:
Dr. Johan Wettergren (RUAG Space AB), and Dr. Rob Maaskant (Chalmers)

Examiner:
Prof. Per-Simon Kildal

Keywords: computational electromagnetics / method of moments / Green's functions / integral equations / waveguides
Subject headings: computational electromagnetics / electric field integral equation

Antenna Group, Department of Signals & Systems
Chalmers University of Technology,
SE-41296, Gothenburg, Sweden.
Telephone: +46 31 772 1000

Cover design: Carl Toft
Press: Chalmers Reproservice, Göteborg

# Abstract

*In recent years, computational methods have started to play an increasingly important part in the design process of antennas. With the development of the new scatterometer-radar antennas for the next generation of MetOp satellites, there is a need for an application specific software that allows for a fast and accurate analysis of waveguides coupled through rectangular slots.*

*The in-house software used at RUAG Space today for the analysis of these structures assumes that the electric field has no polarization longitudinally along the slot apertures, and that the remaining transverse component has no variation transversely across the slot. This assumption is good for moderately and strongly excited slots but is known to yield inaccurate results for weakly excited slots.*

*This thesis removes these assumptions by employing an expansion for the equivalent magnetic current that corresponds to a modal expansion of the electric field inside the slot cavities. In this way, the full behavior of the electric field at the slot apertures can be accounted for, and it is shown by comparison with FEKO and results published previously in the literature that this approach yields accurate values for the scattering parameters even for weakly excited slots. The developed code is several orders of magnitude faster than FEKO for these geometries.*

# Acknowledgements

I would like to extend thanks to my advisors Dr. Johan Wettergren and Dr. Rob Maaskant, without whose support, advice and helpful discussions this thesis would not have been possible. I also wish to express my gratitude towards RUAG Space AB for providing access to the source code of one of their computational programs, as well as for financing the project.

# Contents

# Chapter 1

# Introduction

In recent years, computational methods have started to play an increasingly important role in the design of antennas. They streamline the design process by allowing many different possible antenna geometries to be analyzed and evaluated without the need of physically constructing an antenna demonstrator, and also make it possible to apply advanced optimization algorithms in order to find an antenna that meets the relevant customer specifications.

Today there are many commercial general purpose programs available for use in electromagnetic and microwave simulations, such as HFSS and FEKO. While useful and robust, these programs are sometimes too slow to be used in the initial design stage when a wide range of different antenna geometries are to be tested. Instead, it is here necessary to use application specific software that is designed specifically for the particular geometry at hand, and is therefore also much faster. With the development of the new scatterometer array for the next generation of MetOp satellites, the need has arisen for this kind of accurate and fast analysis software for slot coupled waveguide junctions. The purpose of this thesis is to present a method of moments theory that allows accurate analysis of waveguide coupling junctions, where the full behavior of the field inside the slots is taken into account.

## 1.1 History of the Analysis of Waveguide Coupling Junctions

Slots in rectangular waveguides is a subject that has been analyzed extensively the past decades. Stevenson [1] derived the internal Greens function for a rectangular waveguide and used it to derive an expression for the conductance of a resonant slot as a function of the offset of the slot from the centerline of the waveguide. This theory was later extended by Oliner [2] in which he derived expressions for the susceptance as well as the conductance of longitudinal slots.

The first attempt of using a moment method technique on the slot problem was done by Khac and Carson [3, 4], where they derived an integral equation for the electric field just at the slot aperture, from which the total fields in the structure could be calculated thanks to the Schelkunoff equivalence principle. The integral equation was solved by expanding the unknown electric field in terms of a set of pulse basis functions with unknown coefficients, and then taking the inner product of the integral equation with Dirac delta functions to obtain a set of algebraic equations for the expansion coefficients of the field.

Since then the computing power available in modern computers has increased significantly, and the moment method approach for analyzing rectangular slots in rectangular waveguides has been refined and improved upon significantly. In 1987, Elliott and Stern[5] used the moment method to calculate the resonant length of longitudinal, radiating slots to within one percent of the experimentally measured values, by using an expansion of the electric field in terms of sinusoidal basis functions. A similar analysis was performed by Josefsson [6].

Rengarajan considered the problem of a centered but tilted slot that connected two rectangular waveguides [7], as well as a waveguide with compound (i.e. slots with arbitrary offset from centerline and tilt) radiating slots. Manholm and Hirokawa studied junctions with several waveguides coupled through compound slots, with additional radiating slots[8, 9, 10]. They used an expansion of the transverse electric field in the slot apertures in terms of a sinusoidal basis, and also sinusoidal testing functions to transform the integral equations into a system of algebraic equations. In order to facilitate the evaluation of the slot admittances, they employed an alternative expression for the Green's function in a rectangular waveguide derived by Seki. This method is sometimes referred to as the virtual

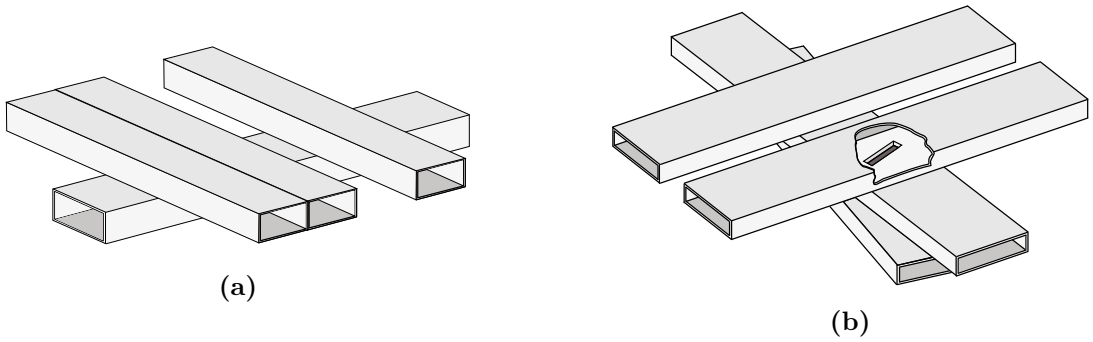

(a) (b)

**Figure 1.1:** Waveguide coupling junction with single feeding waveguide (a), and double feeding layer (b), analyzed by Wettergren. In Fig. (b) one of the top waveguides has been cut open to show the slot that connects it to the middle waveguide.

cavity method, and was also used in [11] when analyzing radiating slots in waveguides by including the shape of the external structure.

Wettergren [12] extended this theory to analyze a feeding waveguide that is connected to an arbitrary number of waveguides above it, shown in Fig. 1.1 (a), as well as the three layered structure shown in Fig. 1.1, where the top layer may include an arbitrary number of waveguides.

Common for all of the above is that they assumed that the tangential electric field at the slot apertures only have a transverse component, i.e. there is no component that is directed longitudinally along the slot. Most also assume that the field can vary longitudinally along the slot but is constant transversely across the slot. For slots that are moderately or strongly excited, in the sense that a non-negligible part of the incident power passes through them, this is a good assumption that corresponds well with measurements and full wave solvers, as shown in the above references. However, as shown by Petersen and Rengarajan[13, 14], this assumption is not true in general and leads to incorrect results for weakly excited slots. For these slots, the longitudinal polarization of the electric field, as well as the transverse variation of the field across the slot must be taken into account.

In her PhD thesis, Petersen developed a method of moments program that analyzed longitudinal slots by expanding the longitudinal and transverse electric field in the slot apertures in terms of a polynomial basis that allowed for variation in both directions along the slot[14], and showed that the longitudinal field contributed significantly to the scattering for weakly excited slots.

## 1.2 Purpose of this thesis

The purpose of this thesis is to develop a method of moments theory for rectangular waveguides coupled through compound slots, where both components of the aperture electric field are taken into account, as well as the transverse variation of this field across the slot. Specifically, the theory can be used to analyze the structures in Fig. 1.1, and is valid even for very weakly excited slots.

This is accomplished by expanding both components of the field in terms of trigonometric functions. The reason for choosing trigonometric functions is twofold. Firstly, it is a very natural expansion since it corresponds to the modal expansion of the electric field inside the slot cavity. Secondly, when neglecting the transverse variation, this approach reduces to the one by Manholm and Hirokawa[8, 9, 10], and their equations and MATLAB code was available for comparison and could be used as a guide. The derivations in this thesis are thus generalizations of their calculations.

## 1.3 Outline of the Thesis

Roughly, the work consists of the following three parts: (i) derivation of a matrix equation for the expansion coefficients of the tangential electric fields in the apertures, with respect to a given basis, (ii) derivation of expressions for the matrix elements and the right hand side vector in this matrix equation and (iii) validation of the previous calculations by considering a few specific examples.

Chapter 2 discusses the theory behind the method of moments and gives expressions for the Green's functions that are encountered throughout the work. In Chapter 3, the matrix equation for the expansion coefficients of the aperture fields are derived, as well as expressions for the scattering parameters of the structures in terms of these coefficients. The matrix elements are given in terms of the slot admittances. Expressions for these admittances are derived in appendix E. Chapter 4 presents numerical results obtained by applying the developed theory to a few specific waveguide geometries, as well as comparisons of these results with values calculated by the commercial FEKO software and with results published previously in the literature.

# Chapter 2

# Theory

The analysis of slot coupled waveguides presented in this thesis is accomplished by deriving a system of governing integral equations for the electric fields in the regions connecting the waveguides and then solving these through the method of moments - a general purpose method for solving linear functional equations. This chapter reviews and examines the mathematical tools needed to cast the Maxwell equations into the form of a system of integral equations and the subsequent discretization and solution of this system by the moment method.

The structure of this chapter is as follows: we will first examine the concepts of Huygen's surfaces and domain decomposition and see how these can be used to derive integral equations for the electric field at surfaces that connect different canonical regions in the geometry. Following this, the method of moments will be discussed and it will be shown how it can be used to solve these equations, and thereafter expressions for the Green's functions for the magnetic field due to a magnetic current are given for some common waveguide geometries. This completes our toolbox, and we are in a position to solve a simple problem involving two orthogonal, aperture coupled waveguides (the T-Junction waveguide). This example contains all the vital methods needed to understand the more complicated problem of analyzing waveguide coupling junctions, which forms the main part of the thesis.

For more information, Harrington[15] gives an excellent introduction to the method of moments.

## 2.1 Domain Decomposition

The slot coupled waveguide structure introduced in the previous chapter has a complex geometry, and trying to solve Maxwell's equations for the entire structure as it is without resorting to a commercial numerical software would be extremely difficult.

There is however a way of reducing the problem to several smaller subproblems, each of which can be solved with relative ease, and then "welding" together the solutions of the subproblems to create the global solution. This method is known as domain decomposition.

In the case of aperture or slot coupled waveguides, the decomposition would loosely mean treating each waveguide or slot separately, and then forcing the two individual solutions to produce the same fields at the interface between the different regions so that the electric and magnetic fields are continuous across this surface.

Consider for example the two aperture coupled waveguides shown in Fig 2.1 where the top walls have been removed. This is called a T-Junction waveguide, and consists of an infinitely long waveguide connected to a semi-infinitely long waveguide through an aperture of width $w$. The task of calculating the total fields (incident field plus fields scattered at the aperture) when a wave is incident from the lower left in the geometry as it is would be very challenging. Instead, it is possible to treat the two waveguides separately. Waveguide 1 is then simply an infinite waveguide, and waveguide 2 is a shorted (semi-infinite) waveguide, and the fields inside these simpler geometries have known solutions (the waveguide walls are assumed to be infinitely thin). By then matching the fields over the aperture we obtain the solution to the global problem.

So far we have been very vague about how these steps are actually done in practice and exactly why they work, and it is the purpose of this section to go through this method step by step. At the end of the chapter, the problem of the T-Junction mentioned above will be solved in detail.

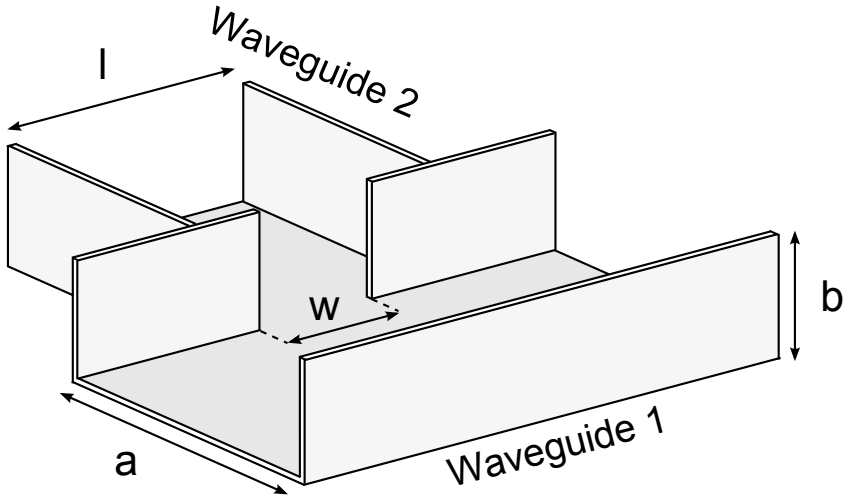


**Figure 2.1:** Interior of a T-Junction waveguide (top cover removed). Only the region in the vicinity of the aperture is shown, and the waveguides are actually infinite in extent and continue indefinitely to the lower left, upper left and upper right.

### 2.1.1 An analogy with image theory

Domain decomposition is quite similar, in spirit, to image theory, in that it allows one to simplify the geometry of the problem by employing auxiliary sources.

As an example of what this means, consider the well-known problem from electrostatics of calculating the electric field due to an electric charge in free space, held fixed above a large, infinitely conducting plane (see Fig. 2.2).

To calculate the field at any point above the plane, we first have to calculate the field from the charge $q$ itself, but we also have to account for the field generated by the surface charges induced on the plane due to the presence of $q$.

However, since we know the electric field inside a perfect conductor is identically zero, we are really only interested in the field in region I, i.e., above the conductor. In this region the scalar potential $\Phi$ satisfies the Poisson equation

$$\nabla^2\Phi = -\frac{\rho}{\epsilon_0} \tag{2.1}$$

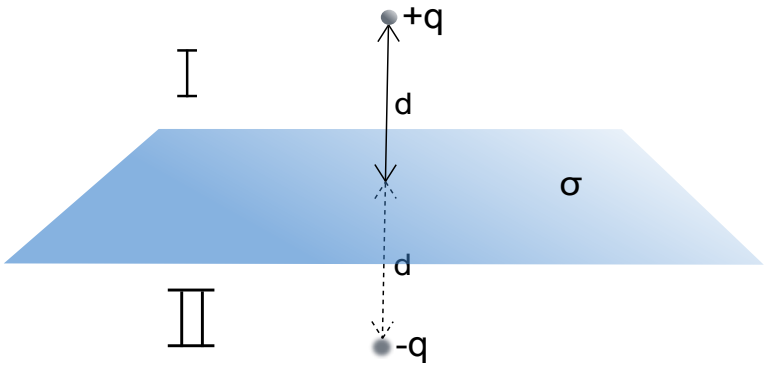


**Figure 2.2:** A charge $q$ above an infinite perfectly conducting plane. The charge induces a surface charge density $\sigma$ on the plane. For the purposes of calculating the fields in the region above the plane, the surface charges may be considered to be concentrated into an "image charge" of charge $-q$ a distance $d$ below the plane, and hence the ground plane can be removed.

where $\rho$ is the electric charge density, with the Dirichlet boundary condition $\Phi(\vec{r}) = 0$ on the surface of the conductor. Now, since the solution to the Poisson equation with Dirichlet boundary conditions is unique[16], all that is left to do is to find a function $\Phi$ such that it vanishes on the metal interface and satisfies (2.1) *inside region I*. Outside region I however, the scalar potential need not satisfy the Poisson equation since we are only concerned with finding the correct field in region I.

In other words, we can change the geometry and sources in the problem, as long as the sources within the region of interest are kept same, and the appropriate boundary conditions of $\Phi$ are still satisfied. The solution $\Phi$ inside this region will be then be identical in both cases.

For the problem of a charge above a conducting plane, this means that we can completely remove the plane and just place an "image charge" $-q$ at the position where the mirror image of $q$ would have been (see Fig 2.2). Since the charge distribution $\rho$ in region I was not changed, and it is easily seen that $\Phi$ is zero where the metal surface previously was, the field in region I created by this configuration must be unique and therefore identical to the one in the original problem with the conducting plane. Though in region II both the geometry and charge distributions were changed, so here the two configurations are not equivalent and will result in different fields.

In summary, what we have accomplished thus far, is that we started with a problem we

did not know how to solve straight away (in this case electric charges in the presence of a conductor), but by changing the geometry and sources of the problem *outside* the region of interest, it was possible to turn the problem into one we knew how to solve (charges in free, unbounded space), but that still gave the same field in the region of interest, and that the change in geometry (half space to free space) was compensated for by the introduction of fictitious charges outside the region of interest.

In the analysis of the T-Junction waveguide in Chapter 3, the two waveguides will be sealed off from one another by adding an infinitely thin, perfectly conducting wall in the aperture, in addition to introducing auxiliary sources to account for this change in geometry. This way, the two initially connected waveguides will become one infinite and one semi-infinite waveguide with no aperture connecting them, and the problem then reduces to calculating the fields generated by the auxiliary sources in these two simpler geometries. This is explained in detail in Section 2.5.

### 2.1.2 Huygen's Equivalence Theorem

In the above example, the field in a new geometry was calculated by changing the geometry into one where it was known how to calculate fields due to a given charge distribution, and adding fictitious charges to compensate for the change in geometry. The important point was that both configurations gave rise to the same field in the region of interest.

The approach was based on the uniqueness of the solution of the Poisson equation satisfied by the scalar potential. Later, when we will calculate scattered fields in more complex waveguide geometries, we will no longer have a time independent problem and will work directly with the time harmonic $\vec{E}$ and $\vec{H}$ fields themselves. Hence, when changes are made to the external geometry, a uniqueness theorem based on the electric and magnetic fields will be needed to ensure that the fields in the region that we are interested in are identical in both configurations.

#### Uniqueness Theorem

In a time harmonic situation, the electric and magnetic fields in a volume $V$ are uniquely determined by Maxwell's equations if all sources inside $V$ are specified, as well as the

tangential component of $\vec{E}$ or $\vec{H}$ over the boundary of $V$, or, more formally:[17, pp. 312–314]

**THEOREM** *A time-harmonic field inside a volume $V$ in a lossy medium is uniquely determined if the sources $\vec{J}$ and $\vec{M}$ inside $V$ are known, as well as one of the following three alternatives:*

*(1). The tangential component of $\vec{E}$ over the entire boundary $\partial V$.*

*(2). The tangential component of $\vec{H}$ over the entire boundary $\partial V$.*

*(3). The tangential component of $\vec{E}$ over one part of the boundary, and the tangential component of $\vec{H}$ over the rest.*

*The lossless case is treated as the limit of the lossy case as the dissipation tends to zero.* □

In other words, for the purpose of calculating the electric and magnetic fields inside some given volume $V$, we are always allowed to change the sources outside the volume as long as these sources produce the same tangential components of the fields over the boundary $\partial V$. This is the foundation of the domain decomposition technique.

### A Comment on the Magnetic Current

The sources $\vec{J}$ and $\vec{M}$ mentioned above correspond to the electric and magnetic currents, respectively. While magnetic currents do not seem to exist in nature, they can be introduced into Faraday's law of induction to make Maxwell's equations more symmetric with respect to the electric and magnetic fields:

$$\nabla \times \vec{E} = -\vec{M} - \frac{\partial \vec{B}}{\partial t}. \tag{2.2}$$

Albeit not "real", these magnetic currents nevertheless constitute a useful theoretical tool since they can be used as fictitious sources to model other electromagnetic configurations that are difficult to analyze using conventional methods, as we will soon see.

If the boundary conditions for the electric and magnetic fields are rederived with the

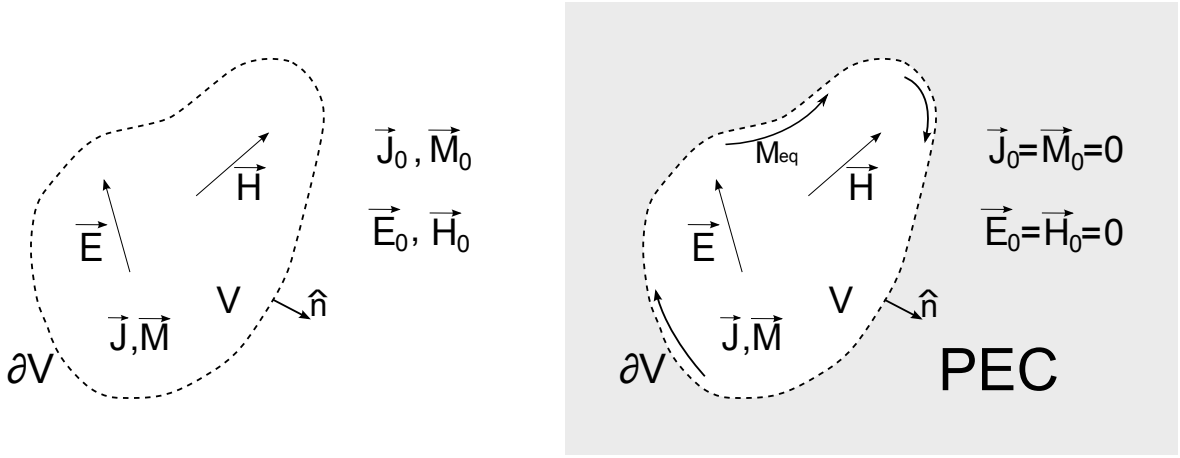


**(a)** **(b)**

**Figure 2.3:** The fields $\vec{E}$ and $\vec{M}$ are generated by the currents $\vec{J}$ and $\vec{M}$ inside $V$, as well as $\vec{J}_0$ and $\vec{M}_0$ outside $V$, as illustrated in the figure on the left. The region exterior to $V$ is then replaced by a PEC and the currents $\vec{J}_0$ and $\vec{M}_0$ are removed. Furthermore, a magnetic current $\vec{M}_{\text{eq}} = \vec{E} \times \hat{n}$ is introduced just at the surface of the PEC, as shown to the right. Since both the sources within $V$ and the tangential component of $\vec{E}$ across $\partial V$ are identical in both cases, the fields $\vec{E}$, $\vec{H}$ inside $V$ are also identical.

magnetic current term included in the Maxwell equations, one finds that the boundary condition for the tangential electric field has changed and is

$$\vec{M} = -\hat{n} \times (\vec{E}_2 - \vec{E}_1) \quad \text{for } \vec{r} \in S, \tag{2.3}$$

where $\hat{n}$ is a unit vector on the interface $S$ between the two media, pointing from media 1 into media 2, $\vec{E}_1$ and $\vec{E}_2$ are the electric fields in these regions, and $\vec{M}$ is the surface magnetic current on the interface.

### Surface Equivalence Principle

Next, with help from the uniqueness theorem, we will see how the geometry of a problem can be changed while the fields are kept the same through adding fictitious magnetic currents outside the region of interest.

Consider the situation in Fig. 2.3a, where we have a field generated by some sources $\vec{J}$ and $\vec{M}$, and where we are interested in calculating the field inside the volume $V$. From the

uniqueness theorem, we are assured that if the tangential component of, say, $\vec{E}$ is known across the boundary $\partial V$, as well as the sources within the volume, then the fields in $V$ are uniquely determined. This means that we are free to change the geometry outside $V$, both media and sources, as long as this new configuration gives rise to the same tangential electric field on the boundary $\partial V$ as our initial problem, since then on account of the uniqueness theorem both situations generate the same field internal to $V$.

The method that is used extensively throughout this thesis is to fill the region exterior to $V$ with a PEC (cf. Fig. 2.3b). This removes the tangential component of $\vec{E}$ and makes it identically zero. However, if the new configuration is to provide identical fields in $V$ as in the original case, they must have the same tangential $\vec{E}$ component at the interface $\partial V$ between the regions. To this end, a fictitious surface magnetic current $\vec{M} = \vec{E} \times \hat{n}$ can be introduced just inside the PEC to ensure the tangential $\vec{E}$ take the same value as in the original problem. This implies that the two different configurations, which have the same sources inside $V$, now also have the same tangential component of the electric field across the surface of $V$, and hence on account of the uniqueness theorem both have the same fields inside $V$, so whichever approach is more convenient can be used to determine the fields.

One might question the usefulness of this technique, since if the goal is to calculate the fields in the region, the new geometry would require us to calculate the fields generated by fictitious magnetic currents that are defined in terms of the unknown fields! This is true. For this technique to be worthwhile, we must know how to calculate the fields generated by given magnetic currents in the new geometry (all the relevant Green's functions for this will be derived in Sec. 2.4), and then the magnetic currents have to be treated as the new unknowns to be determined.

We will now consider the example of the T-Junction and see how an integral equation for the unknown magnetic current can be derived.

### 2.1.3 Domain Decomposition of T-Junction Waveguide

Consider again the T-Junction waveguide that was mentioned briefly above. A schematical picture of the situation is shown in Fig. 2.4. A field is incident from the left, generated by sources at infinity. This field will be scattered at the aperture, reflecting some of the

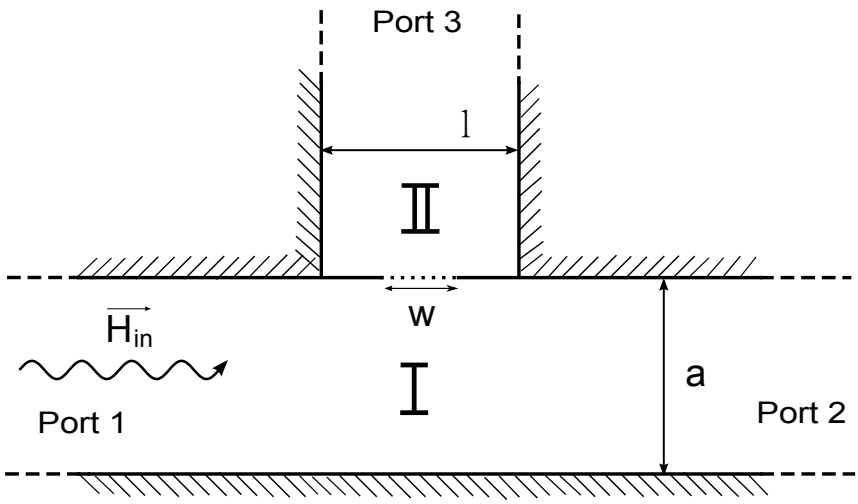


**Figure 2.4:** Schematic picture of the T-Junction waveguide. The geometry is composed of two canonical regions: one infinite and one semi-infinite waveguide, denoted as regions I and II, respectively.

energy back to the left, while the remaining part is split between the other two exits. The ultimate goal is to find the fraction of energy scattered in each direction.

We now subdivide this problem into two subproblems using the domain decomposition technique as discussed above. First, we subdivide the geometry into two canonical regions, region I and II. If the aperture $S$ joining the two waveguides was filled with a PEC, region I transforms into an infinite waveguide, and region II turns into a semi-infinite waveguide. These geometries are much simpler than the T-Junction waveguide since the electric and magnetic fields in these structures are known in closed form (in Sec. 2.4 we will derive exact expressions for the magnetic field Green's function in these geometries).

By the uniqueness theorem, we are allowed to fill the aperture with a PEC, if we first add a compensating magnetic current $\vec{M}(\vec{r}) = \pm\vec{E}(\vec{r}) \times \hat{n}, \quad \vec{r} \in S$, on both sides of the aperture, where the plus sign is for the magnetic current in region I, and the minus sign for the current in region II. The sign difference is due to the fact that the normal to the PEC is in opposite directions on different sides of the aperture (see Fig. 2.5).

We are now assured by the uniqueness theorem that the fields in the regions I and II are unaltered by the introduction of both the PEC and magnetic currents. For example, in

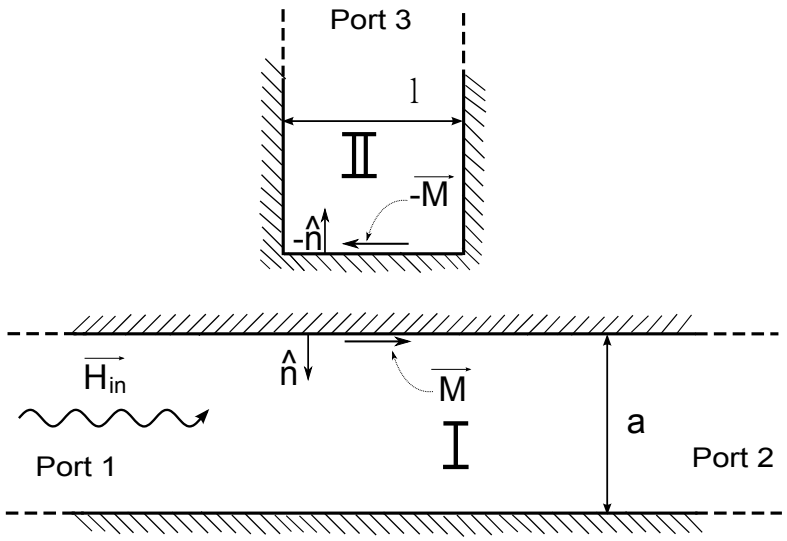


**Figure 2.5:** T-Junction waveguide where each canonical region is treated separately. It is permitted to fill the aperture $S$ with PEC material if a ficticious magnetic current is introduced at the interface in each region. This current has opposite sign in the two regions due to the opposite facing surface normals $\hat{n}$ and $-\hat{n}$.

region I, the tangential $\vec{E}$ component vanishes at the waveguide walls, but the magnetic current was chosen precisely such that the tangential component of the electric field just outside the aperture attains its actual value, i.e., is unaffected by the introduction of the PEC. The same is valid in region II.

As mentioned earlier, the magnetic current is still unknown, but if this can be determined, the problem is solved, since the Green's functions $\overleftrightarrow{G}^m_{Im}$ and $\overleftrightarrow{G}^m_{IIm}$ for the magnetic field generated by magnetic currents are known in both regions (these will be derived in later sections, but for now we assume they are known). We will now derive an integral equation for the unknown magnetic current $\vec{M}$.

The magnetic field in region I can be written in terms of the magnetic current as

$$\vec{H}_I(\vec{r}) = \vec{H}_{\text{in}}(\vec{r}) + \iint_S \overleftrightarrow{G}^m_{Im}(\vec{r}, \vec{r}_s)\vec{M}(\vec{r}_s)\mathrm{d}S_s, \tag{2.4}$$

and the field in region II is given by

$$\vec{H}_{II}(\vec{r}) = -\iint_S \overleftrightarrow{G}^m_{IIm}(\vec{r},\vec{r}_s)\vec{M}(\vec{r}_s)\mathrm{d}S_s, \tag{2.5}$$

where the quantities $\overleftrightarrow{G}^m_{Xm}$ are the Green's functions for the magnetic field in region $X$ generated by a magnetic current in the same region, and $\vec{H}_{\text{in}}$ is the incident magnetic field.

By considering the original T-Junction geometry, it is clear that the $\vec{H}$-field must be everywhere continuous in the T-Junction due to the absence of sources in the original problem. Specifically, the magnetic field must be continuous across the aperture $S$, i.e. $\vec{H}_I(\vec{r}) = \vec{H}_{II}(\vec{r})$ for all $\vec{r}$ on $S$ and hence

$$\vec{H}_{\text{in}}(\vec{r}) + \iint_S \overleftrightarrow{G}^m_{Im}(\vec{r},\vec{r}_s)\vec{M}(\vec{r}_s)\mathrm{d}S_s = -\iint_S \overleftrightarrow{G}^m_{IIm}(\vec{r},\vec{r}_s)\vec{M}(\vec{r}_s)\mathrm{d}S_s \tag{2.6}$$

This equation must be true for all points $\vec{r}$ on $S$. [1] This is an integral equation that completely determines the unknown magnetic current, provided that both the incident field and Green's functions are known. Once solved, the total magnetic and electric fields can be calculated everywhere in the T-Junction through the relevant Green's functions.

In summary, the task of solving Maxwell's equations (which is a set of partial differential equations), applied to the T-Junction waveguide geometry, has been reduced to solving an integral equation for the fictitious magnetic current $\vec{M}$ in the aperture. This procedure of subdividing the geometry into several canonical regions with known Green's functions, adding magnetic currents to ensure the fields are unchanged, and then deriving integral equations for the magnetic currents by requiring the magnetic field to be continuous across the apertures, is a general procedure that is applicable to a wide range of electromagnetic scattering and radiation problems. Specifically, it is exactly this procedure that will be followed when analyzing the system of slot coupled waveguides that form the main part of this thesis.

The final task that now remains is to solve the integral equation in (2.6). This is done numerically using the method of moments as discussed in the next section.

[1] We are actually only required to impose the continuity of the tangential $\vec{H}$-field, but in this case both waveguides are made of the same media so we might as well impose continuity of the total field.

## 2.2 The Method of Moments

The method of moments is a general method for numerically solving linear functional equations [15, pp. 1–21], i.e. equations of the form

$$\mathcal{L}f = g. \tag{2.7}$$

In the above equation, $f$ and $g$ are elements of two different vector spaces, and $\mathcal{L}$ is a linear operator between these spaces. $\mathcal{L}$ and $g$ are assumed to be known, so the task is to find the vector $f$ such that its image under the operator $\mathcal{L}$ is $g$.

This kind of functional equation is interesting to us since both partial differential equations and integral equations can be cast into functional equation form. For example, for the integral equation (2.6) describing the fields in the T-Junction waveguide, the unknown $f$ to be determined would be the magnetic current $\vec{M}$, the right hand side would be $g = -\vec{H}_{\text{in}}$, and the operator would be the sum of the two integrals

$$\mathcal{L}X = \iint_S \overleftrightarrow{G}^m_{Im}(\vec{r}, \vec{r}_s) X(\vec{r}_s) \mathrm{d}S_s + \iint_S \overleftrightarrow{G}^m_{IIm}(\vec{r}, \vec{r}_s) X(\vec{r}_s) \mathrm{d}S_s. \tag{2.8}$$

Note that since $\mathcal{L}$ just consists of a sum of two weighted integrals, it is a linear operator, and this problem is thus actually a linear functional equation.

Returning to the general form (2.7), the idea of the method of moments is to expand the unknown vector $f$ in terms of a known basis, and then by weighting the result with a set of testing functions, obtain a matrix equation for the unknown expansion coefficients. If we denote the basis functions by $\{f_i\}$, we obtain

$$f = \sum_i \alpha_i f_i, \tag{2.9}$$

where the $\alpha_i$ are the unknowns to be determined. In theory, an infinite number of expansion terms may be needed for the equality in (2.9) to hold, but in practice only a finite number of terms need to be included to obtain a good approximation in most cases.

Since $\mathcal{L}$ is linear, equation (2.7) becomes

$$\sum_i \alpha_i \mathcal{L} f_i = g. \tag{2.10}$$

Equation (2.10) can be turned into $M$ scalar equations by forming the inner product of this equation with each element of a set of $M$ *testing functions* $\{w_j\}_{j=1}^{M}$.

We thus obtain the system of $M$ equations

$$\sum_{i=1}^{M} \alpha_i \langle w_j, \mathcal{L} f_i \rangle = \langle w_j, g \rangle, \quad j = 1, 2, ..., M. \tag{2.11}$$

In the T-Junction waveguide, an appropriate inner product between two vectors is to form the symmetric product between the vectors and to integrate the result over the aperture $S$,

$$\langle \vec{A}, \vec{B} \rangle = \iint_S \vec{A}(\vec{r}) \cdot \vec{B}(\vec{r}) \mathrm{d}S. \tag{2.12}$$

For the problems discussed in this thesis, it also has the property of making the operator $\mathcal{L}$ self-adjoint, in the sense that

$$\langle \vec{A}, \mathcal{L}\vec{B} \rangle = \langle \mathcal{L}\vec{A}, \vec{B} \rangle \qquad \text{for all } \vec{A} \text{ and } \vec{B}. \tag{2.13}$$

This self-adjointness (called reciprocity in electromagnetics) will be useful when calculating the matrix elements in situations more complicated than the T-Junction.

In equation (2.11), every quantity, except for the coefficients $\alpha_i$, are known, so this is just a matrix equation for these expansion coefficients once the inner products $\langle w_j, \mathcal{L} f_i \rangle$ and $\langle w_j, g \rangle$ have been calculated.

In this thesis, the weighting functions $w_j$ will be chosen to be identical to the basis functions $f_j$, i.e.,

$$w_j = f_j \quad \text{for } j = 1, ..., M, \tag{2.14}$$

a choice that is referred to as *Galerkin's method*.

What remains is the choice of basis functions $f_i$. Ideally, the expansion functions should be able to accurately model the actual field with as few terms as possible to keep the matrix size as small as possible. This is facilitated by employing basis functions that already satisfy the relevant boundary conditions[14].

Throughout this text, we will use an expansion of the magnetic current into trigonometric functions in the slots and apertures. It has been found that for moderately and strongly excited slots a sinusoidal expansion of the longitudinal magnetic current closely models the actual field with relatively few terms[5, 6, 9], while incorporating the boundary conditions as the magnetic current tends to zero at the edges of the apertures due to the vanishing tangential electric field above the metal.

To apply the method of moments to the T-Junction waveguide, the Green's functions in infinite and semi-infinite waveguides occuring in Eq. (2.8) have to be determined. Before these are derived in Sec. 2.4, we will first take a brief look at the different fields that can exist inside a rectangular waveguide or cavity.

## 2.3 Modes in a Rectangular Waveguide

The magnetic field in a waveguide of uniform cross section, filled with a homogeneous dielectric with dielectric parameter $\epsilon$ can be expanded in terms of a set of eigenfunctions, or modal functions. In a rectangular waveguide, there exists two different kinds of modes: transverse electric (TE) and transverse magnetic (TM) modes. The TE modes have a completely transverse electric field, i.e., the electric field has no $z$-component, whereas the TM modes have a completely transverse magnetic field, i.e., the magnetic field has no $z$-component.

Both TE and TM modes are labeled by two sets of integer indices, $m$ and $n$, and can travel in either the positive or negative $z$-direction. In this thesis the TE mode travelling in the $\pm z$-direction will sometimes be written as $\vec{H}_{mn}^{\mathrm{TE}\pm}$, and the corresponding TM mode is written as $\vec{H}_{mn}^{\mathrm{TM}\pm}$. However, more often the more compact notation $H_u^{\pm}$ will be used, where it is assumed that the index $u$ contains information about both $m$ and $n$, as well as whether the mode is a TE or TM mode.

This means that any possible time harmonic field configuration can be written as the sum

$$\vec{H}(\vec{r}) = \sum_u \left( A_u \vec{H}_u^+ + B_u \vec{H}_u^- \right), \tag{2.15}$$

where the $A_u$ and $B_u$ are complex constants. The sum over $u$ implies that the sum is taken over all TE and TM modes for all possible values of the indices $m$ and $n$.

A more thorough explanation of waveguide modes is given in appendix B, where expressions for the modes in a rectangular waveguide are derived and useful orthogonality conditions between the modes are listed.

## 2.4 Green's Functions

### 2.4.1 Introduction

As described in the preceding sections, we need to determine for the Green's functions $\overleftrightarrow{G}^m_{Im}$ and $\overleftrightarrow{G}^m_{IIm}$ for the magnetic field due to a given magnetic current in the two waveguide regions. We start with a short reminder about Green's functions.

The Green's function $G(\vec{r}, \vec{r}')$ to a linear, scalar valued, partial differential equation (PDE)

$$\mathcal{L}y(\vec{r}) = f(\vec{r}), \tag{2.16}$$

is the solution when the right hand side equals the Dirac delta function, $f(\vec{r}) = \delta(\vec{r} - \vec{r}')$, and thus it satisfies

$$\mathcal{L}G(\vec{r}, \vec{r}') = \delta(\vec{r} - \vec{r}'). \tag{2.17}$$

It can be thought of as the impulse response of the system. From this fundamental solution, the solution for any right hand side $f(\vec{r})$ can be formed by weighting $G$ with $f$ according to

$$y(\vec{r}) = \int G(\vec{r}, \vec{r}') f(\vec{r}') \mathrm{d}^3 x'. \tag{2.18}$$

By applying the operator $\mathcal{L}$ to $y$, it is seen that this is indeed a solution to the linear

equation (2.16),

$$\mathcal{L}y(\vec{r}) = \mathcal{L}\int G(\vec{r},\vec{r}')f(\vec{r}')\mathrm{d}^3x' = \int \left[\mathcal{L}G(\vec{r},\vec{r}')f(\vec{r}')\right]\mathrm{d}^3x' = \tag{2.19}$$
$$= \int \left[\delta(\vec{r}-\vec{r}')\right] f(\vec{r}')\mathrm{d}^3x' = f(\vec{r}).$$

Hence, if the Green's function for a linear PDE can be found, any inhomogenous solution can be found through (2.18).

This technique has one significant shortcoming for our purpose; the approach taken above is only valid for scalar valued functions $y$ (such as the potential $\phi$ in electrostatics). In our case, we seek the magnetic field, a vector-valued function of the spatial coordinates $\vec{r}$. The Green's function will therefore not be scalar-valued as in the above example, but will rather be tensorial, called a *Dyadic Green's function*. The reason the Green's function is not a scalar function anymore is that if it were, then by equation (2.18), the response $\vec{y}$ would always point in the same direction as the source $\vec{f}$, which does not have to be the case.

### Dyadic Green's Functions

We now examine the vector equation

$$\mathcal{L}\vec{A} = \vec{B}, \tag{2.20}$$

where $\mathcal{L}$ is yet again a linear operator. Consider now three vector fields $\vec{G}_i(\vec{r},\vec{r}')$ such that

$$\mathcal{L}\vec{G}_i = \hat{n}_i\delta(\vec{r}-\vec{r}') \quad \text{for } i \in \{1,2,3\}, \tag{2.21}$$

where $\hat{n}_i$ denotes the $x, y$- or $z$-direction respectively. Next, form the 3x3 tensor

$$\overleftrightarrow{G}(\vec{r},\vec{r}') = \left[\vec{G}_1|\vec{G}_2|\vec{G}_3\right], \tag{2.22}$$

where each of the above Green's functions form the columns.

The solution to (2.20) is then given by

$$\vec{A}(\vec{r}) = \int \overleftrightarrow{G}(\vec{r},\vec{r}\,')\vec{B}(\vec{r}\,')\mathrm{d}^3x'. \tag{2.23}$$

Again, this is verified by a straightforward application of $\mathcal{L}$:

$$\mathcal{L}\vec{A} = \int \mathcal{L}\left[\overleftrightarrow{G}(\vec{r},\vec{r}\,')\vec{B}(\vec{r}\,')\right]\mathrm{d}^3x'. \tag{2.24}$$

The expression in brackets can be rewritten as

$$\mathcal{L}\left[\overleftrightarrow{G}(\vec{r},\vec{r}\,')\vec{B}(\vec{r}\,')\right] = \mathcal{L}\left[\vec{G}_1B_1 + \vec{G}_2B_2 + \vec{G}_3B_3\right] = B_1\mathcal{L}\vec{G}_1 + B_2\mathcal{L}\vec{G}_2 + B_3\mathcal{L}\vec{G}_3 = \tag{2.25}$$

$$= (B_1\hat{x} + B_2\hat{y} + B_3\hat{z})\delta(\vec{r}-\vec{r}\,') = \vec{B}(\vec{r}\,')\delta(\vec{r}-\vec{r}\,'). \tag{2.26}$$

And hence the integral (2.24) becomes simply

$$\mathcal{L}\vec{A} = \int \vec{B}(\vec{r}\,')\delta(\vec{r}-\vec{r}\,')\mathrm{d}^3x' = \vec{B}(\vec{r}). \tag{2.27}$$

In summary, for the vector equation $\mathcal{L}\vec{A} = \vec{B}$, if the tensorial – or *dyadic*, as it is commonly called in electromagnetics – Green's function $\overleftrightarrow{G}(\vec{r},\vec{r}\,')$ is known, then the solution for any right hand side $\vec{B}$ can be found through (2.23).

When analyzing waveguides by means of the the domain decomposition technique, fictitious magnetic currents are placed in the waveguides where two different regions have been sealed off from one another by closing the connecting aperture with a PEC. These magnetic currents will radiate and generate electric and magnetic fields in the waveguide as discussed in the previous section, so for this analysis it is imperative to know the dyadic Green's functions $\overleftrightarrow{G}_m^{\,m}$ for the magnetic field generated by the magnetic currents in the different regions. These are listed in the following section.

### 2.4.2 Magnetic Field Green's Functions in Different Waveguide Geometries

Below are listed the Green's functions for the magnetic field generated by a magnetic current in an infinitely long rectangular waveguide, a rectangular cavity and a shorted (semi-infinite) waveguide. Two forms for Green's function in the infinitely long waveguide are presented. The first is very simple but takes on different forms depending on whether the observation point is in front of or behind the source point, longitudinally. The second, called the Seki Green's function, or Seki's alternative expression, is more complicated but has the advantage of being independent of whether the observation point is in front of or behind the source point. Detailed derivations and explanations of all Green's functions can be found in appendix D.

#### Infinite Rectangular Waveguide

In an infinitely long rectangular waveguide with its axis along the $z$-axis, the Green's function $\overleftrightarrow{G}{}^{m}_{m}$ for the magnetic field due to a magnetic current can be expressed in terms of the waveguide modes $\vec{H}_u^{\pm}$ as

$$\overleftrightarrow{G}{}^{m}_{m}(\vec{r},\vec{r}_s) = \begin{cases} \dfrac{1}{2}\displaystyle\sum_u \vec{H}_u^-(\vec{r})\vec{H}_u^+(\vec{r}_s) & \text{for } z < z_s, \\ \dfrac{1}{2}\displaystyle\sum_u \vec{H}_u^+(\vec{r})\vec{H}_u^-(\vec{r}_s) & \text{for } z > z_s, \end{cases} \tag{2.28}$$

where the product of two vectors $\vec{A}\vec{B}$ used above is neither a dot product nor a vector product, but should be regarded as the outer product of the two vectors and is thus an operator (or a matrix). The action of $\vec{A}\vec{B}$ on some vector $\vec{C}$ is

$$(\vec{A}\vec{B})\vec{C} = \vec{A}(\vec{B}\cdot\vec{C}). \tag{2.29}$$

The sum is over all TE and TM modes, for all possible values of the indices $m$ and $n$ for the waveguide modes.

For example, if the magnetic current is confined to some volume $V$, then the magnetic field

scattered by this current $\vec{M}$ at some observation point $\vec{r}$ far into the waveguide ($z << z_s$) is given by

$$\vec{H}(\vec{r}) = \int_V \overleftrightarrow{G}{}^m_m(\vec{r},\vec{r}')\vec{M}(\vec{r}_s)\mathrm{d}^3x' = \frac{1}{2}\sum_u \vec{H}_u^-(\vec{r})\left[\int_V \vec{H}_u^+(\vec{r}')\cdot\vec{M}(\vec{r}')\mathrm{d}^3x'\right]. \tag{2.30}$$

Note that the integral in the bracket is a scalar, and the entire expression is simply an eigenfunction expansion of the magnetic field scattered by the current.

### Green's function in a rectangular cavity

Consider a rectangular cavity that extends from $z = -l_1$ to $z = l_2$. This can be considered to be a rectangular waveguide that has been cut off at these two $z$-coordinates, and thus has the same modal functions $\vec{H}_u^{\pm}$ as an infinite rectangular waveguide. The Green's function in this geometry is given by

$$\overleftrightarrow{G}{}^m_m(\vec{r},\vec{r}_s) = \begin{cases} \dfrac{1}{4}\displaystyle\sum_u \frac{1}{\sinh(\gamma_u l)}\left[\vec{H}_u^-(\vec{r})e^{\gamma_u l_1} - \vec{H}_u^+(\vec{r})e^{-\gamma_u l_1}\right] \\ \qquad\qquad \left[e^{\gamma_u l_2}\vec{H}_u^+(\vec{r}_s) - e^{-\gamma_u l_2}\vec{H}_u^-(\vec{r}_s)\right] \quad \text{for } -l_1 < z < z_s \\ \dfrac{1}{4}\displaystyle\sum_u \frac{1}{\sinh(\gamma_u l)}\left[\vec{H}_u^+(\vec{r})e^{\gamma_u l_2} - \vec{H}_u^-(\vec{r})e^{-\gamma_u l_2}\right] \\ \qquad\qquad \left[e^{\gamma_u l_1}\vec{H}_u^-(\vec{r}_s) - e^{-\gamma_u l_1}\vec{H}_u^+(\vec{r}_s)\right] \quad \text{for } z_s < z < l_2. \end{cases} \tag{2.31}$$

The modes $\vec{H}_u^{\pm}$ above denote modes travelling in the $z$-direction. However, this direction has no special significance for a rectangular cavity, and an analogous expansion in $y$-modes or $x$-modes could have been used instead.

### Seki's alternative expression for the infinite waveguide Green's function

The expression (2.28) is very useful due to its simplicity, but in some circumstances it is more convenient to use a different form of the Green's function for an infinitely long waveguide. This Green's function is derived by introducing a "virtual cavity" of length $l$ of the magnetic current, and extending from $z = -l_1$ to $z = l_2$. This alternate form has

the same functional dependence, irrespective of whether $z < z_s$ or $z > z_s$. It is called the Seki Green's function and is given by

$$\begin{aligned}\overleftrightarrow{G}_{\text{Seki}}(\vec{r},\vec{r}_s) = \overleftrightarrow{G}_c^{\,y}(\vec{r},\vec{r}_s) &+ \frac{1}{4}\sum_u \frac{e^{-\gamma_u l_1}}{\sinh(\gamma_u l)}\left[\vec{H}_u^+(\vec{r})e^{\gamma_u l_2} - \vec{H}_u^-(\vec{r})e^{-\gamma_u l_2}\right]\vec{H}_u^+(\vec{r}_s) + \\ &+ \frac{1}{4}\sum_u \frac{e^{-\gamma_u l_2}}{\sinh(\gamma_u l)}\left[\vec{H}_u^-(\vec{r})e^{\gamma_u l_1} - \vec{H}_u^+(\vec{r})e^{-\gamma_u l_1}\right]\vec{H}_u^-(\vec{r}_s),\end{aligned} \tag{2.32}$$

where $\overleftrightarrow{G}_c^{\,y}$ is the Green's function for a cavity where the modal expansion is done in terms of $y$-travelling modes, instead of in terms of $z$-travelling modes as in (2.31). Note that if the magnetic current is confined to the upper or lower wall, $y$ will always be less than (or greater than) $y_s$ and hence the same form for the cavity Green's function will be used everywhere.

One last thing that must be discussed is the choice of length $l$ for the virtual cavity. We have to avoid making $\sinh(\gamma_u l)$ zero since this term occurs in a denominator in the Seki Green's function. This is impossible for evanescent modes, since for these $\gamma_u$ is real and larger than zero. However, for a propagating mode, $\gamma_u$ is purely imaginary, so $\gamma_u = i\beta_u$, where $\beta_u$ is a real, positive number. Our condition on $l$ is then

$$\sinh(\gamma_u l) = i\sin(\beta_u l) \neq 0, \tag{2.33}$$

but since $\beta_u$ is the wavenumber of the wave, the above condition becomes

$$l \neq \frac{n}{2}\lambda_u, \tag{2.34}$$

where $n$ is any integer and $\lambda_u$ is the wavelength of the propagating mode. In practice, the dimensions of the waveguide are often chosen such that it allows only one propagating mode, and the length of the virtual cavity is then chosen halfway between the first two "forbidden" lengths,

$$l = \frac{3}{4}\lambda_{\text{in}}, \tag{2.35}$$

where $\lambda_{\text{in}}$ is the wavelength of the propagating mode.

**Semi-infinite waveguide**

The Green's function for a semi-infinite waveguide extending from $z = -\infty$ and ending at $z = l$ is given by

$$\overleftrightarrow{G}_m^m(\vec{r},\vec{r}_s) = \begin{cases} \frac{1}{2}\sum_u e^{-\gamma_u l}\vec{H}_u^-(\vec{r})\left[\vec{H}_u^+(\vec{r}_s)e^{\gamma_u l} - \vec{H}_u^-(\vec{r}_s)e^{-\gamma_u l}\right] & \text{for } z < z_s, \\ \frac{1}{2}\sum_u e^{-\gamma_u l}\left[\vec{H}_u^+(\vec{r})e^{\gamma_u l} - \vec{H}_u^-(\vec{r})e^{-\gamma_u l}\right]\vec{H}_u^-(\vec{r}_s) & \text{for } z > z_s. \end{cases} \tag{2.36}$$

This completes the theory needed to perform an analysis of slot and aperture coupled waveguides using the MoM approach, and it will in the next section be shown how it can be used to calculate the scattering parameters in a T-Junction waveguide.

## 2.5 Example: S-Matrix Calculation for a T-Junction Waveguide

In this section we will perform a thorough analysis of the T-Junction waveguide shown in Fig. 2.6.

The geometry consists of two waveguides connected via an aperture $S$ of width $w$. A wave $\vec{H}_{\text{in}}$ is incident from the left, and we wish to calculate the amplitudes of the waves leaving each port, or equivalently, the fraction of power scattered into each port. As discussed in Sec. 2.1, the aperture can be closed if a fictitious magnetic current is introduced on either side of the aperture, as shown in Fig. 2.6. The field in region I is then the sum of the incident field and the field radiated by the magnetic current $\vec{M}$. The field in region II is the field radiated by the magnetic current $-\vec{M}$. Since the Green's functions in both a shorted waveguide and an infinite waveguide are known, the radiated fields can be easily calculated from the magnetic currents by

$$\vec{H}(\vec{r}) = \int \overleftrightarrow{G}(\vec{r},\vec{r}_s)\vec{M}(\vec{r}_s)\mathrm{d}V. \tag{2.37}$$

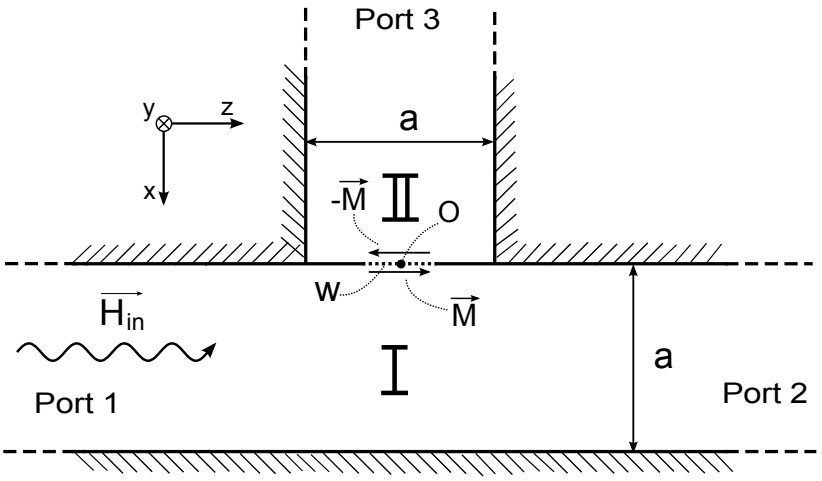


**Figure 2.6:** The T-Junction waveguide consisting of one infinite and one semi infinite waveguide connected through an aperture of width $w$. The origin of coordinates is placed in the top wall at the center of the aperture, with axes as shown in the top left. The height of the waveguides (dimension along $y$) is $b$.

In Sec. 2.1, we also required that the magnetic field be continuous across the aperture $S$, leading to the integral equation (2.6), i.e.,

$$\vec{H}_{\text{in}}(\vec{r}) + \iint_S \overleftrightarrow{G}^m_{Im}(\vec{r},\vec{r}_s)\vec{M}(\vec{r}_s)\mathrm{d}S_s = -\iint_S \overleftrightarrow{G}^m_{IIm}(\vec{r},\vec{r}_s)\vec{M}(\vec{r}_s)\mathrm{d}S_s, \quad \text{for } \vec{r}\in S. \tag{2.38}$$

The above equation simply states that the field, at some observation point $\vec{r}$, as calculated in region I should be identical to the field as calculated in region II when the observation point approaches the aperture $S$. The two functions $\overleftrightarrow{G}^m_{Im}$ and $\overleftrightarrow{G}^m_{IIm}$ simply denote the Green's functions in region I and II, respectively.

Equation (2.38) can be solved for the unknown magnetic current $\vec{M}$, and once known, the fields anywhere – and most interesting to us, far into each port – can be calculated through the Green's functions.

Equation (2.38) can be rewritten into the equivalent but more compact Dirac notation according to

$$|\vec{H}_{\text{in}}\rangle + \overleftrightarrow{G}^m_{Im}|\vec{M}\rangle = -\overleftrightarrow{G}^m_{IIm}|\vec{M}\rangle, \tag{2.39}$$

where we have defined

$$\overleftrightarrow{G}^{m}_{Xm}|\vec{A}\rangle = \iint_S \overleftrightarrow{G}^{m}_{Xm}(\vec{r},\vec{r}_s)\vec{A}(\vec{r}_s)\mathrm{d}S. \tag{2.40}$$

### 2.5.1 Transformation of the Integral Equation into a Matrix Equation

The first step in our MoM approach is to expand the unknown current $\vec{M}$, in terms of a set of known basis functions $\{\vec{m}_j\}_{j=1}^{N}$. We choose the basis functions to be directed along $\hat{z}$ and have a sine variation across the aperture according to

$$\vec{m}_j(z) = \sin\left[\frac{j\pi}{w}\left(z+\frac{w}{2}\right)\right]\hat{z}. \tag{2.41}$$

This choice of basis automatically incorporates the boundary conditions that $\vec{E}\times\hat{n}$, and thus $\vec{M}$, should vanish at the aperture edges $z=-\frac{w}{2}$ and $z=\frac{w}{2}$.

Using this basis, the unknown current is expanded according to

$$\vec{M}(\vec{r}) = \sum_{j=1}^{N} A_j\vec{m}_j(\vec{r}). \tag{2.42}$$

We do not know a priori how many terms $N$ will be needed to obtain accurate results, and this variable will have to be examined for convergence at the end. We have now transformed the problem of determining the unknown magnetic current into the problem of determining the (scalar) expansion coefficients $A_j$ above.

Substituting the expansion (2.42) into the integral equation (2.39) gives

$$|\vec{H}_{\mathrm{in}}\rangle + \sum_{j=1}^{N} A_j\overleftrightarrow{G}^{m}_{Im}|\vec{m}_j\rangle = -\sum_{j=1}^{N} A_j\overleftrightarrow{G}^{m}_{IIm}|\vec{m}_j\rangle, \tag{2.43}$$

where we have used the linearity of the operators $\overleftrightarrow{G}$ to move the expansion coefficients outside the operators.

The next step is to form the symmetric product of the above equation with the testing function $\vec{m}_i$ (see also Sec. 2.2), i.e.,

$$\langle \vec{A} | \vec{B} \rangle = \iint_S \vec{A}(\vec{r}) \cdot \vec{B}(\vec{r}) \mathrm{d}S. \tag{2.44}$$

This leads to the equation

$$\langle \vec{m}_i | \vec{H}_{\mathrm{in}} \rangle + \sum_{j=1}^{N} A_j \langle \vec{m}_i | \overleftrightarrow{G}^{m}_{Im} | \vec{m}_j \rangle = - \sum_{j=1}^{N} A_j \langle \vec{m}_i | \overleftrightarrow{G}^{m}_{IIm} | \vec{m}_j \rangle. \tag{2.45}$$

We rewrite this slightly and realize that this is valid for all basis functions $\vec{m}_i$, that is, it is true for all $i = 1, ..., N$:

$$\sum_{j=1}^{N} A_j \left[ \langle \vec{m}_i | \overleftrightarrow{G}^{m}_{Im} | \vec{m}_j \rangle + \langle \vec{m}_i | \overleftrightarrow{G}^{m}_{IIm} | \vec{m}_j \rangle \right] = - \langle \vec{m}_i | \vec{H}_{\mathrm{in}} \rangle, \quad i = 1, ..., N. \tag{2.46}$$

Note that the above represents a matrix equation that can be written symbolically as

$$\begin{bmatrix} \langle \vec{m}_i | \overleftrightarrow{G}^{m}_{Im} | \vec{m}_j \rangle \\ + \\ \langle \vec{m}_i | \overleftrightarrow{G}^{m}_{IIm} | \vec{m}_j \rangle \end{bmatrix} \begin{bmatrix} \\ A_j \\ \\ \end{bmatrix} = \begin{bmatrix} \\ - \langle \vec{m}_i | \vec{H}_{\mathrm{in}} \rangle \\ \\ \end{bmatrix}, \tag{2.47}$$

where $i$ and $j$ each run from 1 to $N$. Since the Green's functions $\overleftrightarrow{G}^{m}_{Im}$ and $\overleftrightarrow{G}^{m}_{IIm}$ as well as the incident field $\vec{H}_{\mathrm{in}}$ and the basis functions $\vec{m}_i$ are known, we can calculate the RHS and all the elements of the matrix. From the definitions (2.40) and (2.44) it is seen that the matrix elements are given by

$$\langle \vec{m}_i | \overleftrightarrow{G}^{m}_{Xm} | \vec{m}_j \rangle = \iint_S \mathrm{d}S \; \vec{m}_i(\vec{r}) \cdot \iint_S \overleftrightarrow{G}^{m}_{Xm}(\vec{r}, \vec{r}_s) \vec{m}_j(\vec{r}_s) \mathrm{d}S_s, \tag{2.48}$$

and

$$\langle \vec{m}_i | \vec{H}_{\mathrm{in}} \rangle = \iint_S \vec{m}_i(\vec{r}_s) \cdot \vec{H}_{\mathrm{in}}(\vec{r}_s) \mathrm{d}S_s. \tag{2.49}$$

The above integrals are often referred to as *reaction integrals*, and they describe the self and mutual coupling between different basis functions in the aperture in the regions I and

II, and the coupling between the basis functions and the incident field. The next step is to evaluate these integrals.

### 2.5.2 Evaluation of the Reaction Integrals

Let us start with evaluating the reaction integral $\langle \vec{m}_i | \overleftrightarrow{G}^{m}_{Im} | \vec{m}_j \rangle$, which consists of a double surface integral. This means that the source coordinate $\vec{r}_s$ will sweep over the aperture $S$ for every value of $\vec{r}$. Specifically, this means that if we were to use the conventional Green's function (2.31) for an infinite waveguide, the integrals would have to be split up depending on whether $z > z_s$ or $z < z_s$, and to avoid this we employ the Seki Green's function (2.32) since this has the same functional form for all $z$ and $z_s$. The length $d$ of the virtual cavity is chosen to be three quarters of the wavelength of the propagating mode in the waveguide.

The Seki Green's function is composed of two parts: first a contribution from the aperture current directly, as if it were radiating in a cavity, and then secondly a contribution from the ficticious currents on the virtual cavity walls. We thus write the Green's function as [2]

$$\overleftrightarrow{G}^{m}_{Im}(\vec{r}, \vec{r}_s) = \overleftrightarrow{G}^{c}_{x}(\vec{r}, \vec{r}_s) + \overleftrightarrow{G}_{\text{walls}}(\vec{r}, \vec{r}_s). \tag{2.50}$$

The reaction integral then takes the form

$$\langle \vec{m}_i | \overleftrightarrow{G}^{m}_{Im} | \vec{m}_j \rangle = \langle \vec{m}_i | \overleftrightarrow{G}^{c}_{x} | \vec{m}_j \rangle + \langle \vec{m}_i | \overleftrightarrow{G}_{\text{walls}} | \vec{m}_j \rangle. \tag{2.51}$$

We start by evaluating the first RHS term.

The cavity Green's function is given by (2.31). With $l_1 = 0$ and $l = l_2 = a$, this becomes

$$\overleftrightarrow{G}^{c}_{x}(\vec{r}, \vec{r}_s) = \frac{1}{4} \sum_{u} \frac{1}{\sinh(\gamma_{ux} a)} \left[ \vec{H}^{+}_{u}(\vec{r}) e^{\gamma_{ux} a} - \vec{H}^{-}_{u}(\vec{r}) e^{-\gamma_{ux} a} \right] \left[ \vec{H}^{-}_{u}(\vec{r}_s) - \vec{H}^{+}_{u}(\vec{r}_s) \right] \tag{2.52}$$

where $\gamma_{ux}$ is the propagation constant for modes travelling in the $x$-direction in the virtual

[2] Compare this with equation (2.32). In this case we have $\overleftrightarrow{G}^{c}_{x}$ instead of $\overleftrightarrow{G}^{c}_{y}$ since our coordinate system is oriented differently here. The rest of the expression (the two double sums, corresponding to the contribution from the walls) is exactly $\overleftrightarrow{G}_{\text{walls}}$.

cavity. The integral $\langle \vec{m}_i | \overleftrightarrow{G}_x^c | \vec{m}_j \rangle$ then separates products of surface integrals according to

$$\langle \vec{m}_i | \overleftrightarrow{G}_x^c | \vec{m}_j \rangle = \frac{1}{4} \sum_u \frac{1}{\sinh(\gamma_{ux} a)} \int_S \mathrm{d}S \left[ \vec{H}_u^+(\vec{r}) e^{\gamma_{ux} a} - \vec{H}_u^-(\vec{r}) e^{-\gamma_{ux} a} \right] \cdot \vec{m}_i(\vec{r}) \times \\ \times \int_S \left[ \vec{H}_u^-(\vec{r}_s) - \vec{H}_u^+(\vec{r}_s) \right] \cdot \vec{m}_j(\vec{r}_s) \mathrm{d}S_s. \tag{2.53}$$

The sum above is over all modes, both TE and TM. From the equations in appendix B, it can be shown that the $z$-component at $x = 0$ of the TE and TM waves travelling in the $x$-direction is given by

$$\left(H_{nm}^{\mathrm{TE}\pm}\right)_z = \pm \frac{n\pi}{k_{cux} d} \sqrt{\frac{\gamma_u \epsilon_n \epsilon_m}{jk\eta db}} \sin\left[\frac{n\pi}{d}\left(z + \frac{d}{2}\right)\right] \cos\left[\frac{m\pi}{b}\left(y + \frac{b}{2}\right)\right], \tag{2.54}$$

$$\left(H_{nm}^{\mathrm{TM}\pm}\right)_z = \mp \frac{m\pi}{k_{cux} b} \sqrt{\frac{jk\epsilon_n \epsilon_m}{\gamma_u \eta db}} \sin\left[\frac{n\pi}{d}\left(z + \frac{d}{2}\right)\right] \cos\left[\frac{m\pi}{b}\left(y + \frac{b}{2}\right)\right],$$

where $j$ is the imaginary unit (not to be confused with the basis function index $j$), $\eta$ is the impedance of the medium, in this case free space, and $\epsilon_n$ is given by (B.13). Specifically, note that for both TE and TM modes, $\left(H_{nm}^+\right)_z = -\left(H_{nm}^-\right)_z$. The reaction integral (2.53) then becomes

$$\langle \vec{m}_i | \overleftrightarrow{G}_x^c | \vec{m}_j \rangle = -\sum_u \coth(\gamma_{ux} a) \int_S H_{nm}^{z+}(\vec{r}) m_i(\vec{r}) \mathrm{d}S \int_S H_{nm}^{z+}(\vec{r}) m_j(\vec{r}) \mathrm{d}S. \tag{2.55}$$

Note from equation (2.54) that the $z$-component of the TE and TM waves differ only by a proportionality constant. In fact, they have identical $y$ and $z$ dependencies. The surface integrals in (2.55) will then be proportional to

$$\int_{y=-b/2}^{b/2} \int_{z=-w/2}^{w/2} \sin\left[\frac{n\pi}{d}\left(z + \frac{d}{2}\right)\right] \cos\left[\frac{m\pi}{b}\left(y + \frac{b}{2}\right)\right] \sin\left[\frac{k\pi}{w}\left(z + \frac{w}{2}\right)\right] \mathrm{d}y \mathrm{d}z = \\ = b\delta_{m0} \mathrm{i}_{\mathrm{II}nk}(d), \tag{2.56}$$

where $k = i$ or $j$ is the index of the basis function and where $b\delta_{m0}$ results from the integration over $y$, and $\mathrm{i}_{\mathrm{II}nk}(d)$ is given by

$$\mathrm{i}_{\mathrm{II}nk}(d) = \int_{z=-w/2}^{w/2} \sin\left[\frac{n\pi}{d}\left(z + \frac{d}{2}\right)\right] \sin\left[\frac{k\pi}{w}\left(z + \frac{w}{2}\right)\right] \mathrm{d}z, \tag{2.57}$$

which can easily be evaluated analytically and can be found in appendix A.1.

An important point to make is that the surface integral contains a factor $\delta_{m0}$. This means that only modes with $m = 0$ contribute to the sum. But in equation (2.54) we see that the TM modes are proportional to $m$, so all TM modes vanish from the sum, leaving only the TE modes. As a result, by combining equations (2.54), (2.55) and (2.56) the final form of the reaction integral is found:

$$\langle \vec{m}_i | \overleftrightarrow{G}^c_x | \vec{m}_j \rangle = -\sum_{n=1}^{\infty} \coth(\gamma_{ux} a) \frac{2\gamma_{ux} b}{jk\eta d} \mathrm{i}_{\mathrm{II}ni}(d) \mathrm{i}_{\mathrm{II}nj}(d), \tag{2.58}$$

where we have used that for $m = 0, n \geq 1$ modes, the cut-off wavenumber $k_{cux}$ is given by $k_{cux} = n\pi/d$, and $\epsilon_n \epsilon_m = 2$.

All quantities in equation (2.58) are known, so the first part of the region I reaction integral (2.51) can be calculated. We will now derive an expression for the integral $\langle \vec{m}_i | \overleftrightarrow{G}_{\text{walls}} | \vec{m}_j \rangle$, i.e., the contribution from the virtual cavity walls to the self-admittance.

As discussed previously, the Green's function $\overleftrightarrow{G}_{\text{walls}}$ is given by the two double sums in Eq. (2.32), and hence the reaction integral becomes

$$\begin{aligned}\langle \vec{m}_i | \overleftrightarrow{G}_{\text{walls}} | \vec{m}_j \rangle = \frac{1}{4} \sum_u \frac{1}{\sinh(\gamma_{uz} d)} \iint_S \mathrm{d}S\, \vec{m}_i(\vec{r}) \cdot \iint_S \Big\{ \left[ \vec{H}_u^+(\vec{r}) - e^{-\gamma_{uz} d} \vec{H}_u^-(\vec{r}) \right] \vec{H}_u^+(\vec{r}_s) + \\ + \left[ \vec{H}_u^-(\vec{r}) - e^{-\gamma_{uz} d} \vec{H}_u^+(\vec{r}) \right] \vec{H}_u^-(\vec{r}_s) \Big\} \vec{m}_j(\vec{r}_s) \mathrm{d}S_s.\end{aligned} \tag{2.59}$$

where $\gamma_{uz}$ is the propagation constant for modes travelling in the $z$-direction.

The above expression contains double surface integrals over four terms for each mode $u$, which decouple into products of surface integrals due to the simple dependence on $\vec{r}$ and $\vec{r}_s$. By splitting the expression into four double surface integrals we obtain

$$\langle \vec{m}_i | \overleftrightarrow{G}_{\text{walls}} | \vec{m}_j \rangle = \frac{1}{4} \sum_u \frac{1}{\sinh(\gamma_{uz} d)} \Big\{ y_{ui}^+ y_{uj}^+ - e^{-\gamma_{uz} d} y_{ui}^- y_{uj}^+ + y_{ui}^- y_{uj}^- - e^{-\gamma_{uz} d} y_{ui}^+ y_{uj}^- \Big\}, \tag{2.60}$$

where the factors $y_{uk}^{\pm}$ denote the coupling between the mode $\vec{H}_u^{\pm}$ and the basis function

$\vec{m}_k$, and is given by the integral

$$y_{uk}^{\pm} = \iint_S \vec{H}_u^{\pm}(\vec{r}) \cdot \vec{m}_k(\vec{r}) \mathrm{d}S. \tag{2.61}$$

Note that the coupling (2.61) is only nonzero for TE modes since $\vec{m}_k$ is directed completely along $z$. The $z$-component of TE waves travelling along $z$ is given by

$$\vec{H}_{nm}^{+} \cdot \hat{z} = \frac{k_{cuz}}{\gamma_{uz}} \sqrt{\frac{\gamma_{uz}\epsilon_n\epsilon_m}{jk\eta ab}} \cos\left[\frac{m\pi y}{b}\right] e^{\mp\gamma_{uz}z}, \tag{2.62}$$

and hence the coupling becomes

$$\iint_S \vec{H}_u^{\pm}(\vec{r}) \cdot \vec{m}_k(\vec{r}) \mathrm{d}S = \frac{k_{cuz}}{\gamma_{uz}} \sqrt{\frac{\gamma_{uz}\epsilon_n\epsilon_m}{jk\eta ab}} b\delta_{m0} i_{Ink}^{\mp} \tag{2.63}$$

where $b\delta_{m0}$ comes from the integration over $y$ from 0 to $b$, and $i_{Ink}^{\mp}$ is the $z$-part of the integral,

$$i_{Ink}^{\mp} = \int_{z=-w/2}^{z=w/2} e^{\mp\gamma_{uz}z} \sin\left[\frac{k\pi}{w}\left(z + \frac{w}{2}\right)\right] \mathrm{d}z, \tag{2.64}$$

which has a closed form expression (see appendix A.1).

Substituting this into equation (2.60) finally gives

$$\begin{aligned} \langle \vec{m}_i | \overleftrightarrow{G}_{\text{walls}} | \vec{m}_j \rangle = \sum_{n=1}^{\infty} \frac{n^2\pi^2 b}{2a^3\gamma_{uz}jk\eta \sinh(\gamma_{uz}d)} \Big\{ & i_{Ini}^{-} i_{Inj}^{-} + \\ & - e^{-\gamma_{uz}d} i_{Ini}^{+} i_{Inj}^{-} + i_{Ini}^{+} i_{Inj}^{+} - e^{-\gamma_{uz}d} i_{Ini}^{-} i_{Inj}^{+} \Big\} \end{aligned} \tag{2.65}$$

where we used that the cut-off wavenumber is given by $k_{cuz} = n\pi/a$.

The above expression consists completely of known quantities and can hence be calculated numerically. We have thus found expressions for the reaction integral $\langle \vec{m}_i | \overleftrightarrow{G}_{Im}^{m} | \vec{m}_j \rangle$, as given by (2.51).

We must now find an expression for the self-admittance in region II; i.e., for $\langle \vec{m}_i | \overleftrightarrow{G}_{IIm}^{m} | \vec{m}_j \rangle$. Region II is a semi infinite waveguide shorted at $x = 0$, and the Green's function $\overleftrightarrow{G}_{IIm}^{m}$ is

thus found from (2.36) to be

$$\overleftrightarrow{G}^{m}_{IIm}(\vec{r},\vec{r}_s) = \frac{1}{2}\sum_u \vec{H}_u^-(\vec{r})\left[\vec{H}_u^+(\vec{r}_s) - \vec{H}_u^-(\vec{r}_s)\right]. \tag{2.66}$$

The reaction integral thus becomes

$$\langle\vec{m}_i|\overleftrightarrow{G}^{m}_{IIm}|\vec{m}_j\rangle = \frac{1}{2}\sum_u \left[\iint_S \vec{H}_u^-(\vec{r})\cdot\vec{m}_i(\vec{r})\mathrm{d}S\right]\left[\iint_S [\vec{H}_u^+(\vec{r}) - \vec{H}_u^-(\vec{r})]\cdot\vec{m}_j(\vec{r})\mathrm{d}S\right] \tag{2.67}$$

The $z$-components of $x$-travelling TE and TM modes at the wall $x = 0$ are given by

$$\vec{H}^{\mathrm{TE}\pm}_{nm}\cdot\hat{z} = \pm\frac{n\pi}{k_{cuy}a}\sqrt{\frac{\gamma_{uy}\epsilon_n\epsilon_m}{abjk\eta}}\sin\left[\frac{n\pi}{a}\left(z+\frac{a}{2}\right)\right]\cos\left[\frac{m\pi y}{b}\right], \tag{2.68}$$

$$\vec{H}^{\mathrm{TM}\pm}_{nm}\cdot\hat{z} = \mp\frac{m\pi}{k_{cuy}b}\sqrt{\frac{jk\epsilon_n\epsilon_m}{ab\gamma_{uy}\eta}}\sin\left[\frac{n\pi}{a}\left(z+\frac{a}{2}\right)\right]\cos\left[\frac{m\pi y}{b}\right].$$

Note specifically that $\vec{H}_u^- = -\vec{H}_u^+$, and hence the reaction integral (2.67) thus becomes

$$\langle\vec{m}_i|\overleftrightarrow{G}^{m}_{IIm}|\vec{m}_j\rangle = -\sum_u \left[\iint_S \vec{H}_u^+(\vec{r})\cdot\vec{m}_i(\vec{r})\mathrm{d}S\right]\left[\iint_S \vec{H}_u^+(\vec{r})\cdot\vec{m}_j(\vec{r})\mathrm{d}S\right], \tag{2.69}$$

where the surface integrals are found to be

$$\iint_S \vec{H}_u^+(\vec{r})\cdot\vec{m}_i(\vec{r})\mathrm{d}S = \frac{n\pi}{k_{cuy}a}\sqrt{\frac{\gamma_{uy}\epsilon_n\epsilon_m}{abjk\eta}}b\delta_{m0}i_{IIni}(a), \tag{2.70}$$

where the factor $b\delta_{m0}$ comes from the integral over $y$, and $i_{IIIni}$ is the integral over $z$, given by

$$i_{IIni}(a) = \int_{-w/2}^{w/2}\sin\left[\frac{n\pi}{a}\left(z+\frac{a}{2}\right)\right]\sin\left[\frac{i\pi}{w}\left(z+\frac{w}{2}\right)\right]\mathrm{d}z, \tag{2.71}$$

which can be evaluated analytically (see appendix A.1). The contribution from the TM waves vanish since the factor $\delta_{m0}$ forces $m$ to zero, and the amplitude of the TM waves is proportional to $m$ according to (2.68). Inserting this into equation (2.69) gives

$$\langle\vec{m}_i|\overleftrightarrow{G}^{m}_{IIm}|\vec{m}_j\rangle = -\sum_{n=1}^{\infty}\frac{2b\gamma_{uy}}{ajk\eta}i_{IIni}(a)i_{IInj}(a). \tag{2.72}$$

This concludes the derivation of the matrix elements in the matrix equation (2.47).

The RHS of (2.47) is readily found since it is the coupling between the incident $\mathrm{TE}_{10}^{+}$ mode in region I and the basis functions $\vec{m}_i$ in the aperture, and this is given by equation (2.63). Specifically for the $\mathrm{TE}_{10}^{+}$ mode, this becomes

$$-\langle \vec{m}_i | \vec{H}_{\mathrm{in}} \rangle = \frac{k_{cuz}}{\gamma_{uz}} \sqrt{\frac{2b\gamma_{uz}}{jk\eta a}}\, i_{I1i}^{-}. \tag{2.73}$$

### 2.5.3 Evaluation of the Scattering Parameters

In the previous section, we performed the rather tedious task of calculating the reaction integrals that comprise the matrix and right hand side of the matrix equation (2.47) for the magnetic current. For a given width $a$ and height $b$, as well as aperture width $w$, the matrix and right hand side can be calculated numerically from the expressions derived in the previous section, by including only a finite number of terms in the infinite summations, but sufficiently many for convergence. The expansion coefficients $A_j$ are then obtained by solving the matrix equation.

Once these are obtained, the scattering parameters can be calculated. To find these, the Green's function (2.28) for an infinite waveguide will be used.

The scattering parameter $S_{ij}$ is defined as the ratio of the amplitude of the outgoing wave in port $i$, to the amplitude of the incoming wave in port $j$ when no waves are incident on the other ports. Specifically, for a given $j$, the squared magnitude of the S-parameters, $|S_{ij}|^2$, denote what fraction of the energy incident in port $j$ exits through the other ports of the structure.[18, p. 221]

#### Calculation of S11

Consider the outgoing field at a point $\vec{r}$ sufficiently far into port I that the evanescent modes are negligible. Outgoing means that it is travelling in the negative $z$-direction. This

field is generated by the fictitious magnetic current $\vec{M}$ and is found from

$$\vec{H}_I(\vec{r}) = \iint_S \overleftrightarrow{G}^m_{Im}(z < z_s)\vec{M}(\vec{r}_s)\mathrm{d}S_s = \frac{1}{2}\sum_u \vec{H}_u^-(\vec{r}) \iint_S \vec{H}_u^+(\vec{r}_s)\cdot\vec{M}(\vec{r}_s)\mathrm{d}S_s = \tag{2.74}$$
$$= \sum_u \vec{H}_u^-(\vec{r}) \left[\frac{1}{2}\sum_{i=1}^N A_i \iint_S \vec{H}_u^+(\vec{r}_s)\cdot\vec{m}_i(\vec{r}_s)\mathrm{d}S_s\right]$$

Since the dimensions of the waveguide are such that the only propagating mode is the $\mathrm{TE}_{10}$ mode, all modes except $\mathrm{TE}_{10}$ vanish from the sum over $u$ far into port I, hence

$$\vec{H}_I(\vec{r}) = \vec{H}_{10}^- \left[\frac{1}{2}\sum_{i=1}^N A_i \iint_S \vec{H}_{10}^+(\vec{r}_s)\cdot\vec{m}_i(\vec{r}_s)\mathrm{d}S_s\right] = \tag{2.75}$$
$$= \vec{H}_{10}^- \left[\frac{1}{2}\frac{\pi}{a\gamma_{z10}}\sqrt{\frac{2b\gamma_{10z}}{ajk\eta}}\sum_{i=1}^N A_i\, i_{I1i}^-\right],$$

where equation (2.63) was used to evaluate the coupling between the $\mathrm{TE}_{10}$ mode and the basis functions. The return loss $S_{11}$ is then seen to be

$$S_{11} = \left[\frac{1}{2}\frac{\pi}{a\gamma_{z10}}\sqrt{\frac{2b\gamma_{10z}}{ajk\eta}}\sum_{i=1}^N A_i\, i_{I1i}^-\right]. \tag{2.76}$$

### Calculation of S21

To calculate the insertion loss parameter $S_{21}$, we need the field far into the waveguide at port II, travelling in the $z$-direction. Like for the $S_{11}$ parameter, this is calculated using the Green's function (2.28), but in this case with the form valid for $z > z_s$. A calculation almost identical to the one above yields

$$\vec{H}_{II}(\vec{r}) = \vec{H}_{10}^+(\vec{r}) + \vec{H}_{10}^+ \left[\frac{1}{2}\sum_{j=1}^N A_j \iint_S \vec{H}_{10}^-(\vec{r})\cdot\vec{m}_j(\vec{r})\mathrm{d}S\right], \tag{2.77}$$

where the sum over all modes in the expression for the Green's function disappears since only the $\mathrm{TE}_{10}$ mode is a propagating mode in the waveguide and the first term $\vec{H}_{10}^+$ is the field incident from port I.

Using the expression (2.63) for the surface integral, it is found that the scattering parameter $S_{21}$ takes the form

$$S_{21} = 1 + \frac{\pi}{2a}\sqrt{\frac{2b}{\gamma_{10z} jk\eta a}} \sum_{j=1}^{N} i^{+}_{I1j}\ A_j. \tag{2.78}$$

**Calculation of S31**

To calculate the $\vec{H}$-field far into region III, we use the Green's function (2.66) and find

$$\vec{H}(\vec{r}) = -\iint_S \overleftrightarrow{G}^{m}_{IIm}(\vec{r},\vec{r}_s)\vec{M}(\vec{r}_s)\mathrm{d}S_s = -\frac{1}{2}\sum_u \vec{H}^{-}_u(\vec{r}) \iint_S \left[\vec{H}^{+}_u(\vec{r}_s) - \vec{H}^{-}_u(\vec{r}_s)\right] \cdot \vec{M}(\vec{r}_s)\mathrm{d}S_s \tag{2.79}$$

Again, the only propagating mode is the $\mathrm{TE}_{10}$ mode, and the integral was encountered earlier in equation (2.67), where it was found to be two times the expression in (2.70). The scattering parameter is therefore

$$S_{31} = -\sqrt{\frac{2\gamma_{10z} b}{ajk\eta}} \sum_{j=1}^{N} A_j i_{II1j}(a). \tag{2.80}$$

### 2.5.4 Quick Review

It may now be worthwhile to quickly review what we have done so far.

The geometry under consideration is that of the T-Junction waveguide with the $\mathrm{TE}_{10}$ mode incident from port I as shown in Fig. 2.4. The objective is to find the amplitude of the outgoing waves from ports II and III, as well as the amplitude of the wave reflected back into port I. These amplitudes are the scattering parameters $S_{21}$, $S_{31}$ and $S_{11}$, respectively.

To find these, the geometry was first split up into two canonical regions, the infinite waveguide (region I), and the semi-infinite waveguide (region II), by adding a PEC in the aperture $S$. This was only allowed if a magnetic current $\vec{M}$ and $-\vec{M}$ was added on both sides of the aperture (i.e., in both regions), see Fig. 2.6.

An integral equation for $\vec{M}$ was obtained by requiring the $\vec{H}$-field to be continuous across

the aperture $S$ [see Eq. (2.38)], and this was transformed into the matrix equation (2.47) by expanding the magnetic current in sine functions with unknown coefficients and forming the symmetric product of the resulting expression with each of the basis functions. The matrix elements and the vector on the right hand side were then evaluated, allowing the unknown expansion coefficients to be calculated by solving this equation.

Finally, using this approximate form (finite sine expansion) of the magnetic current, the amplitudes of the outgoing magnetic fields in the different ports are easily calculated from the appropriate Green's function.

The S-parameters were calculated numerically, using MATLAB. First the matrix elements and the right hand side of the system of equations (2.47) is calculated. The matrix elements consist of infinite sums over waveguide modes, but these sums converge rather quickly and in practice only around 50 terms need to be included for accurate results. The system of equations is then solved for the expansion coefficients $\{A_j\}_{j=1}^{N}$, and then the S-parameters are calculated according to the equations in the previous section.

### 2.5.5 Results

The scattering parameters were calculated for a T-Junction waveguide with dimensions $a = 47.55\,\text{mm}$, and $b = 22.15\,\text{mm}$, with an incoming wave of frequency $f = 5\,\text{GHz}$. $N = 5$ basis functions were used in the expansion of the magnetic current, and 100 waveguide modes were included in the mode summations that occur in the expressions for the matrix elements. The S-parameters were calculated for twenty different aperture widths $w$, ranging from $w = 0$, where there is no aperture and the two waveguides are completely sealed off from one another, to $w = a$, where the two waveguides are completely joined and there are no thin walls to either side of the aperture.

The results are plotted in Fig. 2.7. Also plotted are the same S-parameters as calculated by the commercial electromagnetics software FEKO, which show a good agreement to the MoM solution presented in this section.

We see that for small aperture widths, there is little coupling between the waveguides; almost all of the incoming power goes straight ahead into port II and only a little makes it way through the aperture into port III, or is reflected back into port I. For larger aperture

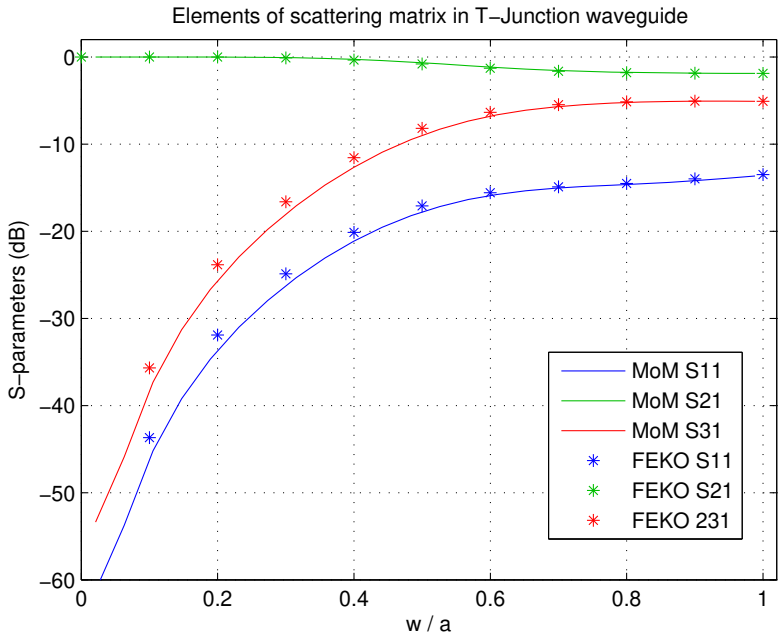


**Figure 2.7:** S-parameters of the T-Junction waveguide at 5 GHz as calculated by the moment method detailed in this chapter, as well as benchmarking values calculated using FEKO.

widths, however, the coupling increases and more power enters port III and reflects back into port I. Since energy is conserved less available power will enter port II and, hence, $S_{21}$ decreases with increasing $w$, as expected. This conservation of energy is expressed in the fact that the sum of the magnitudes of the squared S-parameters should be equal to unity, i.e.,

$$\sum_j |S_{ji}|^2 = 1 \quad \forall\, i. \tag{2.81}$$

This was found to be true to a very high accuracy in the MoM solution.

For this problem, FEKO was used to validate the solution. The calculation of the S-parameters using the method of moments solution presented here was over one hundred times faster than the corresponding computation in FEKO. The MoM code developed here is fast since the fictitious magnetic current is localized to only the small aperture between the waveguides, whereas FEKO solves for the equivalent electric currents induced in the waveguide walls and thus has to solve for a current in a much larger region.

# Chapter 3

# MoM Discretization of Waveguide Coupling Junctions

In the previous chapter a domain-decomposition based MoM technique was introduced and applied to calculate the S-parameters of a T-Junction waveguide.

This chapter presents a systematic treatment of two different waveguide coupling junction structures. The first structure, shown in figure 3.1, consists of a bottom *feeding* waveguide, above which there is an arbitrary number of waveguides, referred to as *branch* waveguides, that intersect the feed waveguide at right angles. Each branch waveguide is connected to the feed waveguide via a slot that may have any transverse and longitudinal offset from the axis of the feed waveguide, as well as an arbitrary tilt relative to its axis (called a compound slot). The second waveguide junction studied is identical to the first, except for an additional feeding waveguide placed below the first one and connected to it through a compound slot (see Fig. 3.3).

The goal of this chapter is to, for both structures, use the MoM approach to derive a general matrix equation from which the scattering parameters are easily calculated. The derivations in this chapter are based on calculations by Johan Wettergren [12].

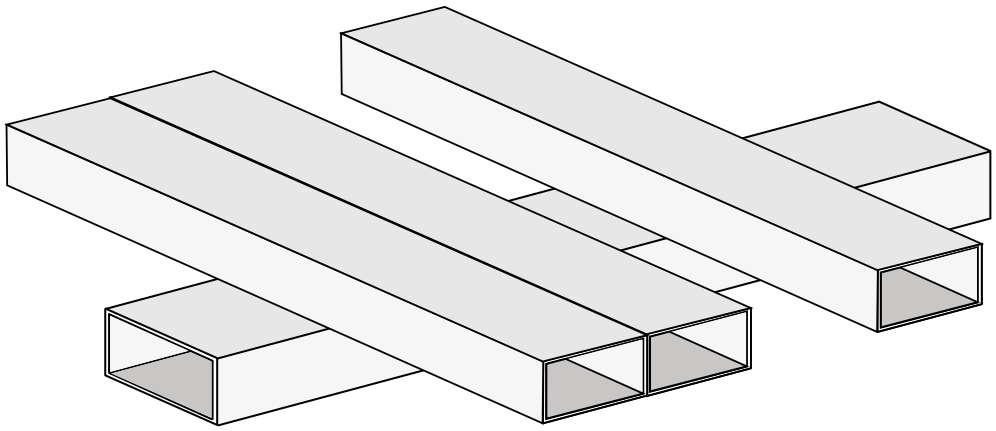

**Figure 3.1:** The geometry of the waveguide junction studied. An arbitrary number of branch waveguides are placed above, and at right angles to, a feed waveguide. Each branch waveguide is connected to the feed waveguide through a slot of arbitrary size, position and tilt.

## 3.1 Multiple Branch Waveguide Junctions with Single Layered Feeding Structure

A multiple branch waveguide junction refers in this thesis to a waveguide coupling junction composed of a feed waveguide connected through slots (with arbitrary tilts and offsets from the centerline) to an arbitrary number $N$ of branch waveguides above it. The branch waveguides are placed at right angles relative to the feed waveguide. All waveguides are assumed to be rectangular (see Fig. 3.1).

Fig. 3.2 shows a cross section of the multiple branch waveguide junction as seen from the side. The feed waveguide is denoted as region 0, the slot cavity between the feed waveguide and the first branch waveguide is denoted as region 1, the cavity between the feed waveguide and branch waveguide number 2 is region 2, and so on. The interior of the first branch waveguide is region $N+1$, the interior of the second is region $N+2$, etc. The bottom aperture of region 1 is surface $S_1$, while the top aperture of region 1 is $S_{N+1}$. The other apertures are named analogously.

The entire geometry can be divided into $2N+1$ canonical regions by adding PEC sheets at each of the $2N$ surfaces $S_q$. The magnetic current added just below surface $S_q$ is denoted

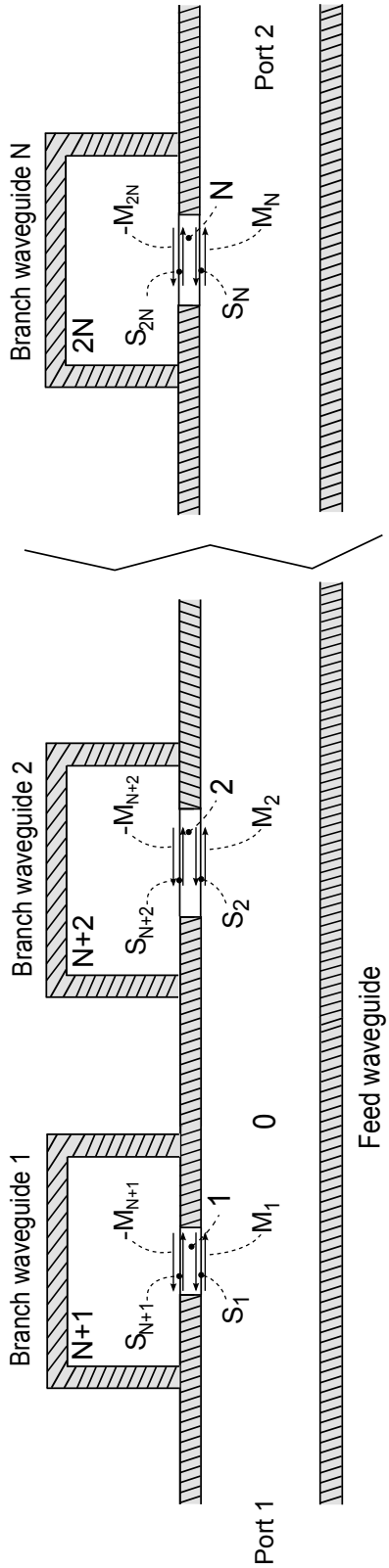


**Figure 3.2:** Side view of the multiple branch waveguide junction.

$\vec{M}_q$, and hence the current just above $S_q$ will be $-\vec{M}_q$.

With these definitions, it is now possible to write down the integral equations representing the continuity of the magnetic field across the $2N$ surfaces. These are given by

$$\begin{aligned} &|\vec{H}^1_{\text{in}}\rangle + \sum_{k=1}^{N} \overleftrightarrow{G}_0 |\vec{M}_k\rangle = -\overleftrightarrow{G}_q |\vec{M}_q\rangle + \overleftrightarrow{G}_q |\vec{M}_{N+q}\rangle \qquad \text{on } S_q, \;\; q = 1, 2, ..., N \\ &-\overleftrightarrow{G}_q |\vec{M}_q\rangle + \overleftrightarrow{G}_q |\vec{M}_{N+q}\rangle = -\overleftrightarrow{G}_{N+q} |\vec{M}_{N+q}\rangle + |\vec{H}^2_{\text{in}}\rangle \quad \text{on } S_{N+q}, \;\; q = 1, 2, ..., N. \end{aligned} \tag{3.1}$$

The first of the two equations above describe continuity across the lower apertures, while the second equation describes continuity across the top surfaces. The vectors $\vec{H}_{\text{in}}$ represent any eventual incident fields. For example, if the waveguide junction is excited from port 1, $\vec{H}^1_{\text{in}}$ would be the plus propagating TE10 mode in the feed waveguide, and $\vec{H}^2_{\text{in}}$ would be zero. When evaluating the S-matrix for the system, each port will be excited in turn.

Now, we introduce a set of basis functions $\{\vec{m}_{kj}\}_{j=1}^{Q}$ for the magnetic current in aperture $k$. At this moment we will not concern ourselves with what particular set of basis functions to choose. All equations derived in this section will have the same symbolic form irrespective of the form of the basis functions.

By expanding the magnetic currents in (3.1) as

$$\vec{M}_k = \sum_{j=1}^{Q} V_{kj} \vec{m}_{kj}, \tag{3.2}$$

and then forming the inner product of equation $q$ with all $\vec{m}_{qi}$, for $i = 1, ..., Q$, we find that each equation of the first set of integral equations in (3.1) becomes, after some rearrangement, the $Q$ scalar equations

$$\begin{aligned} &\sum_{k=1}^{N} \left[ \sum_{j=1}^{Q} V_{kj} \langle \vec{m}_{qi} | \overleftrightarrow{G}_0 | \vec{m}_{kj} \rangle \right] + \sum_{j=1}^{Q} V_{qj} \langle \vec{m}_{qi} | \overleftrightarrow{G}_q | \vec{m}_{qj} \rangle + \\ &- \sum_{j=1}^{Q} V_{N+q,j} \langle \vec{m}_{qi} | \overleftrightarrow{G}_q | \vec{m}_{N+q,j} \rangle = -\langle \vec{m}_{qi} | \vec{H}^1_{\text{in}} \rangle, \quad \text{for } i = 1, ..., Q. \end{aligned} \tag{3.3}$$

Similarly, each of the bottom equations in (3.1) becomes the $Q$ scalar equations

$$\begin{aligned} &-\sum_{j=1}^{Q} V_{qj}\langle \vec{m}_{N+q,i}|\overleftrightarrow{G}_q|\vec{m}_{q,j}\rangle + \sum_{j=1}^{Q} V_{N+q,j}\langle \vec{m}_{N+q,i}|\overleftrightarrow{G}_q|\vec{m}_{N+q,j}\rangle + \\ &+\sum_{j=1}^{Q} V_{N+q,j}\langle \vec{m}_{N+q,i}|\overleftrightarrow{G}_{N+q}|\vec{m}_{N+q,j}\rangle = \langle \vec{m}_{N+q,i}|\vec{H}^2_{\text{in}}\rangle, \quad \text{for } i = 1, ..., Q. \end{aligned} \tag{3.4}$$

The $2NQ$ equations in (3.3) and (3.4) can be written as the matrix equation

$$YV = I, \tag{3.5}$$

where $I$ is the excitation matrix for the structure, i.e., a matrix where column $i$ equals the RHS of the system of equations corresponding to the excitation of port $i$. The excitation vector corresponding to an excitation from port 1 or 2 equals

$$I_1 = \begin{bmatrix} \langle \vec{m}_{1j}|\vec{H}^+_{10}\rangle \\ \langle \vec{m}_{2j}|\vec{H}^+_{10}\rangle \\ \vdots \\ \langle \vec{m}_{Nj}|\vec{H}^+_{10}\rangle \\ \hline 0 \\ ... \\ 0 \end{bmatrix}, \qquad I_2 = \begin{bmatrix} \langle \vec{m}_{1j}|\vec{H}^-_{10}\rangle \\ \langle \vec{m}_{2j}|\vec{H}^-_{10}\rangle \\ \vdots \\ \langle \vec{m}_{Nj}|\vec{H}^-_{10}\rangle \\ \hline 0 \\ ... \\ 0 \end{bmatrix} \tag{3.6}$$

The index $j$ runs from 1 to $Q$, and each 0 is actually a column of $Q$ zeroes. The horizontal line denontes the midpoint of the vector. If the incident wave comes from one of the ports

in branch waveguide $n$, the excitation vector takes the form

$$I_{2n+1} = \left[\begin{array}{c} 0 \\ \vdots \\ 0 \\ \hline 0 \\ \vdots \\ -\langle \vec{m}_{N+n,j} | \vec{H}_{10}^{+} \rangle \\ \vdots \\ 0 \end{array}\right], \quad I_{2n+2} = \left[\begin{array}{c} 0 \\ \vdots \\ 0 \\ \hline 0 \\ \vdots \\ -\langle \vec{m}_{N+n,j} | \vec{H}_{10}^{-} \rangle \\ \vdots \\ 0 \end{array}\right] \tag{3.7}$$

Since the structure has $2N + 2$ ports, the matrix $I$ will have $2N + 2$ columns, while the matrix $V$ will have $2N + 2$ columns, where each column contains all unknown expansion coefficients for the magnetic current corresponding to the given excitation from port $i$. For each column of $V$, the expansion coefficients for the magnetic current in the apertures are listed in the order $V_{1j}, V_{2j}, ..., V_{Nj}$, for $j = 1, ..., Q$. So the $i$th column of $V$, denoted by $V_i$, will be equal to

$$V_i = \left[\begin{array}{c} V_{1j}^{i} \\ V_{2j}^{i} \\ \vdots \\ V_{Nj}^{i} \end{array}\right], \tag{3.8}$$

where $V_{kj}^{i}, j = 1, 2, ..., Q$ is used to denote the expansion coefficients for the current in aperture $k$ when the system is excited from port $i$.

Finally, the matrix $Y$ of admittances is composed of four submatrices

$$Y = \left[\begin{array}{c|c} Y_{11} & Y_{12} \\ \hline Y_{21} & Y_{22} \end{array}\right], \tag{3.9}$$

where each of these submatrices are, in turn, composed of $N \times N$ admittance matrices according to

$$Y_{11} = \left[\begin{array}{cccc} y_{0ij}^{11} + y_{1ij}^{11} & y_{0ij}^{12} & \cdots & y_{0ij}^{1N} \\ y_{0ij}^{21} & y_{0ij}^{22} + y_{2ij}^{22} & \cdots & y_{0ij}^{2N} \\ \vdots & \vdots & \ddots & \vdots \\ y_{0ij}^{N1} & y_{0ij}^{N2} & \cdots & y_{0ij}^{NN} + y_{Nij}^{NN} \end{array}\right], \tag{3.10}$$

$$Y_{12} = \begin{bmatrix} -y_{1ij}^{1,N+1} & 0 & \cdots & 0 \\ 0 & -y_{2ij}^{2,N+2} & & 0 \\ \vdots & & \ddots & 0 \\ 0 & \cdots & 0 & -y_{Nij}^{N,2N} \end{bmatrix}, \tag{3.11}$$

$$Y_{21} = (Y_{12})^T, \tag{3.12}$$

and

$$Y_{22} = \begin{bmatrix} y_{1ij}^{N+1,N+1} + y_{N+1,ij}^{N+1,N+1} & 0 & \cdots & 0 \\ 0 & y_{2ij}^{N+2,N+2} + y_{N+2,ij}^{N+2,N+2} & \cdots & \vdots \\ \vdots & & \ddots & 0 \\ 0 & \cdots & 0 & y_{Nij}^{2N,2N} + y_{2N,ij}^{2N,2N} \end{bmatrix}, \tag{3.13}$$

where, for compactness, we have defined the admittances from aperture $S_n$ to $S_m$ through region $X$ as

$$y_{Xij}^{mn} = -\langle \vec{m}_{m,i} | \overleftrightarrow{G}_X | \vec{m}_{n,j} \rangle. \tag{3.14}$$

For the multiple branch waveguide junction, there are four different kinds of admittances:

1. the self-admittance of an aperture in the infinite waveguide region,
2. the self-admittance of an aperture in the slot cavity region,
3. the mutual admittance between two apertures on the same wall in the infinite waveguide region,
4. the mutual admittance between two apertures in the slot cavity region.

Expressions for the four admittances, as well as for the coupling between basis functions and waveguide modes, are derived in appendix E.

The scattering parameters are derived in the same manner as in Sec. 2.5.3. Since the S-parameters are given by sums over the coupling between the incident waveguide mode and the basis functions in the apertures, weighted by the corresponding expansion coefficient of the magnetic current, it is easy to show that

$$S = \frac{1}{2} V^T I, \tag{3.15}$$

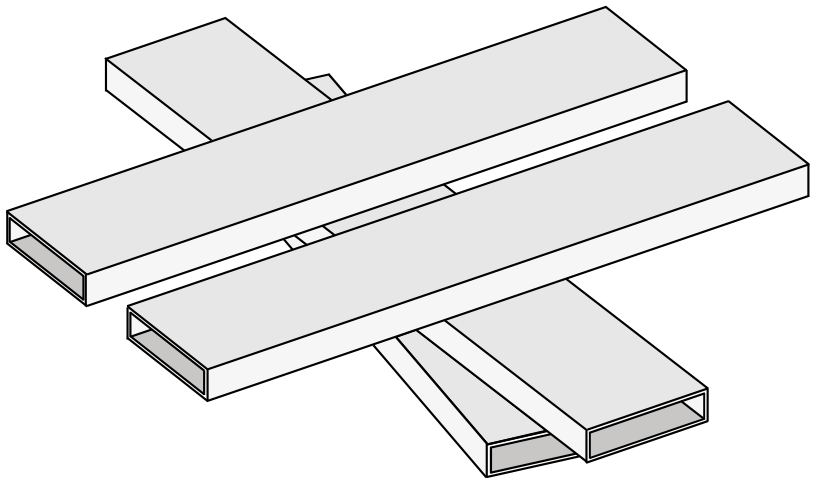

**Figure 3.3:** Waveguide coupling junction with a two layered feeding structure and an arbitrary number of branch waveguides on top.

where $S$ is the scattering matrix for the multiple branch waveguide junction.

## 3.2 Multiple Branch Waveguide Junction with Two Layered Feeding Structure

In this section a waveguide junction consisting of a two layered feeding structure is examined, and a method for calculating the scattering parameters is presented. The geometry is shown in Fig. 3.3, and is identical to the one discussed in the previous section, but with an additional waveguide below the bottom one and connected to this through a compound slot. This new, bottom waveguide can have an arbitrary tilt relative to the middle feed waveguide.

The derivation of the scattering parameters will proceed in a way completely analogous to that in Sec. 3.1, the only difference being the number of integral equations involved.

Fig. 3.4 shows a cross section of the coupling junction. The region inside the bottom feed waveguide is denoted as $w_F$, the upper feed waveguide (middle layer) is region $w_0$, and the branch waveguides are denoted $w_1$, $w_2$ up to $w_N$. Similarly, the slot cavities are denoted as $c_0$, $c_1$, ..., $c_N$.

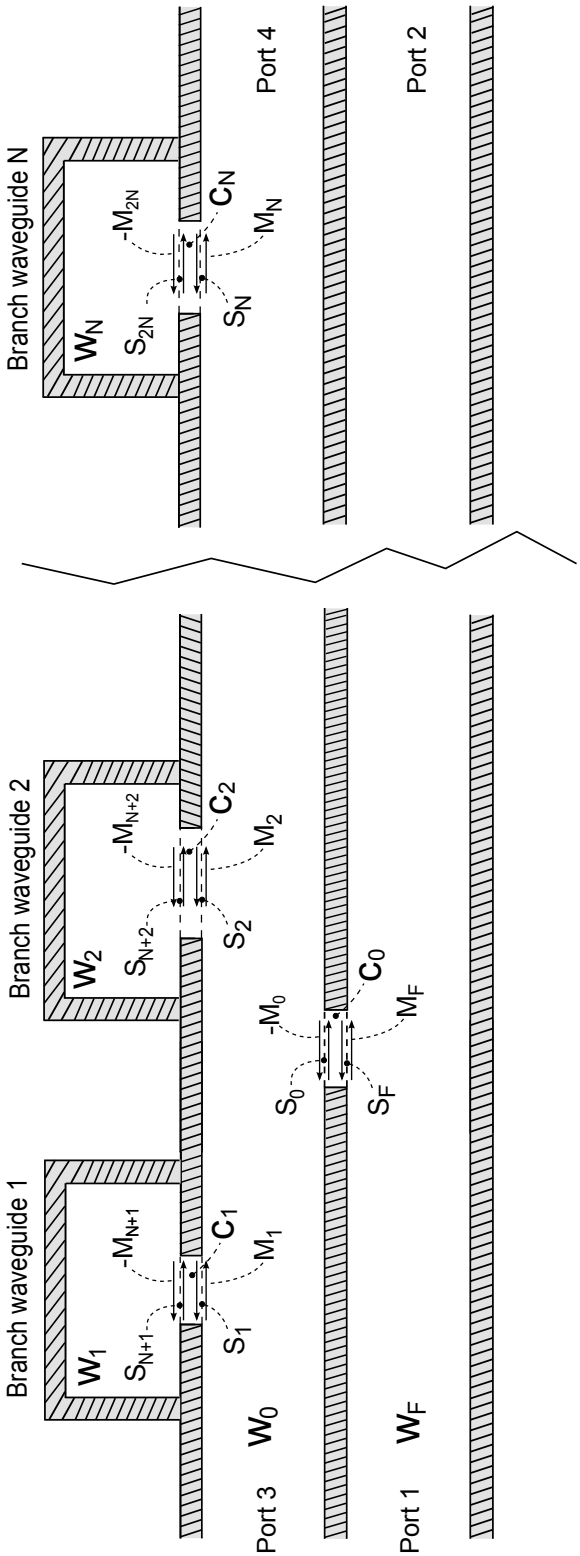


**Figure 3.4:** Cross section of the coupling junction with a two layered feeding structure.

For each surface, an integral equation is obtained by requiring that the magnetic field is continuous across that surface, specifically the following $2N+2$ equations are obtained

$$\begin{aligned}
|\vec{H}^1_{\text{in}}\rangle + \overleftrightarrow{G}_F|\vec{M}_F\rangle &= -\overleftrightarrow{G}_{c_0}|\vec{M}_F\rangle + \overleftrightarrow{G}_{c_0}|\vec{M}_0\rangle, \qquad \vec{r}\in S_F. \\
-\overleftrightarrow{G}_{c_0}|\vec{M}_F\rangle + \overleftrightarrow{G}_{c_0}|\vec{M}_0\rangle &= |\vec{H}^2_{\text{in}}\rangle - \overleftrightarrow{G}_{w_0}|\vec{M}_0\rangle + \sum_{k=1}^{N}\overleftrightarrow{G}_{w_0}|\vec{M}_j\rangle, \qquad \vec{r}\in S_0 \\
|\vec{H}^2_{\text{in}}\rangle + \sum_{k=1}^{N}\overleftrightarrow{G}_{w_0}|\vec{M}_j\rangle &= -\overleftrightarrow{G}_{c_q}|\vec{M}_q\rangle + \overleftrightarrow{G}_{c_q}|\vec{M}_{N+q}\rangle, \qquad \vec{r}\in S_q,\ q=1,2,...,N. \\
-\overleftrightarrow{G}_{c_q}|\vec{M}_q\rangle + \overleftrightarrow{G}_{c_q}|\vec{M}_{N+q}\rangle &= |\vec{H}^3_{\text{in}}\rangle - \overleftrightarrow{G}_{w_{N+q}}|\vec{M}_{N+q}\rangle, \qquad \vec{r}\in S_{N+q},\ q=1,2,...,N.
\end{aligned} \tag{3.16}$$

The first equation describes continuity across the bottom surface $S_F$, the second one describes continuity across $S_0$, and so on.

The magnetic currents $\vec{M}_k$ are expanded according to $\vec{M}_k = \sum_{j=1}^{Q} V_{kj}\vec{m}_{kj}$. The inner product is then taken between the integral equation representing continuity across surface $S_k$ and all basis functions $\vec{m}_{ki},\ i=1,2,...,Q$. The system of integral equations (3.16) then becomes the matrix equation

$$YV = I. \tag{3.17}$$

In the above equation, $V$ is the vector of expansion coefficients, given by

$$V = \begin{bmatrix} V_{Fi} & V_{0i} & V_{1i} & \cdots & V_{2N,i} \end{bmatrix}^T, \tag{3.18}$$

Furthermore, $I$ is the excitation matrix whose columns are given by

$$I_1 = \begin{bmatrix} \langle\vec{m}_{Fj}|\vec{H}^+_{10}\rangle & 0 & \cdots & 0 \end{bmatrix}^T, \tag{3.19}$$

$$I_2 = \begin{bmatrix} \langle\vec{m}_{Fj}|\vec{H}^-_{10}\rangle & 0 & \cdots & 0 \end{bmatrix}^T. \tag{3.20}$$

Each element in the above vectors are actually themselves vectors of length $Q$. When the

junction is excited from port 3 or 4, the corresponding columns of $I$ are

$$I_3 = \left[ \begin{array}{ccccccc} 0 & -\langle \vec{m}_{0j} | \vec{H}_{10}^{+} \rangle & \langle \vec{m}_{1j} | \vec{H}_{10}^{+} \rangle & \cdots & \langle \vec{m}_{Nj} | \vec{H}_{10}^{+} \rangle & 0 & \cdots & 0 \end{array} \right]^T, \tag{3.21}$$

$$I_4 = \left[ \begin{array}{ccccccc} 0 & -\langle \vec{m}_{0j} | \vec{H}_{10}^{-} \rangle & \langle \vec{m}_{1j} | \vec{H}_{10}^{-} \rangle & \cdots & \langle \vec{m}_{Nj} | \vec{H}_{10}^{-} \rangle & 0 & \cdots & 0 \end{array} \right]^T. \tag{3.22}$$

Finally, when the junction is excited from port $2n+3$ or $2n+4$ (these are the two ports in branch waveguide number $n$), the corresponding columns of $I$ are

$$I_{2n+3} = \left[ \begin{array}{ccccccc} 0 & \cdots & 0 & -\langle \vec{m}_{N+n,j} | \vec{H}_{10}^{+} \rangle & 0 & \cdots & 0 \end{array} \right]^T, \tag{3.23}$$

$$I_{2n+4} = \left[ \begin{array}{ccccccc} 0 & \cdots & 0 & -\langle \vec{m}_{N+n,j} | \vec{H}_{10}^{-} \rangle & 0 & \cdots & 0 \end{array} \right]^T. \tag{3.24}$$

Finally, the matrix $Y$ in (3.17) is given by

$$Y = \left[ \begin{array}{cccc} Y_F & Y_{F0} & 0 & 0 \\ (Y_{F0})^T & Y_0 & Y_{0m} & 0 \\ 0 & (Y_{0m})^T & Y_{11} & Y_{12} \\ 0 & 0 & (Y_{12})^T & Y_{22} \end{array} \right], \tag{3.25}$$

where each element is a submatrix, given by

$$Y_F = y_{w_F ij}^{FF} + y_{c_0 ij}^{FF}, \tag{3.26a}$$

$$Y_{F0} = -y_{c_0 ij}^{F0}, \tag{3.26b}$$

$$Y_0 = y_{w_0 ij}^{00} + y_{c_0 ij}^{00}, \tag{3.26c}$$

$$Y_{0m} = \left[ \begin{array}{cccc} -y_{w_0 ij}^{01} & -y_{w_0 ij}^{02} & \cdots & -y_{w_0 ij}^{0N} \end{array} \right], \tag{3.26d}$$

and the matrices $Y_{11}$, $Y_{12}$ and $Y_{22}$ are given by the expressions (3.10), (3.11) and (3.13). Recall that the quantities $y_{Xij}^{mn}$ are admittance matrices of size $Q \times Q$, and given by (3.14).

The mutual admittance between slots in the upper and lower wall of the waveguide is derived in appendix E.

Once the expansion coefficients $V$ have been solved for, the scattering parameters are

calculated from

$$S = \frac{1}{2} V^T I. \tag{3.27}$$

## 3.3 Choice of slot basis functions

The last step in the MoM treatment of the waveguide coupling junctions is to decide what particular set of basis functions to use in the expansion of the magnetic current, since this will determine the form of the admittances and mode couplings that occur in the expressions for the scattering parameters derived above.

Previous analyses of similar problems have assumed that the magnetic current is directed longitudinally along the slot with no variation transversely across the slot. This assumption is good for moderately and strongly excited slot, but fails to accurately model weakly excited slots. Since the purpose of this thesis is to develop a MoM technique for waveguide coupling junctions that is valid even for very weakly excited slots, these transverse effects of the magnetic current must be included in our choice of basis functions.

The magnetic current is directly related to the electric field in the apertures through the relation

$$\vec{M} = \vec{E} \times \hat{n}, \tag{3.28}$$

which means that an expansion of the magnetic current is directly related to a corresponding expansion of the electric field in the aperture, and perhaps the most natural expansion of the electric field is that in terms of TE and TM modes that exist inside the slot cavity. From the expressions for these modes in section B.1 and B.2 it is concluded that a very natural expansion for the magnetic current is $\vec{M}^l(\vec{r}) = \sum_{m,n} a_{mn} \sin\left[\frac{m\pi}{l}\left(s + \frac{l}{2}\right)\right] \cos\left[\frac{n\pi}{w}\left(t + \frac{w}{2}\right)\right] \hat{s}$ for the longitudinal magnetic current, and $\vec{M}^t(\vec{r}) = \sum_{m,n} b_{mn} \cos\left[\frac{m\pi}{l}\left(s + \frac{l}{2}\right)\right] \sin\left[\frac{n\pi}{w}\left(t + \frac{w}{2}\right)\right] \hat{t}$ for the transverse magnetic current. The vectors $\hat{s}$ and $\hat{t}$ are unit vectors directed longitudinally and transversely across the slot, respectively, and $s$ and $t$ are the corresponding coordinates. The center of the $(s, t)$ coordinate system is in the center of the slot aperture.

However, we will not use these expansions, but rather employ a more symmetric expansion that simplifies the calculation of admittances and mode couplings. Specifically we expand

the magnetic currents according to

$$\vec{M}^l(\vec{r}) = \sum_{p,q} a^l_{pq}\vec{m}^l_{pq}(\vec{r}), \qquad \vec{M}^t(\vec{r}) = \sum_{p,q} a^t_{pq}\vec{m}^t_{pq}(\vec{r}) \tag{3.29}$$

where

$$\begin{aligned}\vec{m}^l_{pq}(\vec{r}) &= \sin\left[\frac{p\pi}{l}\left(s+\frac{l}{2}\right)\right]\cos\left[\frac{q\pi}{w}\left(t+\frac{w}{2}\right)\right]\hat{s}, \\ \vec{m}^t_{pq}(\vec{r}) &= \cos\left[\frac{q\pi}{l}\left(\frac{l}{2}-s\right)\right]\sin\left[\frac{p\pi}{w}\left(t+\frac{w}{2}\right)\right]\hat{t}.\end{aligned} \tag{3.30}$$

Note that the transverse basis functions are identical to the longitudinal basis functions of a slot that is tilted an additional 90° and whose length is the original slot's width, and whose width is the original slot's length. Because of this, all expressions for admittances and coupling to waveguide modes that are valid for the longitudinal components can be immediately reused for the transverse components as well. We only have to do these calculations once (see appendix E).

This set of basis functions is used for both the lower and upper aperture in a given slot. For aperture $k$, the expansions in the previous two sections were written more compactly as

$$\vec{M}_k = \sum_{j=1}^{Q} V_{kj}\vec{m}_{kj}, \tag{3.31}$$

where it was assumed that the sum over $j$ include both the transverse and longitudinal polarization of the magnetic current, and for each of these all relevant combinations of the indices $p$ and $q$ for the longitudinal and transverse variations, for a total of $Q$ basis functions for each aperture. In other words we have assumed that for a given $k$ the $\{\vec{m}_{kj}\}_{j=1}^{Q}$ corresponds to some predetermined listing of all basis functions for aperture $k$.

# Chapter 4

# Numerical Results

This chapter presents and discusses the numerical results obtained through using MATLAB to apply the MoM procedures as detailed in Chapter 3 to a variety of waveguide configurations. First, in Secs. 4.1 and 4.2, results for the waveguide junction with a single feeding layer are presented for cases with one and two branch waveguides, respectively, followed by a configuration for the two layered feeding structure in Sec. 4.3.

In this chapter, when discussing the number of basis functions used in a given calculation, it will be written on the form $N = N_p^l \times N_q^l + N_p^t \times N_q^t$. This means that the longitudinal magnetic current has been expanded as

$$\vec{M}^l(\vec{r}) = \sum_{p=1}^{N_p^l} \sum_{q=0}^{N_q^l - 1} a_{pq}^l \vec{m}_{pq}^l(\vec{r}), \tag{4.1}$$

and the transverse magnetic current has been expanded as

$$\vec{M}^t(\vec{r}) = \sum_{p=1}^{N_p^t} \sum_{q=0}^{N_q^t - 1} a_{pq}^t \vec{m}_{pq}^t(\vec{r}). \tag{4.2}$$

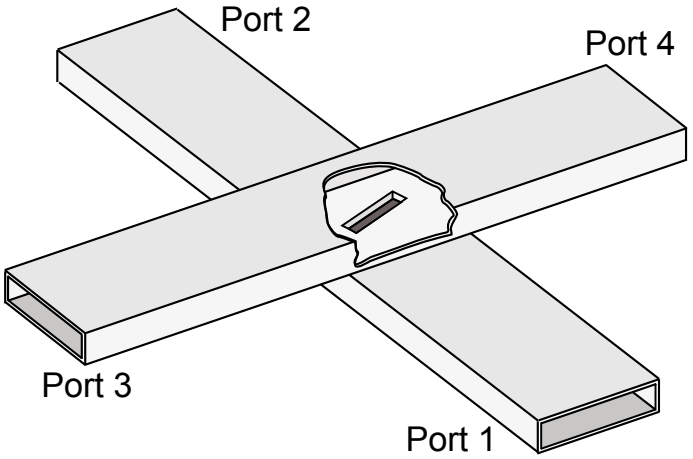


**Figure 4.1:** Two-waveguide coupling junction.

## 4.1 Two-waveguide Coupling Junction

Two different types of junctions with only two waveguides (one feed waveguide and one branch waveguide, cf. Fig 4.1) coupled through a slot were analyzed using the procedure outlined in Sec. 3.1. The difference between the two cases concerned the slot dimension and its tilt angle. In the first case, to be presented in Sec. 4.1.1, the slot was narrow, centered and longitudinal, i.e. straddling the center line of the feed waveguide with no tilt relative to the feed waveguide axis. The second case consists of a centered but tilted very wide slot (its width is on the same order of magnitude as its length), to be presented in Sec. 4.1.2.

### 4.1.1 Centered and longitudinal slot

The reason this case is included is because previous moment method analyses of slot coupled waveguides (with the exception of Cynthia, [14]) have assumed that the magnetic currents on the apertures only have a longitudinal component, and that this component has no transverse variation across the slot. In particular, this means that for a centered, longitudinal slot, the coupling $\langle \vec{m}_{1j} | \vec{H}_{\text{in}} \rangle$ between the basis functions and the incident mode is zero, and hence the RHS (3.6) of the matrix equation vanishes. This means that the magnetic current vanishes, and hence the only non-zero scattering parameter is $S_{21}$, which will be equal to unity. In other words, a longitudinal and centered slot leads to absolutely

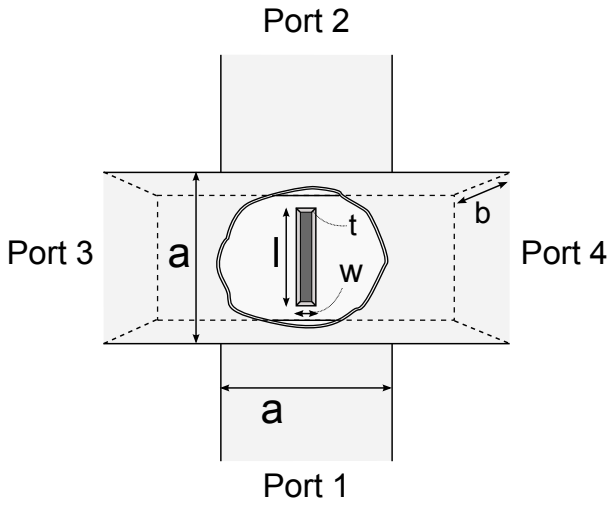


| Dimension | Value |
|---|---|
| f | Varies |
| a | 47.55 mm |
| b | 23.775 mm |
| w | Varies |
| l | 23.775 mm |
| t | 1.18875 mm |

**Table 4.1:** Dimensions of the centered, longitudinal slot and waveguide junction for which the $S_{11}$ parameter is calculated for 30 different cases and compared to Cynthia's results.

no coupling between the waveguides if these assumptions are made; it is as if the slot did not exist at all.

In [14], the $S_{11}$ parameter was listed for different slot dimensions and frequencies for this geometry. To validate the method presented in this thesis, utilizing entire domain trigonometric basis functions, comparisons were made with Cynthia's results in [14]. As we will see, the agreement is very good.

### Scattering parameters

In order to compare the results generated by the method presented in this thesis to those of Cynthia [14], the $S_{11}$ parameter of the two-waveguide junction was calculated at ten different frequencies for three different slot dimensions, for a total of 30 cases. The dimensions are shown in Table 4.1.

All 30 calculated values for $S_{11}$ are shown in Fig. 4.2, together with the corresponding values as calculated by Cynthia. The agreement is very good.

When evaluating the S-parameters, both the longitudinal and transverse currents were expanded into $10 \times 10$ basis functions, for a total of $10 \times 10 + 10 \times 10$ basis functions. In the mode summations (corresponding to the eigenfunction expansions of the Green's

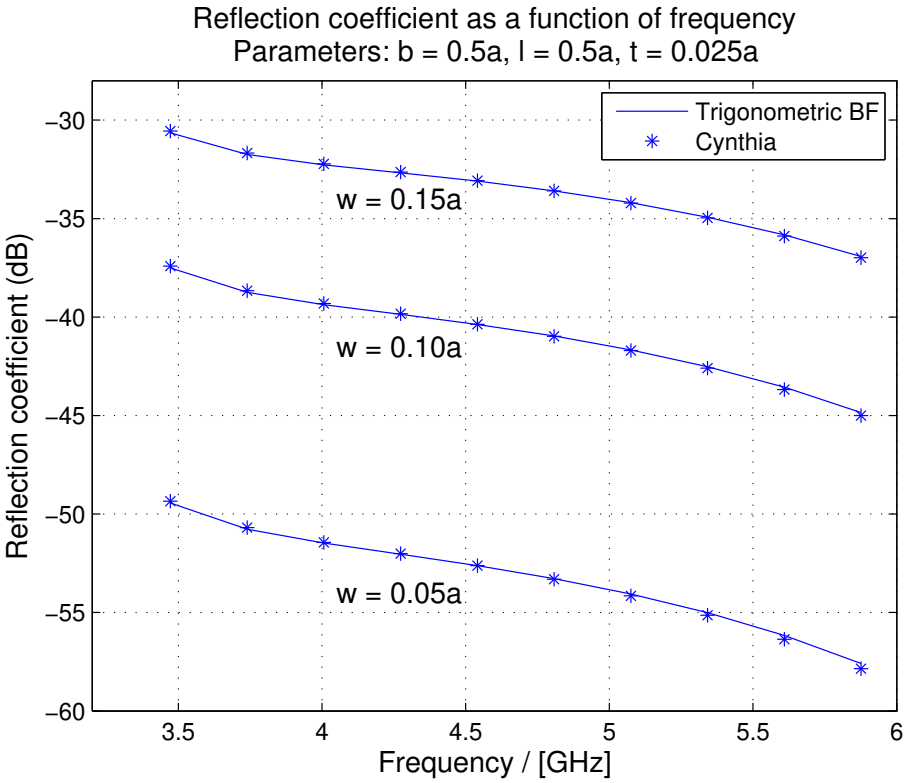


**Figure 4.2:** $S_{11}$ for a centered, longitudinal slot for different frequencies and slot widths, as calculated by Cynthia and as calculated by the trigonometric basis function approach developed in this thesis.

functions), 80,000 waveguide modes in the $y$-direction and 20 waveguide modes in the $z$-direction were included. The calculated S-parameters changed very little ($< 1\%$) when the number of modes or basis functions was increased by 50%, so the convergence seemed good.

Cynthia's scattering parameters were evaluated using a moment method solution employing polynomial basis functions rather than the trigonometric ones described here, and it is thus a very good sign that both MoM approaches yield almost identical results.

### Electric fields in the apertures

The tangential electric field in the aperture was calculated for one particular centered and longitudinal slot, using the relation $\vec{E}_t = \hat{n} \times \vec{M}$. The frequency of operation, as well as

**Table 4.2:** Dimensions of the centered, longitudinal slot and waveguide junction for which $S_{11}$ and the aperture electric field was calculated.

| Quantity | Value |
|---|---|
| f | 9 GHz |
| a | 22.86 mm |
| b | 10.16 mm |
| w | 1.5875 mm |
| l | 15.39494 mm |
| t | 0 mm |

**Table 4.3:** Test for convergence for the slot with parameters listed in Table 4.2. The calculated S-parameters differ by less than one percent, and thus exhibit good convergence.

| Number of basis functions | Modes in $y$-direction | Modes in $z$-direction | $S_{11}$ |
|---|---|---|---|
| $10 \times 10 + 10 \times 10$ | 80 000 | 20 | 0.006188 |
| $10 \times 10 + 10 \times 10$ | 160 000 | 20 | 0.006163 |
| $15 \times 15 + 15 \times 15$ | 100 000 | 20 | 0.006224 |

all relevant geometrical dimensions, are shown in Table 4.2.

Figs. 4.4, 4.5a and 4.5b show the variation of the longitudinal and transverse components of the electric field on the lower aperture surface. The transverse component of the field is negligible at the center line $t = w/2$, so it is not shown. All amplitudes are normalized to the amplitude of the incident field at the center of the feed waveguide. This same behaviour of the fields was reported in [14].

Convergence of the results is something that must be considered. Table 4.3 shows two different runs, with different number of modes included in the mode summation, and a different number of basis functions. The two runs differ by less than 1%, and both of these are in excellent agreement with the value $S_{11} = 0.0062$ published in [14]. Fig. 4.3 shows the calculated $S_{11}$ parameter as a function of the number of $y$-directed modes included, for four different choices of basis functions, and it can be seen that the program seems to converge for around $100,000$ modes and about 10x10+10x10 basis futions.

The $S_{11}$ parameter for this configuration was also calculated by the commercial computational FEKO software, yielding an $S_{11}$ of 0.00654.

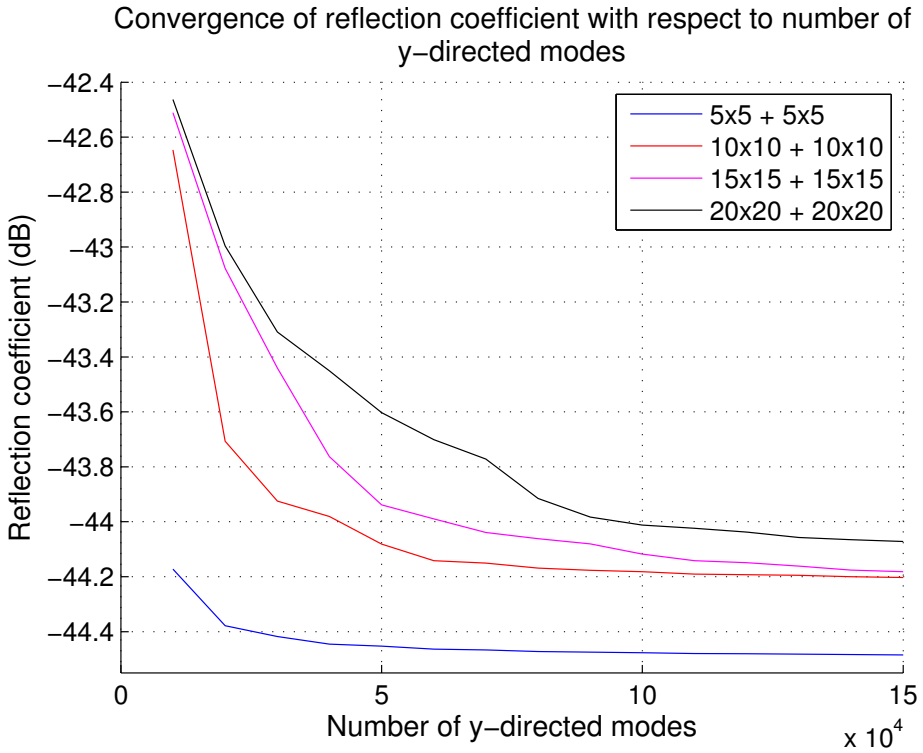


**Figure 4.3:** Convergence of $S_{11}$ parameter with respect to number of basis functions used and number of $y$-directed waveguide modes included in the calculation.

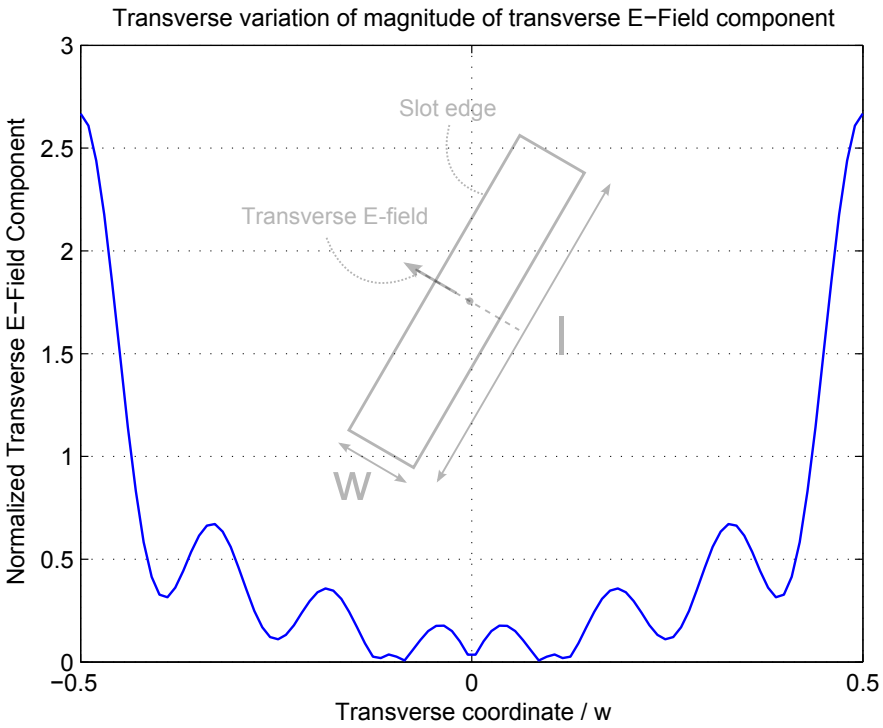


**Figure 4.4:** The transverse variation of the transverse component of the electric field in the lower aperture, evaluated trasnverse across the longitudinal middle (dotted line) of the slot.

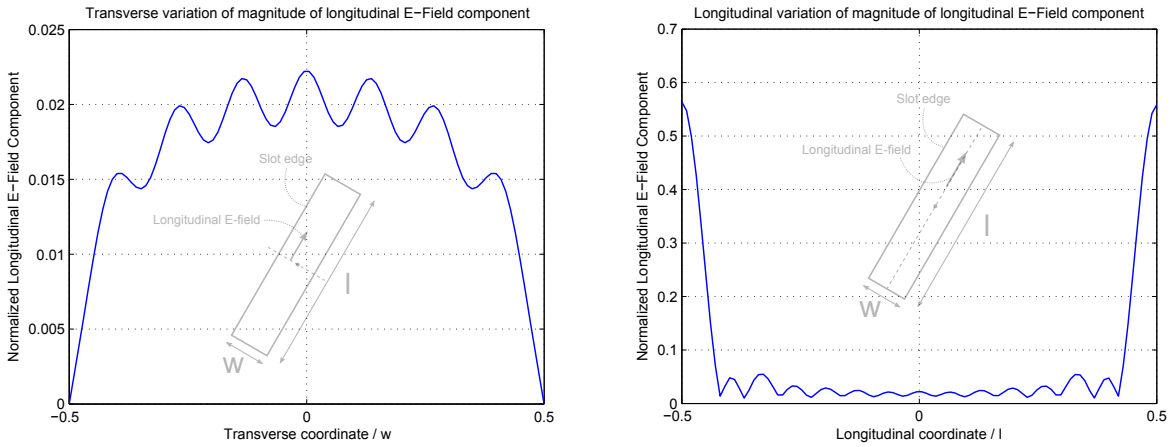


**(a)** **(b)**

**Figure 4.5:** Transverse and longitudinal variation of the longitudinal component of the electric field in the lower aperture. Fig. (a) is evaluated across the longitudinal middle (dotted line) of the slot, and Fig. (b) is evaluated across the transverse middle (dotted line) of the slot.

### 4.1.2 Wide tilted slot

The S-parameters were calculated for the case of a centered, wide slot with different tilt angles between 0° and 90°, in the three following ways

1. using the trigonometric basis functions discussed in this thesis, including both the longitudinal and transverse polarizations;

2. using the trigonometric basis functions, but including only the longitudinal current and neglecting the transverse variation;

3. using the FEKO software.

The reason for choosing this particular geometry is that we are interested in a setup for which the transverse effects of the magnetic current, i.e., transverse polarization and variation, contribute significantly to the coupling between the waveguides. When including only the longitudinal current, the MoM approach described in this thesis reduces to the "old" approach that is known to yield good results for moderately and strongly excited slots (see e.g. [9, 10]). We are thus mainly interested in finding specific setups where the transverse effects play a significant role and can thus be used to validate this extension to the old theory. And intuitively, a very wide slot would seem like a case where the transverse effects would play a significant role. As will be shown below, they do.

The method presented in Sec. 3.1 was used to analyze two waveguides connected through a wide slot for a series of angles ranging from 0° to 90°. These angles were analyzed twice, first including the transverse polarization and variation, and then for only a longitudinal magnetic current that is constant transversely across the slot. FEKO was then used to calculate the S-parameters for the same geometries. The results are shown in Fig. 4.6. All values for the geometrical parameters, as well as the used frequency, are listed in Table 4.7.

Note that the computed values, when including the transverse variation and polarization, agree well with the values given by FEKO, while there is a noticeable difference between the FEKO values and the herein computed values when neglecting the transverse polarization and variation.

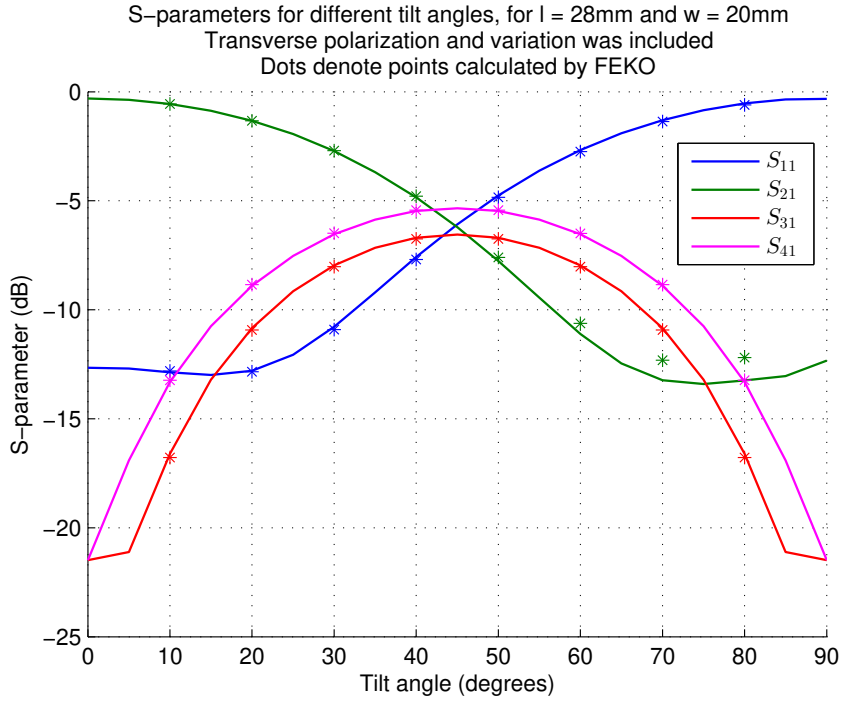


(a)

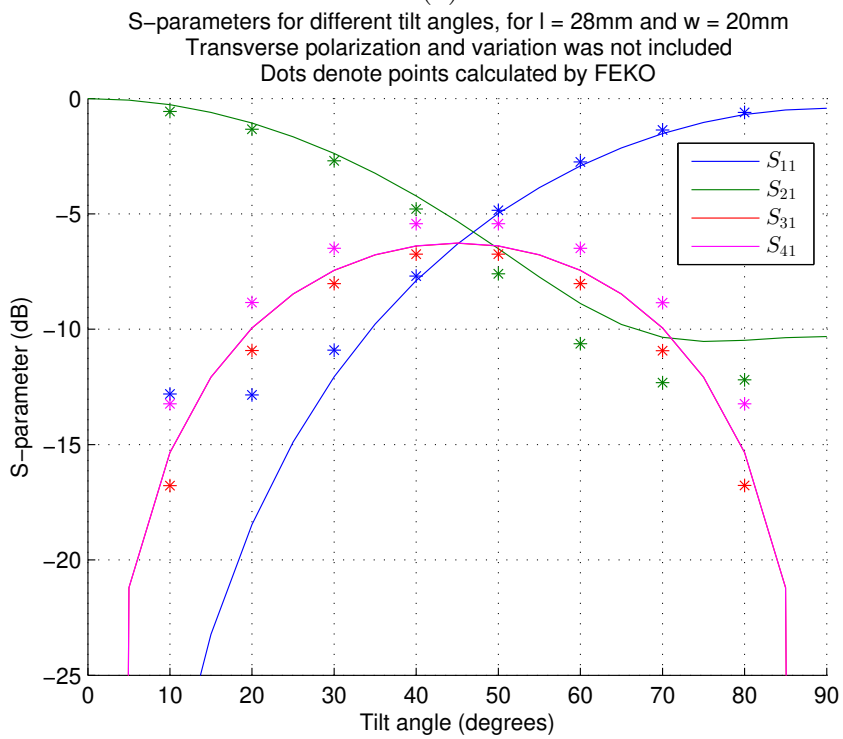


(b)

**Figure 4.6:** The S-parameters in a waveguide junction with a wide slot for different tilt angles as calculated by a MoM approach when the transverse variation and polarization of the magnetic current is (a) accounted for and (b) neglected, together with values that are calculated by the FEKO software for the same geometry.

**Table 4.4:** Frequency and values for geometrical parameters for the wide slot.

| Quantity | Value |
|---|---|
| f | 5 GHz |
| a | 47.55 mm |
| b | 22.15 mm |
| w | 20 mm |
| l | 28 mm |
| t | 1.62 mm |

The moderate disagreement with FEKO for $S_{21}$ at large angles is because these values had not quite converged yet. Attempts to increase the accuracy by including more waveguide modes or basis functions changed the calculated $S_{21}$ values towards the FEKO values, but the number of modes soon became too many for the calculation to be performed in a feasible amount of time. In [9] it was noted that strongly coupled slots required the inclusion of more modes before reaching convergence, and perhaps it is this effect that can be observed here.

Fig. 4.7 shows two plots. In Fig. (a), the convergence properties of $S_{21}$ for the tilt angle $\theta = 20°$ is shown. Note that the S-parameter varies very little when the number of basis functions or the number of $y$-directed waveguide modes are increased. Fig. (b) shows a corresponding plot for the tilt angle $\theta = 80°$, and it is here clear that the S-parameter has not yet reached convergence for 40x40 + 40x40 basis functions when less than 25,000 $y$-directed waveguide modes are included.

## 4.2 Two Branch Waveguide Junction

Two different cases were examined for the waveguide junction consisting of two branch waveguides connected to a single feeding waveguide using the procedure described in Sec. 3.1. In the first case, presented in section 4.2.1 below, one of the slots was oriented completely longitudinally but with an offset, while the other slot was centered and tilted. The second case, presented in Sec. 4.2.2, consists of one centered and longitudinal slot and one slot that is centered and longitudinal, and one that is longitudinal but with a small offset from the center line of the feed waveguide. The general geometry for both cases is shown in fig 4.8.

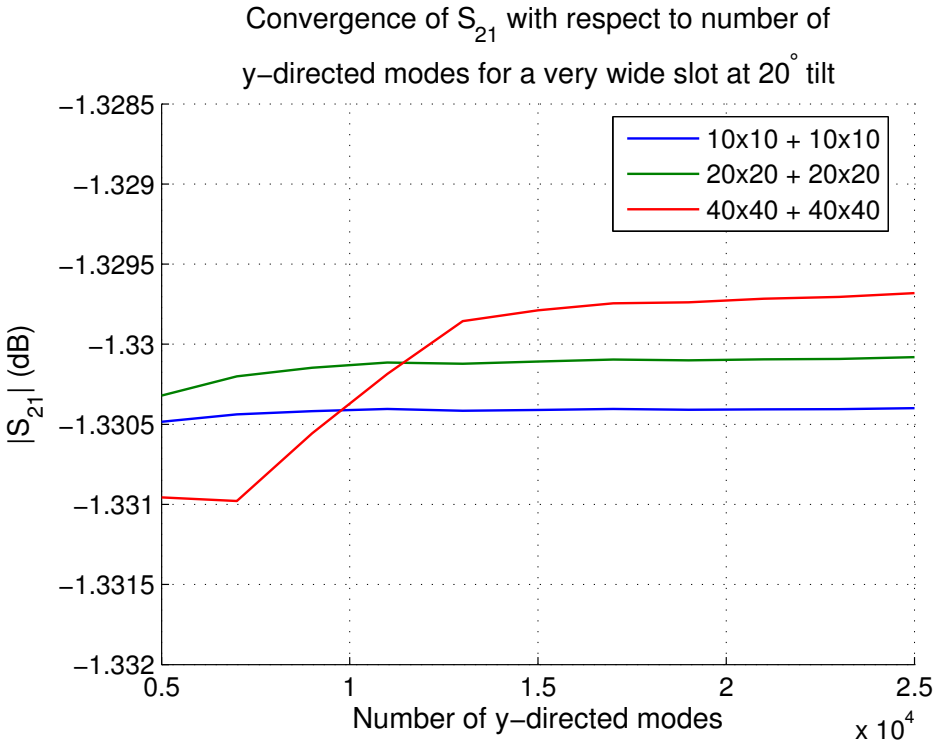


(a)

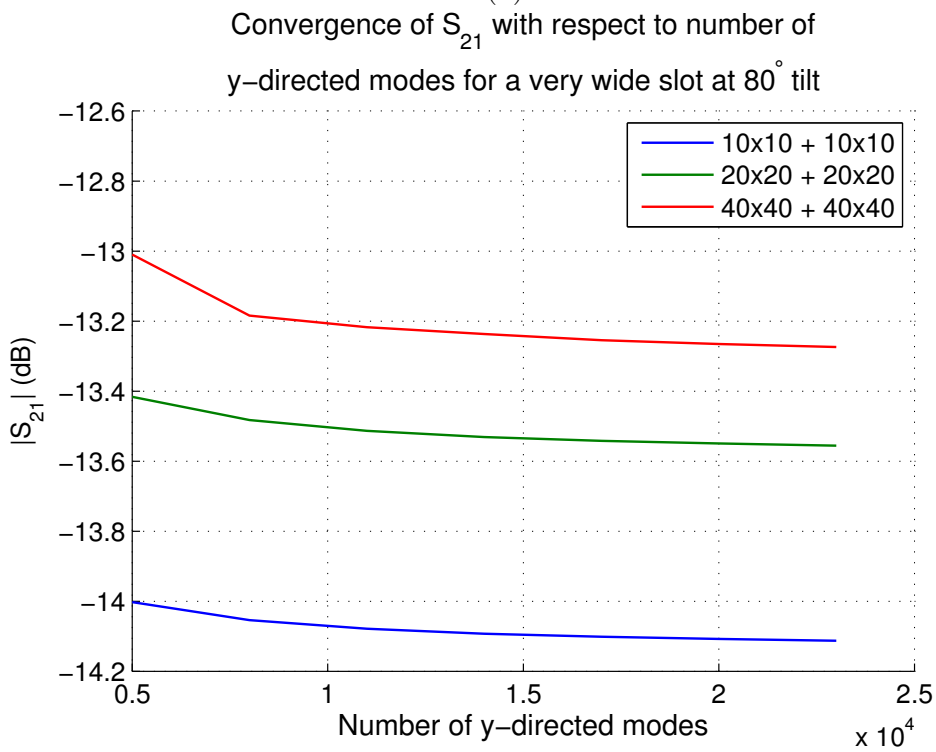


(b)

**Figure 4.7:** The convergence properties for $S_{21}$ for the wide tilted slot. Figure (a) is calculated for a tilt $\theta = 20°$, and figure (b) is for $\theta = 80°$.

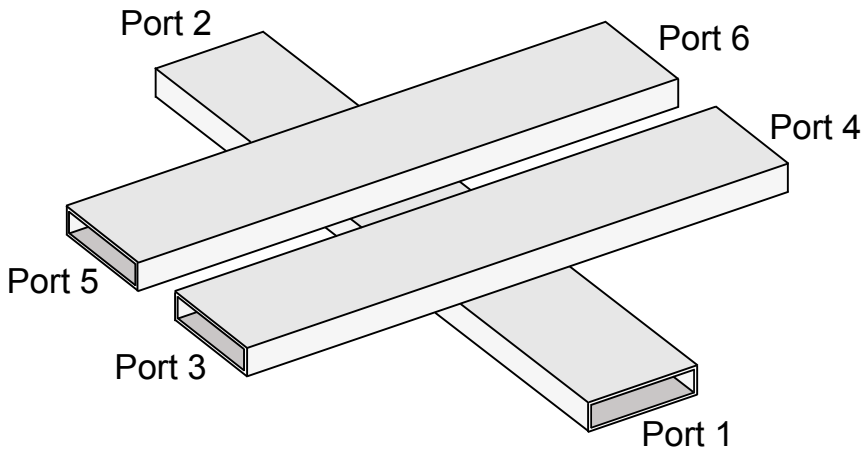


**Figure 4.8:** Waveguide junction consisting of a single feeding waveguide connected to two branch waveguides.

The two slots in the first case are moderately excited, and as will be shown, the transverse polarization and variation play a small but noticeable role. In the second case however, the slots are weakly excited, and the transverse effects must be included to obtain accurate results.

### 4.2.1 Two branch waveguide junction with moderately excited slots

All relevant geometrical parameters are listed in Table 4.5.

The S-parameters in this geometry were computed for 30 linearly spaced frequencies between 5 and 6 GHz, both when the transverse effects of the magnetic current were included and when they were excluded. In addition, FEKO was used to calculate the S-parameters for 11 frequencies in the same interval. The results are shown in Figs. 4.9(a) and 4.9(b).

In Fig. 4.9 (b) (where no transverse effects included), the program has converged for 40 longitudinal basis functions, $30,000$ $y$-directed modes and 20 $z$-directed modes. The difference between the S-parameters calculated by FEKO and by the trigonometric basis function MoM is no larger than around 0.3 dB, except for $S_{11}$, where the difference for frequencies close to 6 GHz is on the order of 0.7 dB.

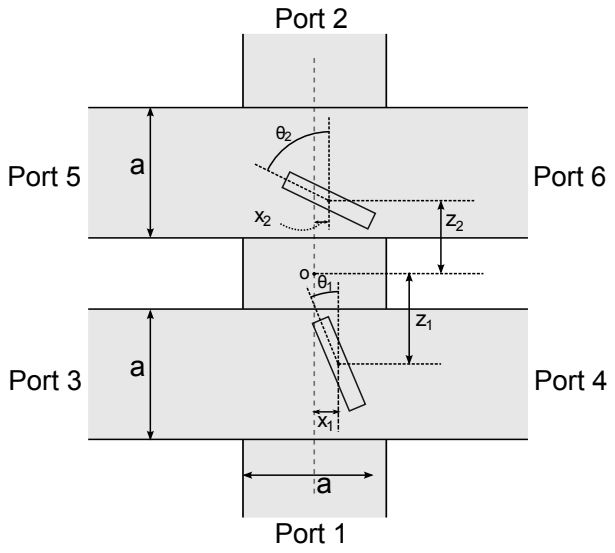


| Dimension | Value |
|---|---|
| a | 38.48 mm |
| b | 10 mm |
| w | 3 mm |
| l | 28 mm |
| t | 1 mm |
| $z_1$ | 3a/4 |
| $z_2$ | 3a/4 |
| $x_1$ | 5 mm |
| $x_2$ | 0 mm |
| $\theta_1$ | 0° |
| $\theta_2$ | 15° |

**Table 4.5:** Geometrical parameters for the two branch waveguide junction with moderately excited slots. $b$ and $t$ are the waveguide height and slot thickness, respectively.

When the transverse polarization and variation are included in the method of moments calculations, the results agree slightly more with FEKO, though the improvement is rather marginal, especially when considering that the run time was around 6 times longer when the transverse effects were included in the calculations. However, both cases were significantly quicker than FEKO (over 100 times faster). When including transverse effects, 20x20 + 20x20 basis functions, 15,000 $y$-directed waveguide modes and 15 $z$-directed ones were sufficient for convergence.

For moderately excited slots, it thus seems that including only longitudinal effects for the magnetic current is sufficient to obtain good results, but if the additional time can be afforded, including the transverse effects will give even more accurate results.

### 4.2.2 Two branch waveguide junction with weakly excited slots

A waveguide junction with two branch waveguides connected to a feeding waveguide through weakly excited slots was also studied. One of the slots was completely centered and oriented longitudinally, while the other slot was longitudinal but offset 0.5 mm from the axis of the feeding waveguide. The geometrical parameters are listed in Table 4.6.

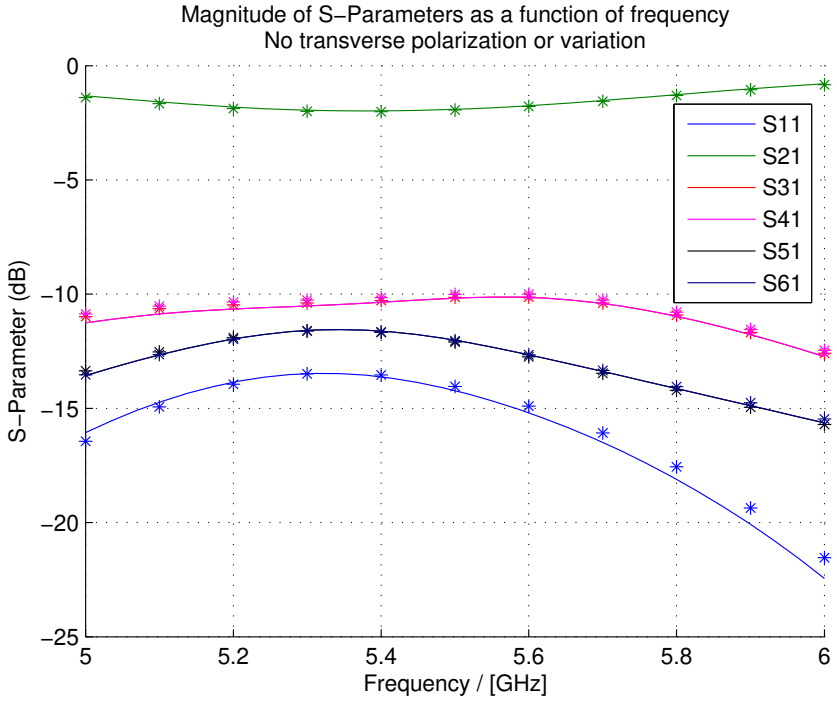


(a)

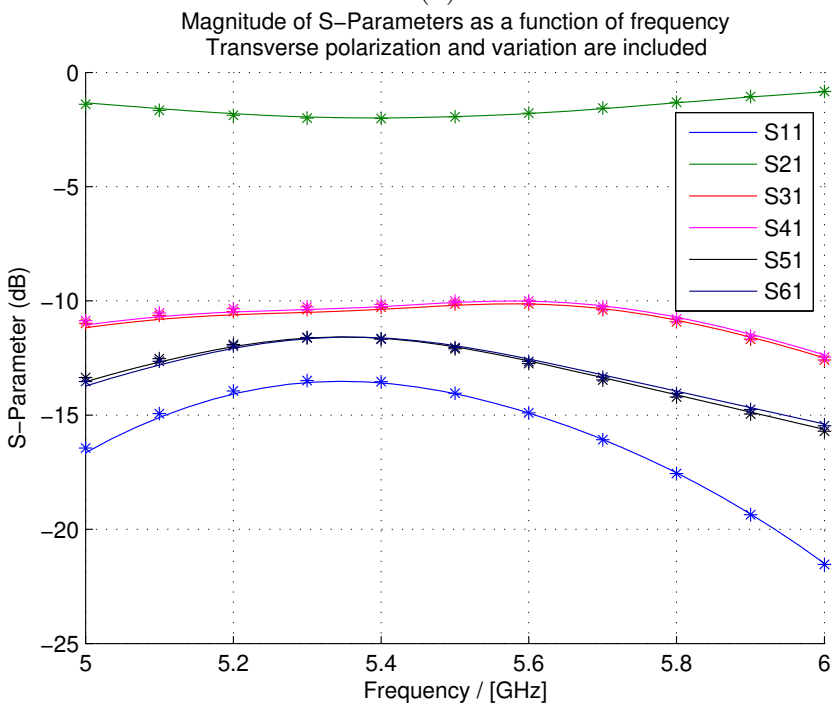


(b)

**Figure 4.9:** S-parameters for different frequencies in the two branch waveguide coupling junction with one offset and one tilted slot, as calculated when transverse effects are included (a) and neglected (b). The dots denote the corresponding points as calculated by FEKO (transverse effects are included in FEKO).

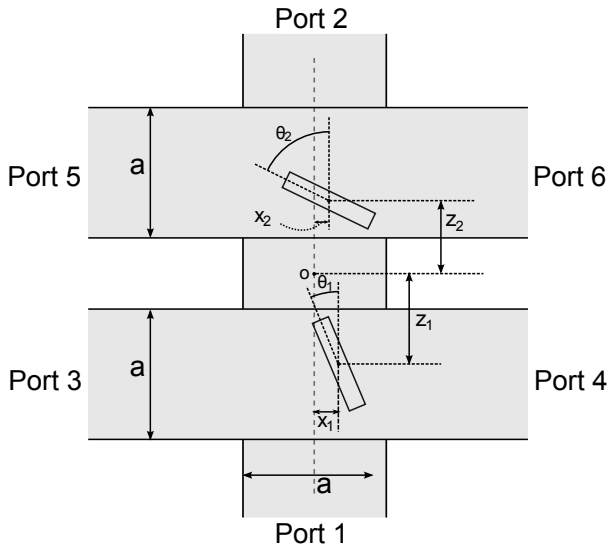


| Quantity | Value |
|---|---|
| a | 38.48 mm |
| b | 10 mm |
| w | 3 mm |
| l | 28 mm |
| t | 1 mm |
| $z_1$ | a/2+3 mm |
| $z_2$ | a/2+3 mm |
| $x_1$ | 0.5 mm |
| $x_2$ | 0 mm |
| $\theta_1$ | 0° |
| $\theta_2$ | 0° |

**Table 4.6:** Geometrical parameters for the two branch waveguide junction with weakly excited slots. $b$ and $t$ are the waveguide height and slot thickness, respectively.

When only the longitudinal effects were included, the method converged at 80 basis functions, $30,000$ $y$-directed waveguide modes and 15 $z$-directed ones. When the transverse effects are included, the program converges for 20x20 + 20x20 basis functions, $30,000$ $y$-directed waveguide modes and 15 $z$-directed ones. The results are shown in Figs 4.10(a) and 4.10(b). The solid lines denote the points as calculated by the trigonometric basis function method described in this thesis, while the dots denote the corresponding points as calculated by the FEKO software.

In this case it is clear that the transverse effects cannot be ignored, as seen in Fig. 4.10 (b).

## 4.3 Two Layered Feeding Structure

The S-parameters of the waveguide junction with two feed waveguides and two branch waveguides shown in Fig. 4.11 were computed using the MoM approach described in 3.2, as well as with FEKO. The results are shown in figure 4.12.

In the MoM program, only longitudinal basis functions with no transverse variation were used. To reach convergence, 160 basis functions were needed, 60,000 $y$-directed waveguide

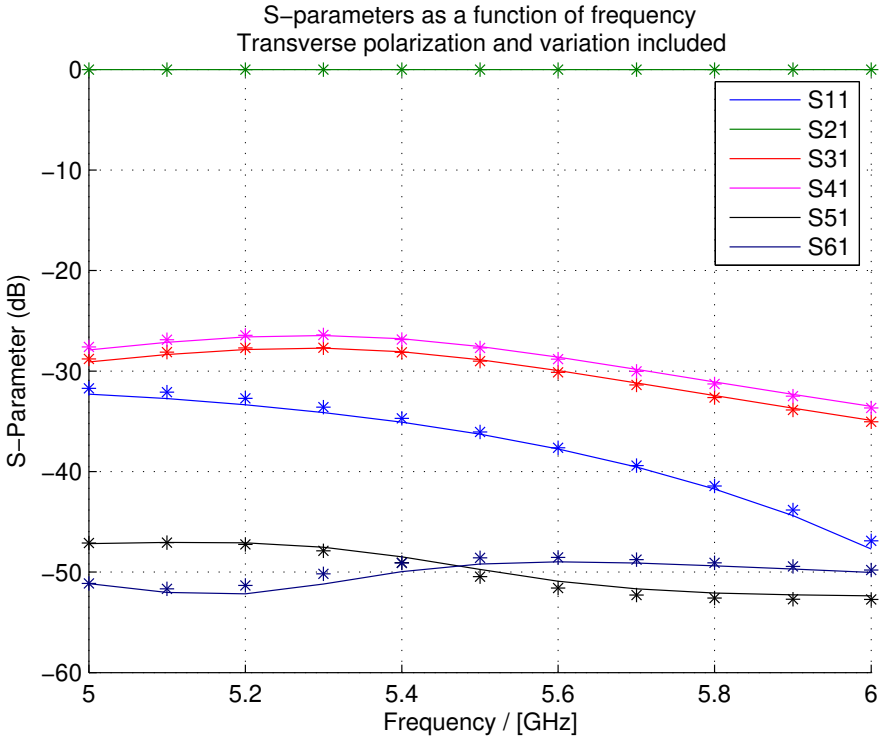


(a)

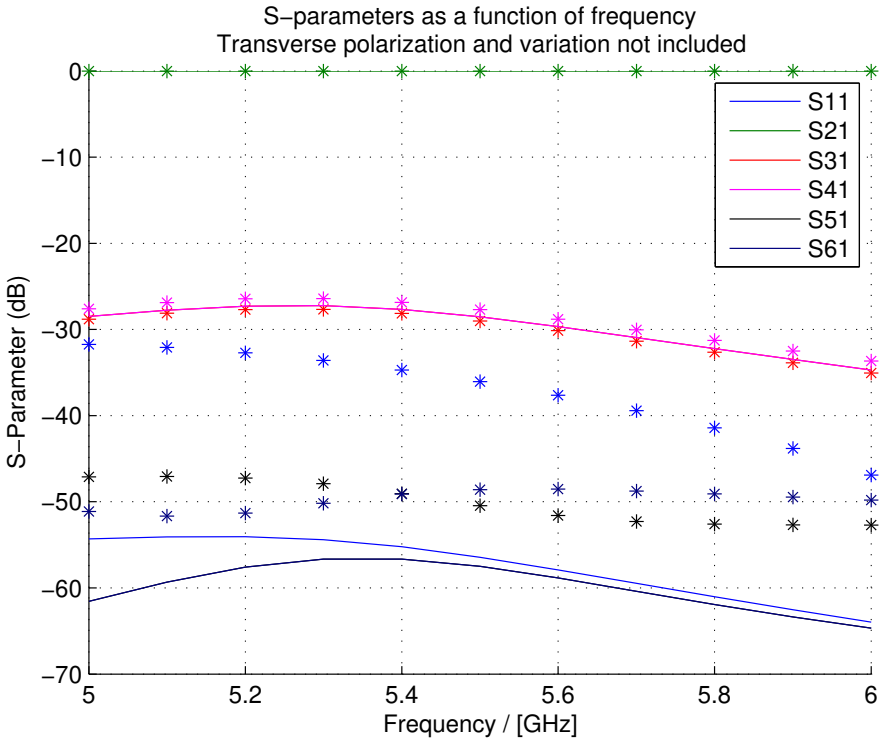


(b)

**Figure 4.10:** S-parameters for different frequencies in the two branch waveguide coupling junction with weakly excited slots, as calculated when the transverse polarization and variation of the magnetic current were included (a) and neglected (b). The dots denote the corresponding points as calculated by FEKO.

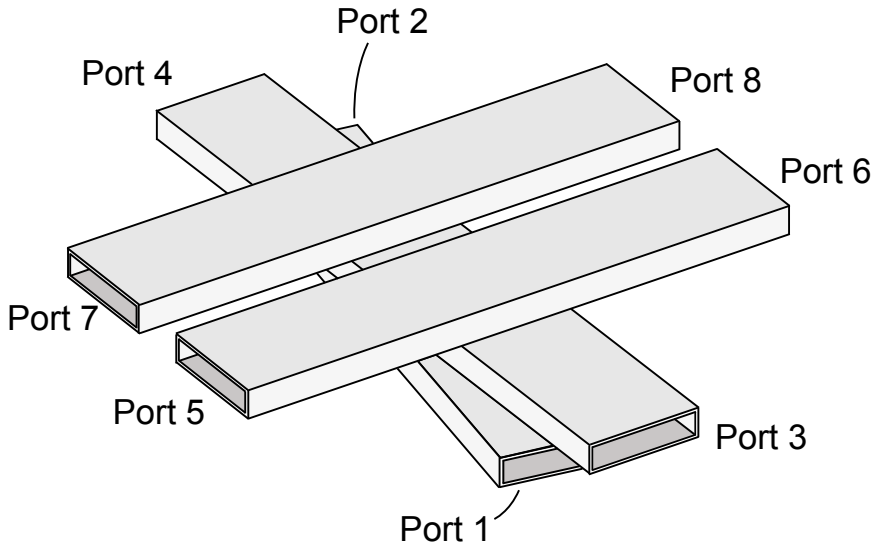


**Figure 4.11:** Waveguide junction with two-layered feeding structure and two branch waveguides.

**Table 4.7:** Frequency and values for geometrical parameters for the waveguide junction with a two layered feeding structure. The parameters for the two upper slots are defined as in the previous section. The slot between the two feeding waveguides is placed such that it is centered in both waveguides, and makes an angle $\theta_F$ with the bottom feeding waveguide, and an angle $\theta_0$ with the middle feeding waveguide.

| Quantity | Value |
|---|---|
| a | 38.78 mm |
| b | 10 mm |
| w | 3 mm |
| l | 28 mm |
| t | 1 mm |
| $x_1$ | 0 mm |
| $x_2$ | 5 mm |
| $z_1$ | 3a/4 |
| $z_2$ | 3a/4 |
| $\theta_F$ | 15° |
| $\theta_0$ | 5° |
| $\theta_1$ | 20° |
| $\theta_2$ | 0° |

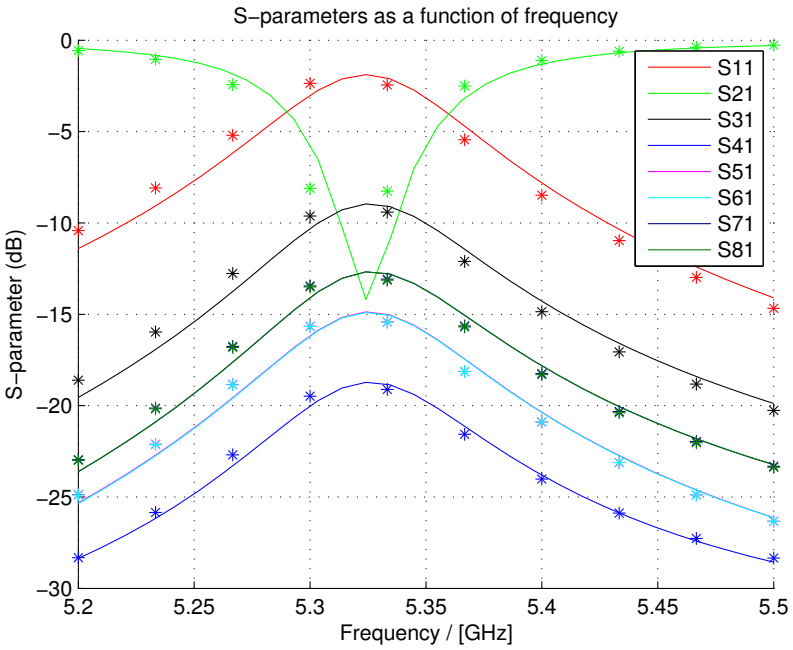


**Figure 4.12:** S-parameters for the waveguide junction with a two-layered feeding structure as computed by the MoM approach described in this thesis, as well as by the FEKO software (dots).

modes and 30 $z$-directed ones. When the transverse polarization and variation were included, good convergence couldn't be achieved, but the general form of the curves was very similar to the ones in Fig. 4.12. Since the slots are moderately excited, no big advantage from including the transverse effects was expected.

FEKO had not converged completely either; when the mesh was refined around the slots, the values changed on the order of several tenths of decibels in the direction of the curve calculated by the MoM approach.

# Chapter 5

# Conclusions

In this work, a method of moments technique was developed that enabled fast and accurate analysis of waveguides coupled through rectangular apertures. By employing a basis function expansion corresponding to the modal expansion of the electric field in the slot cavities, both polarizations of the electric field in the slot apertures, as well as the transverse variation of the fields across the slots, could be accounted for. The finite slot thickness was also included in the analysis.

A MATLAB program was developed to test the theory for specific waveguide configurations, and comparisons were made with the FEKO software and results published previously in the literature. The agreement was good, and the MATLAB program was in all cases significantly faster than the corresponding FEKO computations.

The main disadvantage of the code is that convergence is sometimes an issue. This was seen when examining the wide tilted slot. For small tilt angles the S-parameters converged very quickly, while for large angles good convergence was hard, if not impossible, to achieve. This was also seen for larger structures, such as the waveguide junction with a two layered feeding structure. Convergence was achieved when the transverse polarization of the magnetic current was included, but was, due to memory constraints, not achieved when the transverse component was included. However, it seems that even if convergence is not quite achieved, the computed value still lies in the neighborhood of the actual value.

## 5.1 Future Improvements

The possibility of improvements comes in two different forms: improvements of the theory or of the implementation.

The implementation could be improved by writing the code in a high-performance language, such as C, instead of MATLAB. This would not only make the code faster, but would also require less memory, since an unnecessary amount of data must be stored simultaneously in memory to make use of MATLAB's vectorization features. The parallel nature of the MoM problem could also be taken advantage of. Since all matrix elements can be calculated independently of one another, it might be worthwhile to consider implementing it in a language where one can take advantage of multiple processing cores or the graphics card to accelerate performance.

On the theory side, one might consider using numerically generated basis functions (the characteristic basis function method, CBFM) to decrease computation time for large structures.

# Appendix A

# List of Integrals

This appendix contains a collection of closed form expressions for various integrals encountered when applying the method of moments.

## A.1 Integrals for T-Junction Waveguide

$$
\begin{aligned}
i_{Ink}^{\pm} &= \int_{-w/2}^{w/2} e^{\pm\gamma_{uz} z} \sin\left[\frac{k\pi}{w}\left(z+\frac{w}{2}\right)\right] \mathrm{d}z = \\
&= \frac{\dfrac{k\pi}{w} e^{\mp\gamma_{uz}\dfrac{w}{2}}}{\gamma_u^2 + \dfrac{k^2\pi^2}{w^2}} \left[1 - (-1)^k e^{\pm\gamma_{uz} w}\right]
\end{aligned}
\tag{A.1}
$$

$$
\begin{aligned}
i_{IInk}(a) &= \int_{-w/2}^{w/2} \sin\left[\frac{n\pi}{a}\left(z+\frac{a}{2}\right)\right] \sin\left[\frac{k\pi}{w}\left(z+\frac{w}{2}\right)\right] \mathrm{d}z = \\
&= \frac{\dfrac{k\pi}{w}}{\dfrac{n^2\pi^2}{a^2} - \dfrac{k^2\pi^2}{w^2}} \left\{(-1)^k \sin\left[\frac{n\pi}{2} + \frac{n\pi w}{2a}\right] - \sin\left[\frac{n\pi}{2} - \frac{n\pi w}{2a}\right]\right\}
\end{aligned}
\tag{A.2}
$$

## A.2 Integrals encountered when evaluating y-mode coupling

The two integrals $I^y_{supq\beta}$ and $I^y_{cupq\beta}$ are encountered when evaluating the coupling between the slot basis functions and the $y$-travelling modes in the virtual cavity. These are evaluated below.

### A.2.1 Evaluation of first integral

The integral is given by

$$I^y_{supq\beta} = \int_{s=-l/2}^{l/2}\int_{t=-w/2}^{w/2} \sin\left[\frac{m\pi}{a}\left(x_\beta(s,t)+\frac{a}{2}\right)\right]\cos\left[\frac{n\pi}{c}\left(z_\beta(s,t)+\frac{c}{2}\right)\right]\cdot \sin\left[\frac{p\pi}{l}\left(s+\frac{l}{2}\right)\right]\cos\left[\frac{q\pi}{w}\left(t+\frac{w}{2}\right)\right]\mathrm{d}s\mathrm{d}t. \tag{A.3}$$

To simplify notation, define the following quantities:

$$\alpha = \sin\left[\frac{m\pi}{a}\left(x+\frac{a}{2}\right)\right] \tag{A.4a}$$

$$\beta = \cos\left[\frac{n\pi}{c}\left(z+\frac{c}{2}\right)\right] \tag{A.4b}$$

$$\gamma = \sin\left[\frac{p\pi}{l}\left(s+\frac{l}{2}\right)\right] \tag{A.4c}$$

$$\delta = \cos\left[\frac{q\pi}{w}\left(t+\frac{w}{2}\right)\right] \tag{A.4d}$$

By employing the multiplication formulas for sine and cosine, the integral may be rewritten

as

$$\begin{aligned} I^{y}_{supq\beta} &= \iint_S \frac{1}{2}\left[\sin(\alpha+\beta)+\sin(\alpha-\beta)\right]\frac{1}{2}\left[\sin(\gamma+\delta)+\sin(\gamma-\delta)\right]\mathrm{d}S = \\ &= \frac{1}{4}\iint_S \sin(\alpha+\beta)\sin(\gamma+\delta)\mathrm{d}S + \frac{1}{4}\iint_S \sin(\alpha+\beta)\sin(\gamma-\delta)\mathrm{d}S + \\ &+ \frac{1}{4}\iint_S \sin(\alpha-\beta)\sin(\gamma+\delta)\mathrm{d}S + \frac{1}{4}\iint_S \sin(\alpha-\beta)\sin(\gamma-\delta)\mathrm{d}S. \end{aligned} \tag{A.5}$$

All of the above integrals are of the same general form:

$$I_1 = \iint_S \sin(\alpha+u\beta)\sin(\gamma+v\delta)\mathrm{d}S, \tag{A.6}$$

where the constants $u$ and $v$ are either 1 or -1. Using the product rule for sine, this is in turn written as

$$\begin{aligned} I_1 &= \iint_S \sin(\alpha+u\beta)\sin(\gamma+v\delta)\mathrm{d}S = \\ &= \frac{1}{2}\iint_S \cos(\alpha+u\beta-\gamma-v\delta)\mathrm{d}S - \frac{1}{2}\iint_S \cos(\alpha+u\beta+\gamma+v\delta)\mathrm{d}S \end{aligned} \tag{A.7}$$

By inserting the Eqs. (A.4) and the expressions (E.11) into the above expression, each of the integrals can be evaluated:

$$\begin{aligned} \iint_S \cos(\alpha+u\beta\pm\gamma\pm v\delta)\mathrm{d}S &= \int_{s=-l/2}^{l/2}\int_{t=-w/2}^{w/2}\cos(c_s s + c_t t + c_0)\mathrm{d}s\mathrm{d}t = \\ &= \frac{4\sin\left[c_s\frac{l}{2}\right]\sin\left[c_t\frac{w}{2}\right]\cos\left[c_0\right]}{c_s c_t}, \end{aligned} \tag{A.8}$$

where the coefficients in front of $s$, $t$ and the constant have been labeled $c_s$, $c_t$ and $c_0$, respectively, and are given by

$$c_s = -\frac{m\pi}{a}\sin\theta + u\frac{n\pi}{c}\cos\theta \pm \frac{p\pi}{l}, \tag{A.9}$$

$$c_t = -\frac{m\pi}{a}\cos\theta - u\frac{n\pi}{c}\sin\theta \pm v\frac{q\pi}{w}, \tag{A.10}$$

$$c_0 = \frac{m\pi}{a}x_0 + \frac{m\pi}{2} + u\frac{n\pi}{c}z_0 + u\frac{n\pi}{2} \pm \frac{p\pi}{2} \pm v\frac{q\pi}{2}. \tag{A.11}$$

Every part of the original integral $I^y_{supq\beta}$ have now been evaluated.

### A.2.2 Evaluation of the second integral

In this section we turn towards the evaluation of the second integral

$$I^y_{cupq\beta} = \int_{s=-l/2}^{l/2}\int_{t=-w/2}^{w/2} \cos\left[\frac{m\pi}{a}\left(x_\beta(s,t)+\frac{a}{2}\right)\right]\sin\left[\frac{n\pi}{c}\left(z_\beta(s,t)+\frac{c}{2}\right)\right]\cdot \\ \sin\left[\frac{p\pi}{l}\left(s+\frac{l}{2}\right)\right]\cos\left[\frac{q\pi}{w}\left(t+\frac{w}{2}\right)\right]\mathrm{d}s\mathrm{d}t. \tag{A.12}$$

By using the product formula for sine and cosine, this can be rewritten as

$$\begin{aligned} I^y_{cupq\beta} &= \iint_S \frac{1}{2}\left[\sin(\alpha+\beta)+\sin(\beta-\alpha)\right]\frac{1}{2}\left[\sin(\gamma+\delta)+\sin(\gamma-\delta)\right]\mathrm{d}S = \\ &= \frac{1}{4}\iint_S \sin(\alpha+\beta)\sin(\gamma+\delta)\mathrm{d}S + \frac{1}{4}\iint_S \sin(\alpha+\beta)\sin(\gamma-\delta)\mathrm{d}S + \\ &- \frac{1}{4}\iint_S \sin(\alpha-\beta)\sin(\gamma+\delta)\mathrm{d}S - \frac{1}{4}\iint_S \sin(\alpha-\beta)\sin(\gamma-\delta)\mathrm{d}S. \end{aligned} \tag{A.13}$$

All of the above integrals were encountered and evaluated in the previous section.

## A.3 Integrals encountered when evaluating z-mode coupling

The two integrals $I^z_{supq\beta\pm}$ and $I^z_{cupq\beta\pm}$ are encountered when evaluating the coupling between the slot basis functions and the $z$-travelling modes in the virtual cavity. These are evaluated below.

### A.3.1 Evaluation of first integral

The integral is given by

$$I^z_{supq\beta\pm} = \iint_{S_\beta} \sin\left[\frac{m\pi}{a}\left(x_\beta(s,t)+\frac{a}{2}\right)\right]\sin\left[\frac{p\pi}{l}\left(s+\frac{l}{2}\right)\right]\cos\left[\frac{q\pi}{w}\left(t+\frac{w}{2}\right)\right]e^{\pm\gamma_{uz}z}\mathrm{d}S. \tag{A.14}$$

Using the definitions (A.4) and the sine and cosine product formula, the above is rewritten as

$$\begin{aligned} I^z_{supq\beta\pm} &= \frac{1}{2}\iint_S \sin\alpha\sin(\gamma+\delta)e^{\pm\gamma_u z}\mathrm{d}S + \frac{1}{2}\iint_S \sin\alpha\sin(\gamma-\delta)e^{\pm\gamma_u z}\mathrm{d}S = \\ &= \frac{1}{4}\iint_S \cos(\gamma+\delta-\alpha)e^{\pm\gamma_u z}\mathrm{d}S - \frac{1}{4}\iint_S \cos(\gamma+\delta+\alpha)e^{\pm\gamma_u z}\mathrm{d}S + \\ &+\frac{1}{4}\iint_S \cos(\gamma-\delta-\alpha)e^{\pm\gamma_u z}\mathrm{d}S - \frac{1}{4}\iint_S \cos(\gamma-\delta+\alpha)e^{\pm\gamma_u z}\mathrm{d}S. \end{aligned} \tag{A.15}$$

All of the above integrals are of the form

$$I_2 = \iint_S \cos(\gamma+u\delta+v\alpha)e^{\pm\gamma_u z}\mathrm{d}S, \tag{A.16}$$

where $u$ and $v$ are either 1 or -1. Substutituting back the expressions (A.4), as well as the expressions (E.11), the above integral is rewritten as

$$I_2 = e^{\pm\gamma_u z_0}\int_{s=-l/2}^{l/2}\int_{t=-w/2}^{w/2}\cos\left[c'_s s + c'_t t + c_0\right]e^{\pm\gamma_u s\cos\theta}e^{\mp\gamma_u t\sin\theta}\mathrm{d}s\mathrm{d}t, \tag{A.17}$$

where we have defined

$$c'_s = \frac{p\pi}{l} - v\frac{m\pi}{a}\sin\theta, \tag{A.18}$$

$$c'_t = u\frac{q\pi}{w} - v\frac{m\pi}{a}\cos\theta, \tag{A.19}$$

$$c'_0 = \frac{p\pi}{2} + u\frac{q\pi}{2} + v\frac{m\pi}{2} + v\frac{m\pi}{a}x_0. \tag{A.20}$$

Integrating this yields the result

$$\begin{aligned} I_2 = e^{\pm\gamma_u z_0}\frac{e^{\mp\gamma_u \sin\theta\frac{w}{2}}}{\gamma_u^2\sin^2\theta + c_t'^2}\Bigg[\mp\gamma_u\sin\theta\int_{-l/2}^{l/2} e^{\pm\gamma_u s\cos\theta}\cos(c_s's + c_t'\frac{w}{2} + c_0')\mathrm{d}s + \\ + c_t'\int_{-l/2}^{l/2} e^{\pm\gamma_u s\cos\theta}\sin(c_s's + c_t'\frac{w}{2} + c_0')\mathrm{d}s\Bigg] + \\ - e^{\pm\gamma_u z_0}\frac{e^{\pm\gamma_u \sin\theta\frac{w}{2}}}{\gamma_u^2\sin^2\theta + c_t'^2}\Bigg[\mp\gamma_u\sin\theta\int_{-l/2}^{l/2} e^{\pm\gamma_u s\cos\theta}\cos(c_s's - c_t'\frac{w}{2} + c_0')\mathrm{d}s + \\ + c_t'\int_{-l/2}^{l/2} e^{\pm\gamma_u s\cos\theta}\sin(c_s's - c_t'\frac{w}{2} + c_0')\mathrm{d}s\Bigg], \end{aligned} \tag{A.21}$$

where the two kinds of integrals in this expression are given by

$$\begin{aligned} &\int_{-l/2}^{l/2} e^{\pm\gamma_u s\cos\theta}\cos(c_s's + c_t'A + c_0')\mathrm{d}s = \\ &= \left[\frac{e^{\pm\gamma_u s\cos\theta}}{\gamma_u^2\cos^2\theta + c_s'^2}\left(\pm\gamma_u\cos\theta\cos(c_s's + c_t'A + c_0') + c_s'\sin(c_s's + c_t'A + c_0')\right)\right]_{s=-l/2}^{s=l/2}, \end{aligned} \tag{A.22}$$

and

$$\begin{aligned} &\int_{-l/2}^{l/2} e^{\pm\gamma_u s\cos\theta}\sin(c_s's + c_t'A + c_0')\mathrm{d}s = \\ &= \left[\frac{e^{\pm\gamma_u s\cos\theta}}{\gamma_u^2\cos^2\theta + c_s'^2}\left(\pm\gamma_u\cos\theta\sin(c_s's + c_t'A + c_0') - c_s'\cos(c_s's + c_t'A + c_0')\right)\right]_{s=-l/2}^{s=l/2}, \end{aligned} \tag{A.23}$$

where $A$ is a constant (set to either $w/2$ or $-w/2$ when evaluating Eq. (A.27)). All parts of the expression for $I^z_{supq\beta\pm}$ have now been evaluated.

### A.3.2 Evaluation of the second integral

In this section we turn towards the evaluation of the second integral

$$I^z_{cupq\beta\pm} = \iint_{S_\beta}\cos\left[\frac{m\pi}{a}\left(x_\beta(s,t) + \frac{a}{2}\right)\right]\sin\left[\frac{p\pi}{l}\left(s + \frac{l}{2}\right)\right]\cos\left[\frac{q\pi}{w}\left(t + \frac{w}{2}\right)\right]e^{\pm\gamma_{uz}z}\mathrm{d}S. \tag{A.24}$$

Using the definitions (A.4) and the product rules for sine and cosine, the integral can be

written

$$\begin{aligned} I^z_{cupq\beta\pm} = \frac{1}{4}\iint_S \sin(\gamma+\delta-\alpha)e^{\pm\gamma_u z}\mathrm{d}S + \frac{1}{4}\iint_S \sin(\gamma+\delta+\alpha)e^{\pm\gamma_u z}\mathrm{d}S + \\ + \frac{1}{4}\iint_S \sin(\gamma-\delta-\alpha)e^{\pm\gamma_u z}\mathrm{d}S + \frac{1}{4}\iint_S \sin(\gamma-\delta+\alpha)e^{\pm\gamma_u z}\mathrm{d}S. \end{aligned} \tag{A.25}$$

The above expression consists of integrals of the form

$$I_3 = \iint_S \sin(\gamma + u\delta + v\alpha)e^{\pm\gamma_u z}\mathrm{d}S, \tag{A.26}$$

where $u$ and $v$ are either 1 or -1. Note the similarity to Eq. (A.16). This integral is evaluated in the same way. The result is

$$\begin{aligned} I_3 = e^{\pm\gamma_u z_0}\frac{e^{\mp\gamma_u \sin\theta\frac{w}{2}}}{\gamma_u^2\sin^2\theta + c_t'^2}\Bigg[\mp\gamma_u\sin\theta\int_{-l/2}^{l/2} e^{\pm\gamma_u s\cos\theta}\sin(c_s's + c_t'\frac{w}{2} + c_0')\mathrm{d}s + \\ - c_t'\int_{-l/2}^{l/2} e^{\pm\gamma_u s\cos\theta}\cos(c_s's + c_t'\frac{w}{2} + c_0')\mathrm{d}s\Bigg] + \\ - e^{\pm\gamma_u z_0}\frac{e^{\pm\gamma_u \sin\theta\frac{w}{2}}}{\gamma_u^2\sin^2\theta + c_t'^2}\Bigg[\mp\gamma_u\sin\theta\int_{-l/2}^{l/2} e^{\pm\gamma_u s\cos\theta}\sin(c_s's - c_t'\frac{w}{2} + c_0')\mathrm{d}s + \\ - c_t'\int_{-l/2}^{l/2} e^{\pm\gamma_u s\cos\theta}\cos(c_s's - c_t'\frac{w}{2} + c_0')\mathrm{d}s\Bigg], \end{aligned} \tag{A.27}$$

where the integrals were evaluated in the previous section.

# Appendix B

# Modes in a Rectangular Waveguide

Consider a uniform waveguide with rectangular cross section with its axis parallel to the $z$-axis, as shown in Fig. B.1. Let it be filled with a homogeneous and source-free dielectric with constitutive parameters $\epsilon$ and $\mu$.

In any waveguide of uniform cross section, there will exist a countably infinite set of eigenfunctions, or *modes*, which are fundamental fields into which an arbitrary field in the waveguide can be decomposed. We will in this section derive the modal functions in a rectangular waveguide. This section is not intended to be a thorough introduction to waveguide theory, but rather provides the relevant expressions for the modes, as well as some orthogonality conditions that will be used when deriving Green's functions in the next section. The derivations in this section are based on the ones in [19, pp.xx–yy]. See also [20, pp. 239–246] for similar derivations.

By taking the curl of the time harmonic Faradays's law of induction and Ampere's law, it is observed that in a source free region the $\vec{E}$ and $\vec{H}$ fields satisfy the vector Helmholtz equations:

$$(\nabla^2 + k^2)\vec{E} = 0 \tag{B.1}$$

$$(\nabla^2 + k^2)\vec{H} = 0, \tag{B.2}$$

where $k = \omega\sqrt{\epsilon\mu}$ is the wavenumber of the medium. Since the waveguide is completely uniform along $z$, we further assume a $z$-dependence of $e^{\mp\gamma z}$, where $\gamma$ is called the propaga-

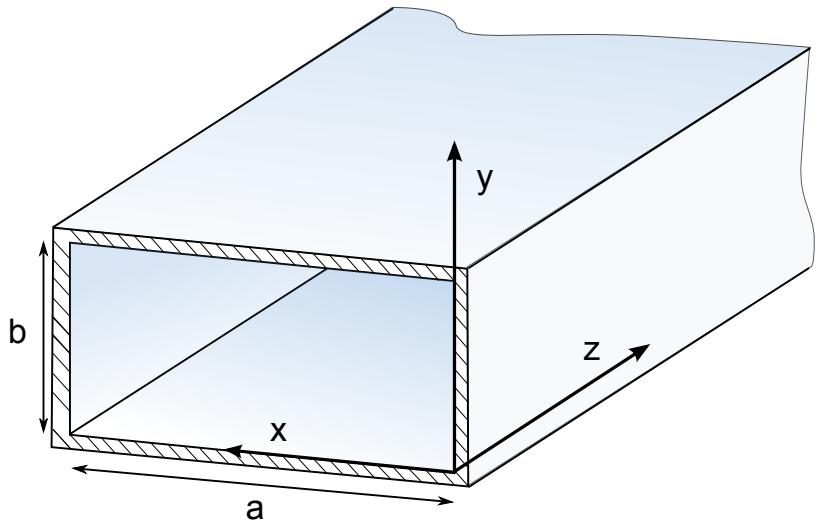


**Figure B.1:** A uniform waveguide with rectangular cross section of dimension $a \times b$. The waveguide may be filled with a dielectric with dielectric constant $\epsilon$.

tion constant of the wave, to be determined. Note that a purely imaginary $\gamma$ corresponds to travelling waves, while a $\gamma$ with a non-zero real component corresponds to exponentially decaying (evanescent) waves. Different $z$-dependencies can be created by a superposition of these waves, and enforcing this can be seen simply as taking the spatial Fourier transform of the fields along $z$. Waves travelling in the positive $z$-direction will have the minus in the exponent, while waves travelling in the negative $z$-direction will have the plus sign.

With this dependence established, the Laplacian takes the form

$$\nabla^2 = \nabla_t^2 + \gamma^2, \tag{B.3}$$

where

$$\nabla_t^2 = \frac{\partial^2}{\partial x^2} + \frac{\partial^2}{\partial y^2} \tag{B.4}$$

is the transverse part of the Laplacian. The Helmholtz equation then takes the form

$$\begin{aligned} \nabla_t^2 \vec{E} + (k^2 + \gamma^2)\vec{E} = 0 \\ \nabla_t^2 \vec{H} + (k^2 + \gamma^2)\vec{H} = 0. \end{aligned} \tag{B.5}$$

Each component of the electric and magnetic fields must satisfy the above Helmholtz

equations, but not all components of $\vec{E}$ and $\vec{H}$ are independent. By expanding the two Maxwell equations $\nabla \times \vec{E} = -j\omega\mu\vec{H}$ and $\nabla \times \vec{H} = j\omega\epsilon\vec{E}$ in Cartesian coordinates and solving for the transverse components of $\vec{E}$ and $\vec{H}$ in terms of the longitudinal components $H_z$ and $E_z$, one obtains the following relations between the components:

$$\begin{aligned} H_x &= -\frac{1}{k_{\text{cu}}^2}\left(\pm\gamma\frac{\partial H_z}{\partial x} - j\omega\epsilon\frac{\partial E_z}{\partial y}\right) \\ H_y &= -\frac{1}{k_{\text{cu}}^2}\left(\pm\gamma\frac{\partial H_z}{\partial y} + j\omega\epsilon\frac{\partial E_z}{\partial x}\right) \\ E_x &= -\frac{1}{k_{\text{cu}}^2}\left(\pm\gamma\frac{\partial E_z}{\partial x} + j\omega\mu\frac{\partial H_z}{\partial y}\right) \\ E_y &= -\frac{1}{k_{\text{cu}}^2}\left(\pm\gamma\frac{\partial E_z}{\partial y} - j\omega\mu\frac{\partial H_z}{\partial x}\right), \end{aligned} \tag{B.6}$$

where we have introduced the cut-off wavenumber $k_{\text{cu}}^2 = \gamma^2 + k^2$, which corresponds to the largest possible wavenumber that is allowed for propagating modes. Modes with wavenumbers larger than this will be evanescent, as will be apparent soon.

Perhaps the most important conclusion from the above equations is that the transverse components of the fields are completely determined by the longitudinal field components; the $z$-component is the only degree of freedom. This means that we only need to concern ourselves with the $z$-components of the vector Helmholtz equations in (B.5), that is,

$$\begin{aligned} \nabla_t^2 E_z + (k^2 + \gamma^2)E_z = 0 \\ \nabla_t^2 H_z + (k^2 + \gamma^2)H_z = 0. \end{aligned} \tag{B.7}$$

The possible field solutions can now be grouped into three distinct categories: (i) Transverse Electric (TE) waves having $E_z = 0, H_z \neq 0$; (ii) Transverse Magnetic (TM) waves satisfying $H_z = 0, E_z \neq 0$, and; (iii) *Transverse ElectroMagnetic* (TEM) waves having $E_z = H_z = 0$. It turns out that TEM waves cannot exist inside our rectangular waveguide, see for example [16] or [21] for a detailed explanation. The troublesome part is the fact that the denominator $k_{\text{cu}}^2$ may be zero, and thus it is not as simple as just letting $E_z = H_z = 0$ and saying that the transverse components vanish in view of equations (B.6)).

Any wave with $E_z \neq 0$ and $H_z \neq 0$ can be treated as a superposition of a TE wave and a TM wave.

## B.1 Transverse Electric Waves

TE waves have a transversely directed electric field, i.e., $E_z = 0$, as the name suggests. By setting $E_z$ to zero in Eqs. (B.6), we observe that the transverse component of the electric and magnetic fields can be calculated from $H_z$ as

$$\vec{H}_t = \mp \frac{\gamma}{k_{\text{cu}}^2} \nabla_t H_z \tag{B.8}$$
$$\vec{E}_t = \frac{1}{k_{\text{cu}}^2} j\omega\mu \, \hat{z} \times \nabla_t H_z.$$

The longitudinal component of the magnetic field is determined from the Helmholtz equation $[\nabla_t^2 + (\gamma + k^2)]H_z = 0$. However for this to be a well-posed problem, we must impose boundary conditions on $H_z$. At the inside of the metal walls of the waveguide, the normal component of the magnetic field must vanish. This implies that $\hat{n} \cdot \vec{H}_t = 0$ on the walls, but from (B.8) we conclude that this is equivalent to the Neumann boundary condition

$$\frac{\partial H_z}{\partial n} = 0, \tag{B.9}$$

where $n$ is a coordinate normal to the waveguide walls.

We are now ready to solve the equations for $H_z$ in our rectangular waveguide. First we separate out the different spatial dependencies of $H_z$ as

$$H_z = \frac{k_{\text{cu}}}{\sqrt{j\gamma k\eta}} \psi(x, y) e^{\mp \gamma z}, \tag{B.10}$$

where $\eta = \sqrt{\mu/\epsilon}$ is the impedance of the medium. The constant in front has been added to make the orthogonality conditions between modes (derived later) more convenient. Note that we are free to scale the fields by any constant, since if some field $H_z$ is a solution to the homogeneous Helmholtz equation, then so is the field obtained by scaling $H_z$ by a constant factor. We are also free to choose a normalization for $\psi$, and we decide that

$$\iint_S |\psi(x, y)|^2 \mathrm{d}S = 1, \tag{B.11}$$

where the surface $S$ is any cross section of the waveguide.

Substituting (B.10) into (B.7), it is clear that $\psi$ (called the Hertz potential), must satisfy the same equation and boundary conditions as $H_z$. It is easily found through a separation of variables procedure that in rectangular coordinates:

$$\psi(x,y) = \psi_{mn}(x,y) = \sqrt{\frac{\epsilon_m \epsilon_n}{ab}} \cos\left[\frac{m\pi}{a}x\right] \cos\left[\frac{n\pi}{b}y\right], \tag{B.12}$$

is a solution, where $m$ and $n$ are any non-negative integers, though both may not be zero, and

$$\epsilon_k = \begin{cases} 2 & \text{for } k \neq 0, \\ 1 & \text{for } k = 0. \end{cases} \tag{B.13}$$

From the separation of variables procedure, the propagation constant $\gamma$ is also found to be

$$\gamma = \sqrt{\left(\frac{m\pi}{a}\right)^2 + \left(\frac{n\pi}{b}\right)^2 - k^2}. \tag{B.14}$$

Recalling from earlier that we defined $k_{\text{cu}}^2 = \gamma^2 + k^2$, it is now clear that the cutoff wavenumber is given by

$$k_{\text{cu}}^2 = \left(\frac{m\pi}{a}\right)^2 + \left(\frac{n\pi}{b}\right)^2. \tag{B.15}$$

The electric and magnetic fields can now be found from (B.10) and (B.8).

The meaning of the cutoff wavenumber is now clear. For $k > k_{\text{cu}}$, the propagation constant $\gamma$ is purely imaginary, and the mode is a propagating mode. However, when $k < k_{\text{cu}}$, $\gamma$ will be a real-valued number and the mode will be evanescent. Since $k^2 = \omega^2 \mu \epsilon$, for a given frequency, the dimensions $a$ and $b$ of the waveguide will determine whether a given mode is propagating or not. Usually the waveguide dimensions are chosen such that only one mode is propagating at the operating frequency. This mode is referred to as the fundamental mode of the waveguide.

## B.2 Transverse Magnetic Waves

TM waves are waves whose magnetic field is transverse to the direction of propagation, i.e., $H_z = 0$. In this case, all fields will be derived from $E_z$ that must satisfy the Helmholtz

equation $[\nabla_t^2 + (\gamma^2 + k^2)]E_z = 0$. The boundary condition in this case is simply $E_z = 0$ on the waveguide walls, since the tangential components of the electric field must vanish at the surface of a PEC. The analysis of TM waves is carried out in a completely analogous way to the analysis of TE waves in the previous section. Finally, one ends up with the following expressions for the field components

$$\begin{aligned}\vec{E}_z &= \pm\hat{z}k_{\text{cu}}\sqrt{\frac{\eta}{j\gamma k}}\psi(x,y)e^{\mp\gamma z} \\ \vec{E}_t &= -\frac{1}{k_{\text{cu}}}\sqrt{\frac{\gamma\eta}{jk}}e^{\mp\gamma z}\nabla_t\psi(x,y) \\ \vec{H}_t &= \pm\frac{jk}{\gamma\eta}\hat{z}\times\vec{E}_t,\end{aligned} \tag{B.16}$$

where $\gamma$ and $k_{\text{cu}}$ are given by the same expressions as before, and

$$\psi(x,y) = \sqrt{\frac{\epsilon_m\epsilon_n}{ab}}\sin\left[\frac{m\pi}{a}x\right]\sin\left[\frac{n\pi}{b}y\right]. \tag{B.17}$$

## B.3 Orthogonality Conditions between Modes

It can be shown through a direct calculation, that the modes obey the following orthogonality conditions:

$$\iint_S(\vec{E}_u^{\pm}\times\vec{H}_v^{+})\cdot\hat{z}\,\mathrm{d}S = \delta_{uv}e^{(\mp\gamma_u-\gamma_v)z}, \tag{B.18a}$$

$$\iint_S(\vec{E}_u^{\pm}\times\vec{H}_v^{-})\cdot\hat{z}\,\mathrm{d}S = -\delta_{uv}e^{(\mp\gamma_u+\gamma_v)z}, \tag{B.18b}$$

where the integral is taken over a cross section $S$ of the waveguide at a given $z$, and the indices $u$ and $v$ each contain information on the two indices $m$ and $n$, as well as if the mode is TE or TM.

If we denote by $\vec{e}_{tu}$ and $\pm\vec{h}_{tu}$ the transverse component of the electric and magnetic field in mode $u$, with the $z$-dependence $e^{\mp\gamma_u z}$ removed, one can show through a direct calculation that these transverse components obey

$$\iint_S(\vec{e}_{tu}\times\vec{h}_{tv})\cdot\mathrm{d}\vec{S} = \delta_{uv}. \tag{B.19}$$

For a general derivation of the orthogonality conditions for waveguides of arbitrary cross section, see for example [22, pp. 329-337].

# Appendix C

# Lorentz Reciprocity Theorem

In this appendix a useful identity known as Lorentz reciprocity theorem is proved[17, pp. xx–yy]. The derivations of all Green's functions used in this thesis are based on this theorem.

Consider two sets of sources $\vec{J_1}$, $\vec{M_1}$ and $\vec{J_2}$, $\vec{M_2}$ in a linear, isotropic medium, producing the fields $\vec{E_1}$, $\vec{H_1}$ and $\vec{E_2}$, $\vec{H_2}$, respectively.

These fields satisfy Maxwell's equations

$$\nabla \times \vec{E_1} = -\vec{M_1} - j\omega\mu\vec{H_1} \tag{C.1a}$$

$$\nabla \times \vec{H_1} = \vec{J_1} + j\omega\epsilon\vec{E_1} \tag{C.1b}$$

for $\vec{J_1}$ and $\vec{M_1}$ and

$$\nabla \times \vec{E_2} = -\vec{M_2} - j\omega\mu\vec{H_2} \tag{C.2a}$$

$$\nabla \times \vec{H_2} = \vec{J_2} + j\omega\epsilon\vec{E_2} \tag{C.2b}$$

for $\vec{J_2}$ and $\vec{M_2}$.

Upon dot-multiplying the first equation by $\vec{H_2}$, the fourth by $\vec{E_1}$, and subsequently subtracting the results yields

$$\vec{E_1} \cdot \nabla \times \vec{H_2} - \vec{H_2} \cdot \nabla \times \vec{E_1} = \vec{E_1} \cdot \vec{J_2} + j\omega\epsilon\vec{E_1} \cdot \vec{E_2} + \vec{H_2} \cdot \vec{M_1} + j\omega\mu\vec{H_2} \cdot \vec{H_1}. \tag{C.3}$$

Now, by using the vector identity

$$\nabla \cdot (\vec{A} \times \vec{B}) = \vec{B} \cdot (\nabla \times \vec{A}) - \vec{A}(\nabla \times \vec{B}), \tag{C.4}$$

we observe that $\vec{E}_1 \cdot \nabla \times \vec{H}_2 - \vec{H}_2 \cdot \nabla \times \vec{E}_1 = \nabla \cdot (\vec{H}_2 \times \vec{E}_1)$ so that (C.3) is rewritten as

$$-\nabla \cdot (\vec{E}_1 \times \vec{H}_2) = \vec{E}_1 \cdot \vec{J}_2 + \vec{H}_2 \cdot \vec{M}_1 + j\omega\epsilon\vec{E}_2 \cdot \vec{E}_1 + j\omega\mu\vec{H}_1 \cdot \vec{H}_2. \tag{C.5}$$

We can perform an analogous procedure by dot multiplying $\nabla \times \vec{H}_1 = \vec{J}_1 + j\omega\epsilon\vec{E}_1$ by $\vec{E}_2$ and $\nabla \times \vec{E}_2 = -\vec{M}_2 j\omega\mu\vec{H}_2$ by $\vec{H}_1$ to obtain

$$-\nabla \cdot (\vec{E}_2 \times \vec{H}_1) = \vec{E}_2 \cdot \vec{J}_1 + \vec{H}_1 \cdot \vec{M}_2 + j\omega\epsilon\vec{E}_2 \cdot \vec{E}_1 + j\omega\mu\vec{H}_1 \cdot \vec{H}_2. \tag{C.6}$$

Subtracting (C.6) from (C.5) leads to the identity

$$-\nabla \cdot (\vec{E}_1 \times \vec{H}_2 - \vec{E}_2 \times \vec{H}_1) = \vec{E}_1 \cdot \vec{J}_2 + \vec{H}_2 \cdot \vec{M}_1 - \vec{E}_2 \cdot \vec{J}_1 - \vec{H}_1 \cdot \vec{M}_2. \tag{C.7}$$

Finally, by integrating this expression over some volume $V$ and using the divergence theorem we obtain the Lorentz reciprocity theorem

$$-\iint_{\partial V} (\vec{E}_1 \times \vec{H}_2 - \vec{E}_2 \times \vec{H}_1) \cdot \hat{n}\mathrm{d}S = \iiint_V (\vec{E}_1 \cdot \vec{J}_2 + \vec{H}_2 \cdot \vec{M}_1 - \vec{E}_2 \cdot \vec{J}_1 - \vec{H}_1 \cdot \vec{M}_2)\mathrm{d}V. \tag{C.8}$$

The derivation of all Green's functions used in this thesis are be based upon this identity.

# Appendix D

# Derivations of Green's Functions for Magnetic Field in Different Geometries

In this appendix the Green's functions for the magnetic field generated by magnetic currents in infinite, rectangular waveguides are derived. The simplest form of this Green's function is derived in Sec. D.1. This particular form has the disadvantage of being piecewise defined, that is, it takes two different forms depending on whether the observation point is in front of or behind the source point (magnetic current), longitudinally. To remove this disadvantage, a different expression for this Green's function is derived in Sec. D.3. This new form is referred to as the Seki Green's function, or Seki's alternate expression for the Green's function, and has the advantage that it is independent on whether the observation point is in front of the source or behind it. However, to derive this form, we need the Green's function for a rectangular cavity, so this is derived in Sec. D.2. In the final section D.4, the Green's function for a shorted (semi-infinite) waveguide is derived.

## D.1 Infinite Rectangular Waveguide

The dyadic Green's function $\overleftrightarrow{G}_m^m$ for the magnetic field due to a magnetic current simply the field generated by a dirac delta current.

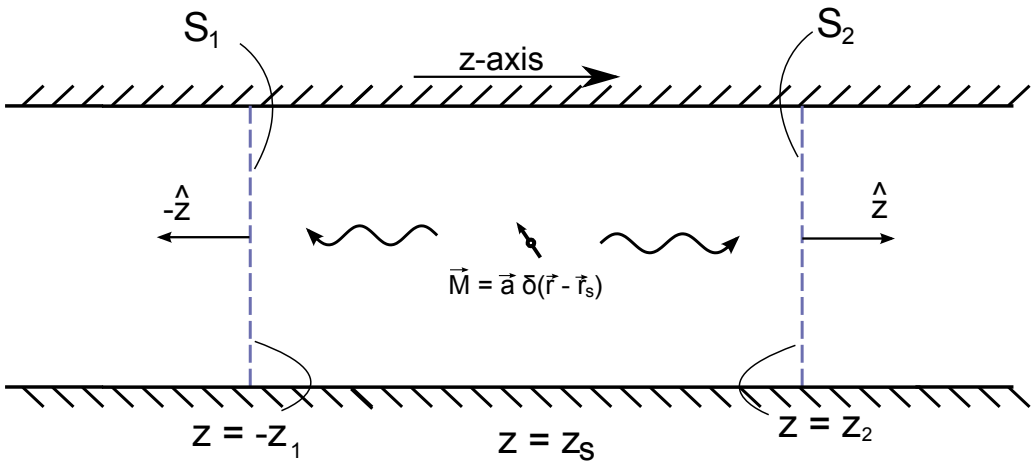


**Figure D.1:** A radiating point magnetic current in an infinite rectangular waveguide. The fields in the waveguide consist of modes propagating in the positive $z$-direction for $z > z_s$, and modes propagating in the negative $z$-direction for $z < z_s$. The fields are determined by applying the Lorentz reciprocity theorem to the volume bounded by the surfaces $z = -z_1$ and $z = z_2$ in the waveguide.

Consider the infinitely long rectangular waveguide in Fig. D.1. At some $\vec{r} = \vec{r}_s$, a magnetic current given by

$$\vec{M} = \vec{a}\delta(\vec{r} - \vec{r}_s). \tag{D.1}$$

is placed.

The corresponding $\vec{E}-$ and $\vec{H}$-fields fields generated by this current can be decomposed into TE and TM modes, $\vec{E}_u^{\pm}$ and $\vec{H}_u^{\pm}$. The index $u$ contains information of mode number and mode type (TE or TM), and the $\pm$ denotes whether the wave travels in the positive or negative $z$-direction.

To the right ($z > z_s$) of the source, the waves travel in the positive $z$-direction, while the waves to the left of $\vec{M}$ travel in the negative $z$-direction. This implies that the eigenmode decomposition of $\vec{E}$ and $\vec{H}$ is expressed accordingly:

$$\vec{E}(\vec{r}) = \begin{cases} \sum_u A_u \vec{E}_u^{+}(\vec{r}) & \text{for } z > z_s, \\ \sum_u B_u \vec{E}_u^{-}(\vec{r}) & \text{for } z < z_s. \end{cases} \tag{D.2}$$

and similarly for $\vec{H}$:

$$\vec{H}(\vec{r}) = \begin{cases} \sum_u A_u \vec{H}_u^+(\vec{r}) & \text{for } z > z_s, \\ \sum_u B_u \vec{H}_u^-(\vec{r}) & \text{for } z < z_s. \end{cases} \tag{D.3}$$

If we can find the coefficients $A_u$ and $B_u$, we will know the form of the fields generated by the magnetic current $\vec{M}$, and hence the magnetic field Green's function $\overleftrightarrow{G}_m^m$. To determine these, the Lorentz reciprocity theorem (appendix C) is used. Consider, in the infinite waveguide, two sets of sources $\vec{J}_1$, $\vec{M}_1$ and $\vec{J}_2$, $\vec{M}_2$, and the corresponding fields $\vec{E}_1$, $\vec{H}_1$ and $\vec{E}_2$, $\vec{H}_2$.

Furthermore, let

$$\begin{aligned} \vec{J}_1 &= 0 \\ \vec{M}_1 &= \vec{a}\delta(\vec{r} - \vec{r}_s) \\ \vec{E}_1 &= \vec{E} \\ \vec{H}_1 &= \vec{H}, \end{aligned} \tag{D.4a}$$

and

$$\begin{aligned} \vec{J}_2 &= 0 \\ \vec{M}_2 &= 0 \\ \vec{E}_2 &= \vec{E}_v^+ \\ \vec{H}_2 &= \vec{H}_v^+. \end{aligned} \tag{D.4b}$$

In other words, for the two independent sets of fields in the Lorentz reciprocity theorem, we use the field generated by the magnetic current $\vec{M}$ in the waveguide (this is the field that we wish to determine), and for the second field we use mode number $v$ travelling in the positive $z$-direction. We are free two choose any two fields we like, since the reciprocity theorem is an identity valid for any two sets of fields. The reason for choosing these particular fields is that expressions for the coefficients $A_u$ and $B_u$ will be found from the calculation (though this is not obvious at the moment).

To apply the Lorentz reciprocity theorem, Eq. (C.8), we must first decide on a volume $V$ for integration; we choose the volume $V$ in the waveguide between the parallel planes $z = -z_1$ and $z = z_2$, see Fig. D.1.

We recall the Lorentz reciprocity theorem for convenience:

$$-\iint_{\partial V} (\vec{E}_1 \times \vec{H}_2 - \vec{E}_2 \times \vec{H}_1) \cdot \hat{n} \mathrm{d}S = \iiint_V (\vec{E}_1 \cdot \vec{J}_2 + \vec{H}_2 \cdot \vec{M}_1 - \vec{E}_2 \cdot \vec{J}_1 - \vec{H}_1 \cdot \vec{M}_2) \mathrm{d}V. \tag{D.5}$$

Consider first the volume integral. Since $\vec{J}_1 = \vec{J}_2 = \vec{M}_2 = 0$, the right hand side reduces to

$$\mathrm{RHS} = \iiint_V \vec{H}_2 \cdot \vec{M}_1 \mathrm{d}V = \iiint_V \vec{H}_v^+ \cdot \vec{a} \delta(\vec{r} - \vec{r}_s) \mathrm{d}V = \vec{H}_v^+(\vec{r}_s) \cdot \vec{a}. \tag{D.6}$$

The surface integral contains three different contributions: the integral over the $S_1$, $S_2$ and the walls of the waveguide. It is immediately evident that the integral over the walls is zero, since the electric field is always perpendicular to the surface of a PEC and hence $\vec{E} \times \vec{H}$ is orthogonal to the surface normal.

The contribution from $S_1$ is

$$\begin{aligned} &-\iint_{S_1} (\vec{E}_1 \times \vec{H}_2 - \vec{E}_2 \times \vec{H}_1) \cdot \hat{n} \mathrm{d}S = \\ &= -\iint_{z=-z_1} \left( \sum_u A_u \vec{E}_u^- \times \vec{H}_v^+ - \vec{E}_v^+ \times \sum_u A_u \vec{H}_u^- \right) \cdot (-\hat{z}) \mathrm{d}S = \\ &= \sum_u A_u \delta_{uv} e^{(+\gamma_u - \gamma_v)(-z_1)} - \sum_u A_u (-\delta_{uv}) e^{(-\gamma_u + \gamma_v)(-z_1)} = \\ &= 2A_v, \end{aligned} \tag{D.7}$$

where the orthogonality property (B.18) of the different modes was used.

The contribution from $S_2$ is

$$\begin{aligned}
&-\iint_{S_2}(\vec{E}_1\times\vec{H}_2-\vec{E}_2\times\vec{H}_1)\cdot\hat{n})\mathrm{d}S=\\
&=-\iint_{z=z_2}\left(\sum_u B_u\vec{E}_u^+\times\vec{H}_v^+-\vec{E}_v^+\times\sum_u B_u\vec{H}_u^+\right)\cdot\hat{z}\mathrm{d}S=\\
&=-\sum_u B_u\delta_{uv}e^{(-\gamma_u-\gamma_v)z_2}+\sum_u B_u(-\delta_{uv})e^{(-\gamma_u-\gamma_v)z_2}=\\
&=0,
\end{aligned} \tag{D.8}$$

where again the orthogonality property of the modes was used.

This means that the total surface integral on the left hand side of the reciprocity theorem (D.5) is

$$\mathrm{LHS}=2A_v, \tag{D.9}$$

but this equals the right hand side (D.6)! We have thus found that

$$A_v=\frac{1}{2}\vec{H}_v^+(\vec{r}_s)\cdot\vec{a}. \tag{D.10}$$

The coefficients for the scattered fields generated by $\vec{M}$ to the left of the source are now known. To find the fields to the right of the source, the coefficients $B_u$ must be determined.

These are found through exactly the same procedure as above, but instead of using the modes $\vec{E}_v^+$ and $\vec{H}_v^+$ as the testing modes in the reciprocity theorem, we use the modes $\vec{E}_v^-$ and $\vec{H}_v^-$ instead, and after an almost identical calculation we find

$$B_v=\frac{1}{2}\vec{H}_v^+(\vec{r}_s)\cdot\vec{a}. \tag{D.11}$$

With the coefficients $A_u$ and $B_u$ known, the fields due to a point source $\vec{M}=\vec{a}\delta(\vec{r}-\vec{r}_s)$ in an infinite waveguide can be written as

$$\vec{E}(\vec{r})=\begin{cases}\dfrac{1}{2}\displaystyle\sum_u\vec{E}_u^-(\vec{r})\left[\vec{H}_u^+(\vec{r}_s)\cdot\vec{a}\right] & \text{for } z<z_s,\\[2ex] \dfrac{1}{2}\displaystyle\sum_u\vec{E}_u^+(\vec{r})\left[\vec{H}_u^-(\vec{r}_s)\cdot\vec{a}\right] & \text{for } z>z_s,\end{cases} \tag{D.12}$$

and

$$\vec{H}(\vec{r}) = \begin{cases} \frac{1}{2}\sum_u \vec{H}_u^-(\vec{r})\left[\vec{H}_u^+(\vec{r}_s)\cdot\vec{a}\right] & \text{for } z < z_s, \\ \frac{1}{2}\sum_u \vec{H}_u^+(\vec{r})\left[\vec{H}_u^-(\vec{r}_s)\cdot\vec{a}\right] & \text{for } z > z_s. \end{cases} \tag{D.13}$$

.

Now that the scattered fields from a point source have been determined, the fields due to any source distribution can be determined through a weighted sum of the fields from all infinitesimal point sources.

From equation (D.13), the Green's function $\overleftrightarrow{G}_m^m$ can be extracted:

$$\overleftrightarrow{G}_m^m(\vec{r},\vec{r}_s) = \begin{cases} \frac{1}{2}\sum_u \vec{H}_u^-(\vec{r})\vec{H}_u^+(\vec{r}_s) & \text{for } z < z_s, \\ \frac{1}{2}\sum_u \vec{H}_u^+(\vec{r})\vec{H}_u^-(\vec{r}_s) & \text{for } z > z_s, \end{cases} \tag{D.14}$$

where the product of two vectors $\vec{A}\vec{B}$ used above is neither a dot product nor a vector product, but should be interpreted as the outer product of the two vectors and is thus an operator (or a matrix). The action of $\vec{A}\vec{B}$ on some vector $\vec{C}$ is defined as

$$(\vec{A}\vec{B})\vec{C} = \vec{A}(\vec{B}\cdot\vec{C}). \tag{D.15}$$

The magnetic field due to an arbitrary magnetic current $\vec{M}(\vec{r})$ can then be found from

$$\vec{H}(\vec{r}) = \int \overleftrightarrow{G}_m^m(\vec{r},\vec{r}_s)\vec{M}(\vec{r}_s)\mathrm{d}V_s. \tag{D.16}$$

Similarly, we have found the Green's function for the electric field due to a magnetic current,

$$\overleftrightarrow{G}_m^e(\vec{r},\vec{r}_s) = \begin{cases} \frac{1}{2}\sum_u \vec{E}_u^-(\vec{r})\vec{H}_u^+(\vec{r}_s) & \text{for } z < z_s, \\ \frac{1}{2}\sum_u \vec{E}_u^+(\vec{r})\vec{H}_u^-(\vec{r}_s) & \text{for } z > z_s. \end{cases} \tag{D.17}$$

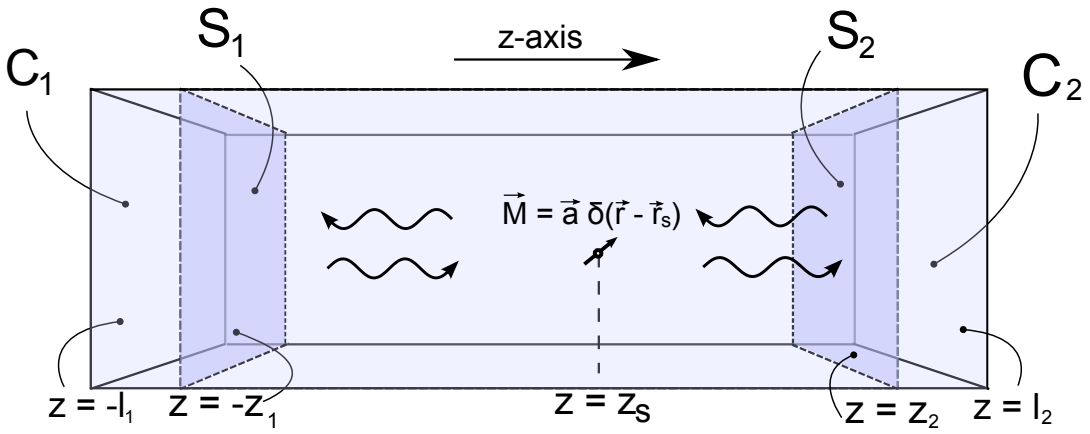


**Figure D.2:** Point magnetic current in a cavity.

Note that the Green's functions are defined in a piecewise manner, that is, they take two different forms depending on whether $z > z_s$ or $z < z_s$. This is not a severe problem when calculating $\vec{H}$ from simple magnetic current distributions, but for more complicated magnetic currents this may pose a problem rather quickly when calculating the matrix elements $\langle w_j, \mathcal{L}f_i \rangle$ in (2.11). For this reason an alternative expression for this Green's function, known as the Seki Green's function[23], that has the same functional form for all $z$ will be derived below. However, to this end, we will first need the magnetic field Green's function in a cavity.

## D.2 Green's Function in a Cavity

Consider a rectangular cavity with walls $C_1$ at $z = -l_1$ and $C_2$ at $z = l_2$, as shown in Fig. D.2. Once again the goal is to find the Green's function by calculating the magnetic field inside the cavity due to a point source.

After placing a magnetic current element $\vec{M} = \vec{a}\delta(\vec{r} - \vec{r}_s)$ at $\vec{r}_s$, we expand the magnetic field to the left and right of the magnetic current in terms of eigenmodes. However, unlike the case with the infinite waveguide, we now have modes travelling in both the negative and positive $z$-direction, since the outgoing waves are reflected off the cavity walls at $z = -l_1$ and $z = l_2$.

We thus have

$$\vec{H}(\vec{r}) = \begin{cases} \sum_u \left[ A_u \vec{H}_u^-(\vec{r}) + B_u \vec{H}_u^+(\vec{r}) \right] & \text{for } -l_1 < z < z_s, \\ \sum_u \left[ C_u \vec{H}_u^+(\vec{r}) + D_u \vec{H}_u^-(\vec{r}) \right] & \text{for } z_s < z < l_2. \end{cases} \tag{D.18}$$

and

$$\vec{E}(\vec{r}) = \begin{cases} \sum_u \left[ A_u \vec{E}_u^-(\vec{r}) + B_u \vec{E}_u^+(\vec{r}) \right] & \text{for } -l_1 < z < z_s, \\ \sum_u \left[ C_u \vec{E}_u^+(\vec{r}) + D_u \vec{E}_u^-(\vec{r}) \right] & \text{for } z_s < z < l_2. \end{cases} \tag{D.19}$$

Two of the unknowns can be removed by imposing the boundary condition that the tangential electric field vanishes at the PEC walls $C_1$ and $C_2$.

Since the tangential electric field for a mode $u$ is given by $\vec{E}_{ut}^{\pm} = \vec{e}_{tu} e^{\mp \gamma_u z}$, and hence

$$\vec{E}_t(z = -l_1) = \sum_u \left[ A_u \vec{e}_{tu} e^{-\gamma_u l_1} + B_u \vec{e}_{tu} e^{\gamma_u l_1} \right] = 0. \tag{D.20}$$

We now take the cross product of this equality with $\vec{h}_{tv}$ from the right and make use of the orthogonality condition (B.19) to obtain

$$\iint_{C_1} \sum_u \left[ A_u \vec{e}_{tu} e^{-\gamma_u l_1} + B_u \vec{e}_{tu} e^{\gamma_u l_1} \right] \times \vec{h}_{tv} \cdot \mathrm{d}\vec{S} = A_v e^{-\gamma_v l_1} + B_v e^{\gamma_v l_1} = 0 \tag{D.21}$$

and hence

$$B_v = -A_v e^{-2\gamma_v l_1}. \tag{D.22}$$

Similarly, for $C_2$, it is found that

$$D_v = -C_v e^{-2\gamma_v l_2}. \tag{D.23}$$

The $\vec{E}$ and $\vec{H}$ fields can thus be written

$$\vec{E}(\vec{r}) = \begin{cases} \sum_u A_u \left[ \vec{E}_u^-(\vec{r}) - \vec{E}_u^+(\vec{r}) e^{-2\gamma_u l_1} \right] & \text{for } -l_1 < z < z_s \\ \sum_u C_u \left[ \vec{E}_u^+(\vec{r}) - \vec{E}_u^-(\vec{r}) e^{-2\gamma_u l_2} \right] & \text{for } z_s < z < l_2, \end{cases} \tag{D.24}$$

and

$$\vec{H}(\vec{r}) = \begin{cases} \sum_u A_u \left[ \vec{H}_u^-(\vec{r}) - \vec{H}_u^+(\vec{r}) e^{-2\gamma_u l_1} \right] & \text{for } -l_1 < z < z_s \\ \sum_u C_u \left[ \vec{H}_u^+(\vec{r}) - \vec{H}_u^-(\vec{r}) e^{-2\gamma_u l_2} \right] & \text{for } z_s < z < l_2. \end{cases} \tag{D.25}$$

As in the case of the infinite waveguide, we now make use of the reciprocity theorem twice, using first right and then left travelling modes as testing functions. The integration volume is the one contained between the surfaces $S_1$ and $S_2$ in Fig. D.2.

For the two sets of fields required in the reciprocity theorem, we choose

$$\vec{E}_1 = \vec{E} \tag{D.26}$$
$$\vec{H}_1 = \vec{H} \tag{D.27}$$
$$\vec{J}_1 = 0 \tag{D.28}$$
$$\vec{M}_1 = \vec{a}\delta(\vec{r} - \vec{r}_s), \tag{D.29}$$

and

$$\vec{E}_2 = \vec{E}_v^+ \tag{D.30}$$
$$\vec{H}_2 = \vec{H}_v^+ \tag{D.31}$$
$$\vec{J}_2 = 0 \tag{D.32}$$
$$\vec{M}_2 = 0. \tag{D.33}$$

We now apply the reciprocity theorem (C.8) to these fields. The volume integral on the right hand side becomes

$$\text{RHS} = \int_V \vec{H}_2 \cdot \vec{M}_1 \mathrm{d}V = \int_V \vec{H}_v^+(\vec{r}) \cdot \vec{a}\delta(\vec{r} - \vec{r}_s) \mathrm{d}V = \vec{H}_v^+(\vec{r}_s) \cdot \vec{a}. \tag{D.34}$$

The surface integral is a little more complicated. Again, the parts of the surface integral over the PEC walls vanish due to the boundary conditions of $\vec{E}$, so we only need to calculate the contribution from $S_1$ and $S_2$. Starting with $S_1$:

$$\begin{aligned}
&-\int_{S_1}(\vec{E}_1\times\vec{H}_2-\vec{E}_2\times\vec{H}_1)\cdot\mathrm{d}\vec{S}=\\
&=-\int_{S_1}\left[\sum_u A_u[\vec{E}_u^--\vec{E}_u^+e^{-2\gamma_y l_1}]\times\vec{H}_v^+-\vec{E}_v^+\times\sum_u A_u[\vec{H}_u^--\vec{H}_u^+e^{-2\gamma_u l_1}]\right]\cdot\mathrm{d}\vec{S}=\\
&=\sum_u A_u\left[\delta_{uv}e^{(+\gamma_u-\gamma_v)(-z_1)}-\delta_{uv}e^{(-\gamma_u-\gamma_v)(-z_1)}e^{-2\gamma_u l_1}\right]+\\
&-\sum_u A_u\left[-\delta_{uv}e^{(-\gamma_v+\gamma_u)(-z_1)}-\delta_{uv}e^{(-\gamma_u-\gamma_v)(-z_1)}e^{-2\gamma_u l_1}\right]=\\
&=2A_v,
\end{aligned}\tag{D.35}$$

where we used the orthogonality property (B.18) of the eigenmodes.

Similarly, for the contribution at $S_2$ we get

$$\begin{aligned}
&-\int_{S_2}(\vec{E}_1\times\vec{H}_2-\vec{E}_2\times\vec{H}_1)\cdot\mathrm{d}\vec{S}=\\
&=-\int_{S_2}\left[\sum_u C_u[\vec{E}_u^+-\vec{E}_u^-e^{-2\gamma_y l_2}]\times\vec{H}_v^+-\vec{E}_v^+\times\sum_u C_u[\vec{H}_u^+-\vec{H}_u^-e^{-2\gamma_u l_2}]\right]\cdot\mathrm{d}\vec{S}=\\
&=-\sum_u C_u\left[\delta_{uv}e^{(-\gamma_u-\gamma_v)z_2}-\delta_{uv}e^{(\gamma_u-\gamma_v)z_2}e^{-2\gamma_u l_2}\right]+\\
&+\sum_u C_u\left[\delta_{uv}e^{(-\gamma_v-\gamma_u)z_2}+\delta_{uv}e^{(-\gamma_v+\gamma_u)z_2}e^{-2\gamma_u l_2}\right]=\\
&=2e^{-2\gamma_v l_2}C_v.
\end{aligned}\tag{D.36}$$

Upon combining the results from equation (D.34), (D.35) and (D.36), we obtain

$$2A_v+2e^{-2\gamma_v l_2}C_v=\vec{H}_v^+(\vec{r}_s)\cdot\vec{a}.\tag{D.37}$$

Next, by applying the reciprocity theorem once again, but choosing $\vec{E}_1$ as $\vec{E}_v^-$ and $\vec{H}_2$ as $\vec{H}_v^-$ yields, after very similar calculations,

$$2C_v + 2e^{-2\gamma_v l_1} A_v = \vec{H}_v^-(\vec{r}_s) \cdot \vec{a}. \tag{D.38}$$

Solving the above two equations for $A_v$ and $C_v$ yields

$$A_v = \frac{e^{\gamma_v l_1}}{4 \sinh(\gamma_v l)} \left[ e^{\gamma_v l_2} \vec{H}_v^+(\vec{r}_s) \cdot \vec{a} - e^{-\gamma_v l_2} \vec{H}_v^-(\vec{r}_s) \cdot \vec{a} \right] \tag{D.39}$$

$$C_v = \frac{e^{\gamma_v l_2}}{4 \sinh(\gamma_v l)} \left[ e^{\gamma_v l_1} \vec{H}_v^-(\vec{r}_s) \cdot \vec{a} - e^{-\gamma_v l_1} \vec{H}_v^+(\vec{r}_s) \cdot \vec{a} \right]. \tag{D.40}$$

where $l = l_1 + l_2$.

We have now determined the magnetic field due to a point source magnetic current. Substituting these results into Eq. (D.25) for the $\vec{H}$-field, we find that the magnetic field Green's function in a cavity due to a magnetic current is given by

$$\overleftrightarrow{G}_m^m(\vec{r}, \vec{r}_s) = \begin{cases} \dfrac{1}{4} \displaystyle\sum_u \dfrac{1}{\sinh(\gamma_u l)} \left[ \vec{H}_u^-(\vec{r}) e^{\gamma_u l_1} - \vec{H}_u^+(\vec{r}) e^{-\gamma_u l_1} \right] \\ \qquad \left[ e^{\gamma_u l_2} \vec{H}_u^+(\vec{r}_s) - e^{-\gamma_u l_2} \vec{H}_u^-(\vec{r}_s) \right] \quad \text{for } -l_1 < z < z_s \\ \dfrac{1}{4} \displaystyle\sum_u \dfrac{1}{\sinh(\gamma_u l)} \left[ \vec{H}_u^+(\vec{r}) e^{\gamma_u l_2} - \vec{H}_u^-(\vec{r}) e^{-\gamma_u l_2} \right] \\ \qquad \left[ e^{\gamma_u l_1} \vec{H}_u^-(\vec{r}_s) - e^{-\gamma_u l_1} \vec{H}_u^+(\vec{r}_s) \right] \quad \text{for } z_s < z < l_2. \end{cases} \tag{D.41}$$

where, as defined above, the product of two vectors $\vec{A}\vec{B}$ denotes the outer product.

## D.3 Seki's Alternative Expression

The Green's function for the infinite waveguide derived above has one major disadvantage: it takes different functional forms depending on whether $z > z_s$ or $z < z_s$. This becomes very problematic when evaluating the matrix elements $\langle w_j, \mathcal{L} f_i \rangle$ in the method of moments [see Eq. (2.11)]. To circumvent this problem, we will now derive an alternative expression for the Green's function that has the same functional form for all $z$, known as the Seki

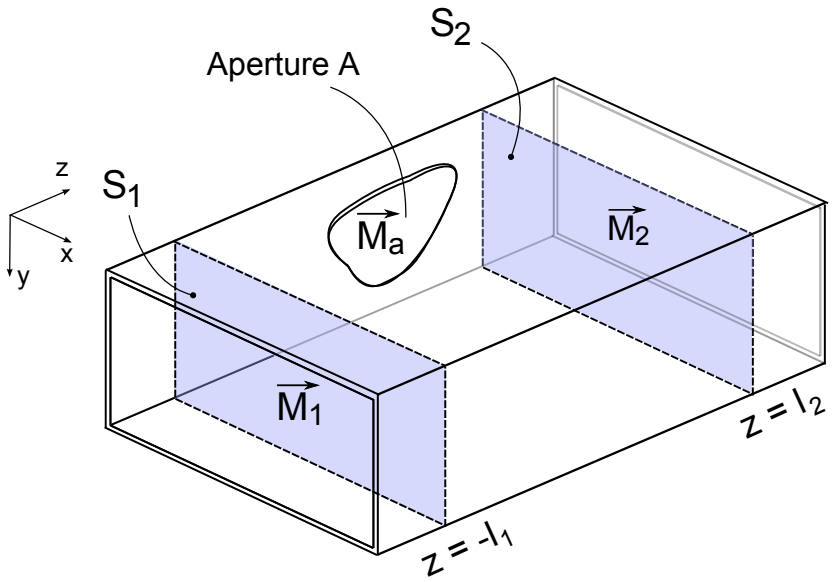


**Figure D.3:** A section of an infinite waveguide with an aperture $A$ in one of its walls. The fields can be analyzed by closing the aperture and the two surfaces $S_1$ and $S_2$ with PEC material and introducing appropriate magnetic currents at the surfaces.

Green's function, that will make the calculation of the matrix elements considerably easier.

To find this expression, consider an infinite waveguide with a magnetic current along the surface of one of its walls. This will be the case in all applications studied throughout this text, since every magnetic current will be the fictitious current due to an aperture in the wall that has been closed with a PEC.

In principle, the magnetic field could be calculated using the Green's function (2.28) for an infinite waveguide, and splitting the integral up over the two parts $z < z_s$ and $z > z_s$ if needed, but we will use a different approach. Instead, we seal off the waveguide with two PEC walls $S_1$ and $S_2$ to create a "virtual cavity". This is allowed if we also add sheets of magnetic current, $\vec{M}_1$ and $\vec{M}_2$, over the respective surfaces, given by

$$\vec{M}_1 = \vec{E}_1 \times \hat{z}, \tag{D.42}$$

$$\vec{M}_2 = \vec{E}_2 \times (-\hat{z}), \tag{D.43}$$

where $\vec{E}_1$ is the electric field at surface $S_1$, and $\vec{E}_2$ is the magnetic field at the surface $S_2$. With these currents, the uniqueness theorem of electromagnetic fields ensures us that the fields in this new geometry (with the PEC walls and magnetic currents) is the same as in

the original situation (without the walls and currents).

The magnetic field in the waveguide can now be calculated by considering this virtual cavity, and instead of using the infinite waveguide Green's function, we are now allowed to use the cavity Green's functions instead. As we will now see, this allows us to find an equivalent Green's function that has the same form for all $z$. The $\vec{H}$-field scattered by the current $\vec{M}_a$ is then

$$\vec{H}(\vec{r}) = \int_{S_a} \overleftrightarrow{G}{}^c_y(\vec{r},\vec{r}_s)\vec{M}_a(\vec{r}_s)\mathrm{d}S_s + \int_{S_1} \overleftrightarrow{G}{}^c_z(\vec{r},\vec{r}_s)\vec{M}_1(\vec{r}_s)\mathrm{d}S_s + \int_{S_2} \overleftrightarrow{G}{}^c_z(\vec{r},\vec{r}_s)\vec{M}_2(\vec{r}_s)\mathrm{d}S_s, \tag{D.44}$$

where the Green's functions in the above expression are all for the magnetic field due to a magnetic current in a cavity. Specifically, the last two terms are identical to the one derived in the previous section, with the fields expanded in terms of modes travelling in the $z$-direction. The first RHS-term uses a Green's function where the fields are expanded in terms of modes travelling in the $y$-direction. The derivation of this Green's function is identical to the derivation in the previous section, except that $z$ should be replaced by $y$. The reason that the $y$-expansion is used for the magnetic current in the aperture is that for every point $\vec{r}$ in the cavity, $y > y_s$ for every source point $\vec{r}_s$ in the aperture. This means that the form of the Green's function for $y > y_s$ can be used in the entire integral in Eq. (D.44).

The same holds true for the magnetic currents at $S_1$ and $S_2$. When evaluating the second integral in Eq. (D.44), $z > z_s$ and only one form of the Green's function is needed, and for the third integral $z < z_s$ so the Green's function takes the same form for the entire surface here as well. This is the key behind the Seki Green's function, derived below.

We now proceed to calculate the magnetic field in the virtual cavity in terms of the magnetic current $\vec{M}_a$ in the aperture by starting with the field due to $\vec{M}_1$.

As stated earlier, $\vec{M}_1 = \vec{E}_1 \times \hat{z}$, where $\vec{E}_1$ is the electric field at the surface $S_1$ and can be calculated from the electric field Green's function in an infinite waveguide [cf. Eq. (D.17)]. The magnetic current is then

$$\vec{M}_1(\vec{r}_s) = \left[\frac{1}{2}\sum_v \vec{E}_v^-(\vec{r}_s)\int_{S_a} \vec{H}_v^+(\vec{r}'_s)\cdot\vec{M}_a(\vec{r}'_s)\mathrm{d}S'_s\right]\times\hat{z}, \tag{D.45}$$

so the magnetic field generated by this current is

$$\begin{aligned}\int_{S_1} \overleftrightarrow{G}^{c}_{z}(\vec{r},\vec{r}'_s)\vec{M}_1(\vec{r}'_s)\mathrm{d}S'_s = \frac{1}{4}\sum_u \frac{1}{\sinh(\gamma_u l)}[\vec{H}^+_u(\vec{r})e^{\gamma_u l_2} - \vec{H}^-_u(\vec{r})e^{-\gamma_u l_2}] \\ \int_{S_1}\mathrm{d}S'_s\left[\vec{H}^-_u(\vec{r}'_s)e^{\gamma_u l_1} - \vec{H}^+_u(\vec{r}'_s)e^{-\gamma_u l_1}\right]\cdot \\ \left[\frac{1}{2}\sum_v \vec{E}^-_v(\vec{r}'_s)\times\hat{z}\int_{S_a}\vec{H}^+_v(\vec{r}_s)\cdot\vec{M}_a(\vec{r}_s)\mathrm{d}S_s\right].\end{aligned} \tag{D.46}$$

The multiplication between the first and second line in the right hand side is an outer product, whereas the multiplication between lines two and three is a dot product. The expression may seem hideous, but we will now rewrite it into a much simpler form.

Using the vector identity $\vec{H}\cdot(\vec{E}\times\hat{z}) = -\hat{z}\cdot(\vec{E}\times\vec{H})$, the above expression can be written as

$$\begin{aligned}\int_{S_1} \overleftrightarrow{G}^{c}_{z}(\vec{r},\vec{r}'_s)\vec{M}_1(\vec{r}'_s)\mathrm{d}S'_s = -\frac{1}{4}\sum_u \frac{1}{\sinh(\gamma_u l)}[\vec{H}^+_u(\vec{r})e^{\gamma_u l_2} - \vec{H}^-_u(\vec{r})e^{-\gamma_u l_2}] \\ \int_{S_1}\frac{1}{2}\sum_v \vec{E}^-_v(\vec{r}'_s)\int_{S_a}\vec{H}^+_v(\vec{r}_s)\cdot\vec{M}_a(\vec{r}_s)\mathrm{d}S_s\times \\ \left[\vec{H}^-_u(\vec{r}'_s)e^{\gamma_u l_1} - \vec{H}^+_u(\vec{r}'_s)e^{-\gamma_u l_1}\right]\cdot\hat{z}\mathrm{d}S'_s.\end{aligned} \tag{D.47}$$

To make sense out of the above equation, note that the integal over $S_a$ on the second line is a constant, so the outer integral over $S_1$ is, after moving all constants outside, the surface integral of $\vec{E}^-_v \times \vec{H}^\pm_u$ over a cross section of the waveguide. But this implies that we can use the orthogonality conditions (B.18) to obtain

$$\begin{aligned}\int_{S_1} \overleftrightarrow{G}^{c}_{z}(\vec{r},\vec{r}'_s)\vec{M}_1(\vec{r}'_s)\mathrm{d}S'_s = -\frac{1}{4}\sum_v \frac{1}{\sinh(\gamma_v l)}[\vec{H}^+_v(\vec{r})e^{\gamma_v l_2} - \vec{H}^-_v(\vec{r})e^{-\gamma_v l_2}]\times \\ \left[\frac{1}{2}(-e^{-\gamma_v l_1} - e^{-\gamma_v l_1})\int_{S_a}\vec{H}^+_v(\vec{r}_s)\cdot\vec{M}_a(\vec{r}_s)\mathrm{d}S_s\right] = \\ = \frac{1}{4}\sum_v \frac{e^{-\gamma_v l_1}}{\sinh(\gamma_v l)}[\vec{H}^+_v(\vec{r})e^{\gamma_v l_2} - \vec{H}^-_u(\vec{r})e^{-\gamma_v l_2}]\times \\ \int_{S_a}\vec{H}^+_v(\vec{r}_s)\cdot\vec{M}_a(\vec{r}_s)\mathrm{d}S_s.\end{aligned} \tag{D.48}$$

An analogous calculation for finding the magnetic field from $\vec{M}_2$ at the opposing surface $S_2$, yields:

$$\int_{S_2} \overleftrightarrow{G}{}^c_z(\vec{r},\vec{r}\,'_s)\vec{M}_2(\vec{r}\,'_s)\mathrm{d}S'_s = \frac{1}{4}\sum_v \frac{e^{-\gamma_v l_2}}{\sinh(\gamma_v l)}\left[\vec{H}_v^-(\vec{r})e^{\gamma_v l_1} - \vec{H}_v^+(\vec{r})e^{-\gamma_v l_1}\right] \int_{S_a} \vec{H}_v^-(\vec{r}_s)\cdot\vec{M}_a(\vec{r}_s)\mathrm{d}S_s. \tag{D.49}$$

Note that we have now transformed the integrals over the two fictitious magnetic currents $\vec{M}_1$ and $\vec{M}_2$ into integrals over the current $\vec{M}_a$ in the aperture. We can thus combine all integrals in the expression (D.44) to obtain an expression for $\vec{H}$ in terms of $\vec{M}_a$ that consists of only one integral over $S_a$:

$$\vec{H}(\vec{r}) = \int_{S_a} \overleftrightarrow{G}_{\text{Seki}}(\vec{r},\vec{r}_s)\vec{M}_a(\vec{r}_s)\mathrm{d}S_s, \tag{D.50}$$

and the Seki Green's function $\overleftrightarrow{G}_{\text{Seki}}$ is given by

$$\overleftrightarrow{G}_{\text{Seki}}(\vec{r},\vec{r}_s) = \overleftrightarrow{G}{}^y_c(\vec{r},\vec{r}_s) + \frac{1}{4}\sum_u \frac{e^{-\gamma_u l_1}}{\sinh(\gamma_u l)}\left[\vec{H}_u^+(\vec{r})e^{\gamma_u l_2} - \vec{H}_u^-(\vec{r})e^{-\gamma_u l_2}\right]\vec{H}_u^+(\vec{r}_s) + \frac{1}{4}\sum_u \frac{e^{-\gamma_u l_2}}{\sinh(\gamma_u l)}\left[\vec{H}_u^-(\vec{r})e^{\gamma_u l_1} - \vec{H}_u^+(\vec{r})e^{-\gamma_u l_1}\right]\vec{H}_u^-(\vec{r}_s), \tag{D.51}$$

which is the Green's function we were after. It provides us with the magnetic field due to a magnetic current on one of the waveguide walls, and has the vital property of having the same functional expression for all $z$ and $z_s$, independent of whether $z$ is greater than or less than $z_s$. It is this form for $\overleftrightarrow{G}$ that is used to calculate the self- and mutual admittances of slots in the waveguide walls in appendix E.

One important aspect that must be discussed is the choice of length $l$ for the virtual cavity. We have to avoid making $\sinh(\gamma_u l)$ zero since this term occurs in a denominator in the Seki Green's function. This is impossible for evanescent modes, since for these $\gamma_u$ is real and larger than zero. However, for a propagating mode, $\gamma_u$ is purely imaginary, so $\gamma_u = i\beta_u$, where $\beta_u$ is a real, positive number. Our condition on $l$ is then

$$\sinh(\gamma_u l) = i\sin(\beta_u l) \neq 0, \tag{D.52}$$

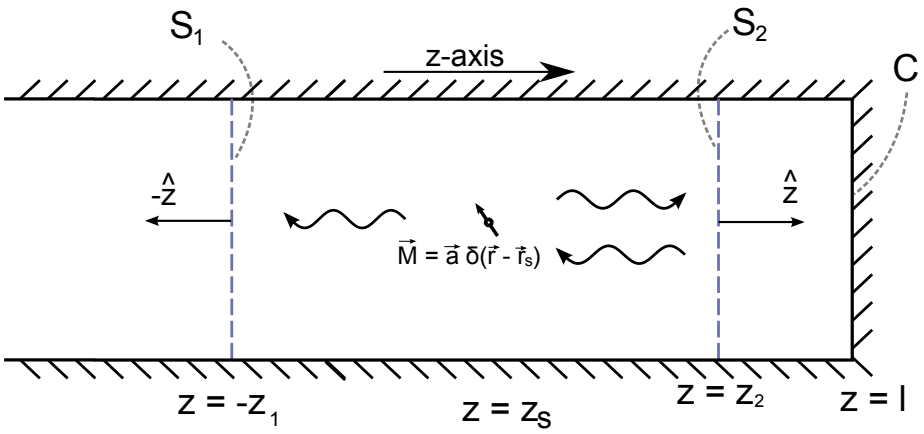


**Figure D.4:** A waveguide shorted at $z = l$ with an incremental magnetic current source at $z = z_s$.

but since $\beta_u$ is the wavenumber of the wave, the above condition becomes

$$l \neq n\frac{\lambda_u}{2}, \tag{D.53}$$

where $n$ is any positive integer and $\lambda_u$ is the wavelength of the propagating mode. In practice, the dimensions of the waveguide are often chosen such that it allows only one propagating mode, and the length of the virtual cavity is then chosen halfway between the first two "forbidden" lengths, i.e.,

$$l = \frac{3}{4}\lambda_u. \tag{D.54}$$

## D.4 Green's function in a shorted waveguide

Consider the shorted waveguide in Fig. D.4. An incremental magnetic current source $\vec{M}$ is placed at some point $\vec{r}_s$. The magnetic field to the left of $z_s$, i.e., with $z < z_s$ consists only of modes travelling in the negative $z$-direction. The waves travelling to the right are reflected at the end surface $C$, which means that the field at $z > z_s$ consists of modes propagating both to the left and right. The magnetic field can thus be decomposed according to

$$\vec{H}(\vec{r}) = \begin{cases} \sum_u A_u \vec{H}_u^-(\vec{r}) & \text{for } z < z_s, \\ \sum_u \left[ B_u \vec{H}_u^-(\vec{r}) + C_u \vec{H}_u^+(\vec{r}) \right] & \text{for } z > z_s. \end{cases} \tag{D.55}$$

A similar decomposition is true for the electric field:

$$\vec{E}(\vec{r}) = \begin{cases} \sum_u A_u \vec{E}_u^-(\vec{r}) & \text{for } z < z_s, \\ \sum_u \left[ B_u \vec{E}_u^-(\vec{r}) + C_u \vec{E}_u^+(\vec{r}) \right] & \text{for } z > z_s. \end{cases} \tag{D.56}$$

We now make use of the boundary condition that the tangential electric field vanishes at $C$ in exactly the same way as we did when deriving the cavity Green's function in Sec. D.2. The tangential electric field for mode $u$ at any $z$ is given by $\vec{E}_{ut}^{\pm} = \vec{e}_{ut} e^{\mp \gamma_u z}$. The boundary condition can thus be written

$$\vec{E}_t(z = l) = \sum_u \left[ B_u \vec{e}_{tu} e^{\gamma_u l} + C_u \vec{e}_{tu} e^{-\gamma_u l} \right] = 0. \tag{D.57}$$

Cross multiplying by $\vec{h}_{tv}$ from the right, integrating over a cross section of the waveguide, and making use of the orthogonality condition (B.19) between $\vec{e}_{tu}$ and $\vec{h}_{tv}$ yields

$$B_v = -C_v e^{-2\gamma_v l}. \tag{D.58}$$

The unknowns $B_u$ have now been removed. To determine $A_u$ and $C_u$, Lorentz reciprocity theorem is applied twice to the volume between surfaces $S_1$ and $S_2$. The fields $\vec{E}$ and $\vec{H}$ in the waveguide are first tested against the modes $\vec{E}_v^+$, $\vec{H}_v^+$, and then against the modes $\vec{E}_v^-$, $\vec{H}_v^-$.

The first application yields

$$A_v + e^{-2\gamma_v l} C_v = \frac{1}{2} \vec{H}_v^+(\vec{r}_s) \cdot \vec{a}, \tag{D.59}$$

and the second application yields

$$C_v = \frac{1}{2} \vec{H}_v^-(\vec{r}_s) \cdot \vec{a}. \tag{D.60}$$

(See section on the Green's function in a cavity for details on how the volume and surface integrals in the reciprocity theorem are evaluated. This case is completely analogous.)

Substituting (D.60) back into Eqs. (D.60) and (D.58) gives

$$A_v = \frac{e^{-\gamma_v l}}{2}\left[\vec{H}_v^+(\vec{r}_s)e^{\gamma_v l} - \vec{H}_v^-(\vec{r}_s)e^{-\gamma_v l}\right]\cdot\vec{a}. \tag{D.61}$$

and

$$B_v = -\frac{e^{-2\gamma_v l}}{2}\vec{H}_v^-(\vec{r}_s)\cdot\vec{a}. \tag{D.62}$$

The above three equations for the expansion coefficients $A_u$, $B_u$ and $C_u$ are now substituted into the original expression (D.55) for the $\vec{H}$ field:

$$\vec{H}(\vec{r}) = \begin{cases} \dfrac{1}{2}\displaystyle\sum_u e^{-\gamma_u l}\vec{H}_u^-(\vec{r})\left[\vec{H}_u^+(\vec{r}_s)e^{\gamma_u l} - \vec{H}_u^-(\vec{r}_s)e^{-\gamma_u l}\right]\cdot\vec{a} & \text{for } z < z_s, \\ \dfrac{1}{2}\displaystyle\sum_u e^{-\gamma_u l}\left[\vec{H}_u^+(\vec{r})e^{\gamma_u l} - \vec{H}_u^-(\vec{r})e^{-\gamma_u l}\right]\vec{H}_u^-(\vec{r}_s)\cdot\vec{a} & \text{for } z > z_s. \end{cases} \tag{D.63}$$

The Green's function for a shorted waveguide can readily be extracted from the above expression:

$$\overleftrightarrow{G}_m^m(\vec{r},\vec{r}_s) = \begin{cases} \dfrac{1}{2}\displaystyle\sum_u e^{-\gamma_u l}\vec{H}_u^-(\vec{r})\left[\vec{H}_u^+(\vec{r}_s)e^{\gamma_u l} - \vec{H}_u^-(\vec{r}_s)e^{-\gamma_u l}\right] & \text{for } z < z_s, \\ \dfrac{1}{2}\displaystyle\sum_u e^{-\gamma_u l}\left[\vec{H}_u^+(\vec{r})e^{\gamma_u l} - \vec{H}_u^-(\vec{r})e^{-\gamma_u l}\right]\vec{H}_u^-(\vec{r}_s) & \text{for } z > z_s. \end{cases} \tag{D.64}$$

# Appendix E

# Self- and Mutual Admittances

Expressions for the self- and mutual admittances of tilted slots in rectangular waveguides are needed to calculate the S-parameters of the waveguide coupling junction studied in this thesis. The admittances of the basis functions in the cavities formed between waveguides due to the non-zero thickness of the waveguide walls are also needed, as well as expressions for the coupling between basis functions and waveguide modes. The sole purpose of this appendix is to derive expressions for these quantities.

The derivations presented here are based on very similar derivations by Lars Manholm and Jiro Hirokawa [8, 10], but their expressions are valid only for longitudinal magnetic currents with no transverse variation, whereas the basis functions used here allow for both transverse polarization and variation of the magnetic current. Hence, the admittances derived in this chapter are generalizations of those in [8, 10], and it is easy to show that they reduce to those equations in the case when no transverse variation is included.

## E.1 Self- and mutual admittances of slots in the upper wall of a rectangular waveguide

We start by deriving expressions for the self- and mutual admittances of slots in the same broad wall of a rectangular waveguide. The derivations are generalizations of the

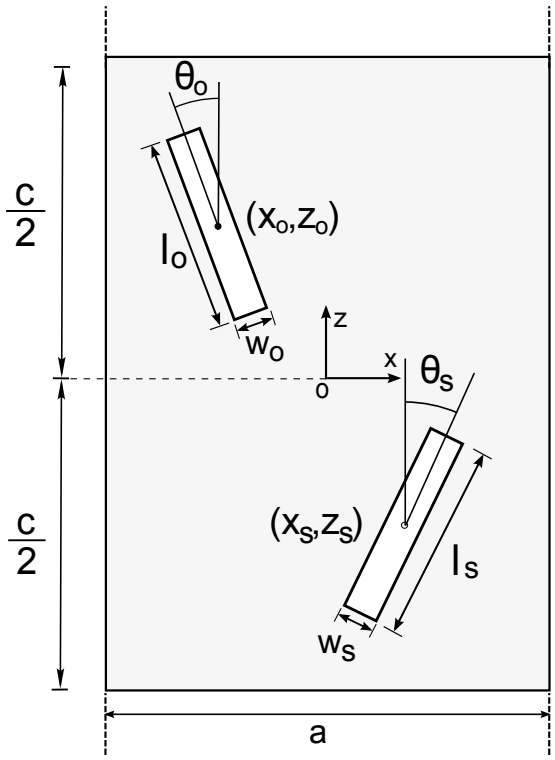


**Figure E.1:** Two slots whose mutual admittance we wish to calculate. The waveguide geometry has been changed into a virtual cavity with the origin at the center of the top wall. Angles are measured counterclockwise to the waveguide axis (meaning that the particular value for $\theta_s$ shown above is negative).

calculations by Manholm and Hirokawa [9, 10].

Consider an infinite waveguide with a rectangular cross section of dimension $a \times b$, with two slots in the upper wall. The fields due to the equivalent magentic current distributions in these slots will be analyzed using the virtual cavity method, and thus Seki's alternative expression (2.32) for the Green's function in a rectangular waveguide will be used. Let the origin be placed in the upper wall, at the center of the virtual cavity, and the slots be located as shown in Fig. E.1. The virtual cavity is chosen to be large enough to enclose both slots. The tilt angles $\theta$ of the slots are defined to be positive in the counterclockwise direction.

The admittance between the slots is defined as the matrix whose elements are given by

$$y_{ij} = -\iint_{S_o} \mathrm{d}S_o\, \vec{m}_i^o(\vec{r}_o) \cdot \iint_{S_s} \overleftrightarrow{G}(\vec{r}_o, \vec{r}_s)\vec{m}_j^s(\vec{r}_s)\mathrm{d}S_s, \tag{E.1}$$

where all quantities with subscript or superscript $o$ belong to the observation slot $S_o$, and all quantities with subscript or superscript $s$ belong to the source slot $S_s$. If the source and observation slot are chosen to be the same slot, the admittance (E.1) becomes the self-admittance of the slot. In this case, the virtual cavity is placed such that the slot is at its center line, i.e. $z_0 = z_s = 0$.

The Seki Green's function is given by equation (2.32) and consists of two distinct contributions, one from the waves travelling in the $y$-direction, and the other from waves travelling in the $z$-direction from the equivalent magnetic currents on the virtual cavity walls. With the coordinate system and geometry as given in figure E.1, the Seki Green's function takes the form

$$\begin{aligned}\overleftrightarrow{G}(\vec{r}_o, \vec{r}_s) = \overleftrightarrow{G}_y^c(\vec{r}_o, \vec{r}_s) + \frac{1}{4}\sum_u \frac{1}{\sinh(\gamma_{uz}c)}\Bigg\{ &\left[\vec{H}_u^+(\vec{r}_o) - \vec{H}_u^-(\vec{r}_0)e^{-\gamma_{uz}c}\right]\vec{H}_u^+(\vec{r}_s) + \\ &\left[\vec{H}_u^-(\vec{r}_o) - \vec{H}_u^+(\vec{r}_o)e^{-\gamma_{uz}c}\right]\vec{H}_u^-(\vec{r}_s)\Bigg\},\end{aligned} \tag{E.2}$$

where $\overleftrightarrow{G}_y^c(\vec{r}_0, \vec{r}_s)$ is the Green's function for a cavity, given by equation (2.31) as

$$\overleftrightarrow{G}_y^c(\vec{r}_0, \vec{r}_s) = \frac{1}{4}\sum_u \frac{1}{\sinh(\gamma_{uy}b)}\left[\vec{H}_u^+(\vec{r}_0)e^{\gamma_{uy}b} - \vec{H}_u^-(\vec{r}_0)e^{-\gamma_{uy}b}\right]\left[\vec{H}_u^-(\vec{r}_s) - \vec{H}_u^+(\vec{r}_s)\right]. \tag{E.3}$$

It should be noted that the modes $\vec{H}_u$ in equation (E.2) travel in the $z$-direction, but in equation (E.3) they are travelling in the $y$-direction. For the cavity Green's function, the form valid for $y_o > y_s$ has been used.

The admittance $y_{ij}$ is split into two parts,

$$y_{ij} = y_{ij}^1 + y_{ij}^2, \tag{E.4}$$

where $y_{pq}^1$ is the contribution from the $y$-travelling modes, and $y_{ij}^2$ is the contribution from the $z$-travelling modes. These will now be evaluated in turn.

### E.1.1 Contribution to admittance from y-travelling modes

The $y$-contribution is given by

$$\begin{aligned} y_{ij}^{1} &= -\iint_{S_o} \mathrm{d}S_o\, \vec{m}_i^{o}(\vec{r}_o) \cdot \iint_{S_s} \overleftrightarrow{G}_y^{c}(\vec{r}_o, \vec{r}_s) \vec{m}_j^{s}(\vec{r}_s) \mathrm{d}S_s \\ &= -\frac{1}{4} \sum_u \frac{1}{\sinh(\gamma_{uy} b)} \iint_{S_o} \left[ \vec{H}_u^{+}(\vec{r}_o) e^{\gamma_{uy} b} - \vec{H}_u^{-}(\vec{r}_o) e^{-\gamma_{uy} b} \right] \cdot \vec{m}_i^{o}(\vec{r}_o) \mathrm{d}S_o \times \\ &\quad \iint_{S_s} \left[ \vec{H}_u^{-}(\vec{r}_s) - \vec{H}_u^{+}(\vec{r}_s) \right] \cdot \vec{m}_j^{s}(\vec{r}_s) \mathrm{d}S_s. \end{aligned} \tag{E.5}$$

To evaluate this, we need expressions for the transverse components of modes propagating in the $y$-direction in the virtual cavity. These are found from the equations in appendix B to be

$$\begin{aligned} (\vec{H}_{mn}^{\mathrm{TE}\pm})_t = \pm \frac{\pi}{k_{cuy}} \sqrt{\frac{\gamma_{uy} \epsilon_n \epsilon_m}{jk\eta ac}} \Bigg\{ \frac{m}{a} \sin\left[ \frac{m\pi}{a} \left( x + \frac{a}{2} \right) \right] \cos\left[ \frac{n\pi}{c} \left( z + \frac{c}{2} \right) \right] \hat{x} + \\ + \frac{n}{c} \cos\left[ \frac{m\pi}{a} \left( x + \frac{a}{2} \right) \right] \sin\left[ \frac{n\pi}{c} \left( z + \frac{c}{2} \right) \right] \hat{z} \Bigg\} e^{\mp \gamma_{uy} y} \end{aligned} \tag{E.6}$$

for TE modes, and

$$\begin{aligned} (\vec{H}_{mn}^{\mathrm{TM}\pm})_t = \pm \frac{\pi}{k_{cuy}} \sqrt{\frac{jk \epsilon_n \epsilon_m}{\gamma_{uy} \eta ac}} \Bigg\{ \frac{m}{a} \cos\left[ \frac{m\pi}{a} \left( x + \frac{a}{2} \right) \right] \sin\left[ \frac{n\pi}{c} \left( z + \frac{c}{2} \right) \right] \hat{z} + \\ - \frac{n}{c} \sin\left[ \frac{m\pi}{a} \left( x + \frac{a}{2} \right) \right] \cos\left[ \frac{n\pi}{c} \left( z + \frac{c}{2} \right) \right] \hat{x} \Bigg\} e^{\mp \gamma_{uy} y} \end{aligned} \tag{E.7}$$

for TM modes. $k_{cuy}$ denotes the cut-off wavenumber for mode $u$ propagating in the $y$-direction. An important remark to make about the expressions for the modes is that at the upper wall, $y = 0$, and hence

$$\vec{H}_{mn}^{-} = -\vec{H}_{mn}^{+} \qquad \text{for } y = 0 \tag{E.8}$$

for both TE and TM waves. Using this relation in equation (E.5) yields

$$y_{ij}^{1} = \sum_u \coth(\gamma_{uy} b) \iint_{S_o} \vec{H}_u^{+}(\vec{r}_o) \cdot \vec{m}_i^{o}(\vec{r}_o) \mathrm{d}S_o \times \iint_{S_s} \vec{H}_u^{+}(\vec{r}_s) \cdot \vec{m}_j^{s}(\vec{r}_s) \mathrm{d}S_s. \tag{E.9}$$

We thus see that the contribution from $y$-travelling modes to the admittance is just the product of the couplings between the respective basis functions to the $+y$ travelling modes, weighted with $\coth(\gamma_{uy}b)$, summed over all modes. This coupling is evaluated next.

### E.1.2 Coupling between basis functions in upper or lower wall and y-travelling modes

In this section the coupling between the basis functions $\vec{m}_{pq}$ in a slot in the upper or lower wall and the modes travelling in the $y$-direction in the virtual cavity is derived.

Consider a slot of length $l$, width $w$ and inclination $\theta$, in the upper or lower wall of the virtual cavity, with its center at $(x_0, z_0)$. The coupling between basis functions and waveguide modes is given by the surface integral

$$i_y^{upq\beta} = \iint_{S_\beta} \vec{H}_u^+(\vec{r}) \cdot \vec{m}_{pq}^\beta(\vec{r}) \mathrm{d}S. \tag{E.10}$$

The parameter $\beta$ denotes for which slot the coupling is calculated, and it is either the observation slot $o$, or the source slot $s$. We have here written out the two basis function indices $p$ and $q$. Sometimes these will be written more compactly as $i$ or $j$, such as the $\vec{m}_i^\beta$ used in the previous section, but it should still be remembered that the $i$ in this case actually corresponds to *two* indices, as seen in the expressions for the magnetic current in (E.12) below.

To evaluate this integral, we introduce the coordinates $s$ and $t$ as shown in Fig. E.2. Using this coordinate system, the $xz$-coordinates corresponding to a given $s$ and $t$ are

$$x_\beta(s,t) = x_\beta - s\sin\theta - t\cos\theta, \tag{E.11a}$$

$$z_\beta(s,t) = z_\beta + s\cos\theta - t\sin\theta. \tag{E.11b}$$

As was discussed in section 3.3, there are two different kinds of basis functions in the slot, one that is longitudinal to the slot, i.e. directed along $\hat{s}$, and the other is transverse to the

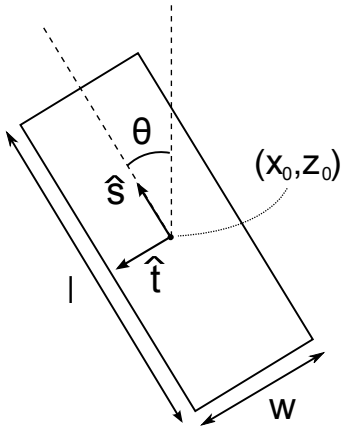


**Figure E.2:** To evaluate the surface integral over the slot, a local coordinate system $(s, t)$ is introduced. The origin of this system coincides with the slot center $(x_0, z_0)$.

slot, i.e. directed along $\hat{t}$. More precisely, they were given by

$$\vec{m}^{l}_{pq} = \sin\left[\frac{p\pi}{l}\left(s+\frac{l}{2}\right)\right]\cos\left[\frac{q\pi}{w}\left(t+\frac{w}{2}\right)\right]\hat{s}, \tag{E.12}$$
$$\vec{m}^{t}_{uv} = \sin\left[\frac{u\pi}{w}\left(t+\frac{w}{2}\right)\right]\cos\left[\frac{v\pi}{l}\left(\frac{l}{2}-s\right)\right]\hat{t}.$$

The coupling (E.10) is now evaluated for the longitudinal magnetic current. The coupling to the corresponding transverse current can then be found by interchanging $l$ and $w$, and increasing $\theta$ by $\pi/2$.

Using expressions (E.6) and (E.7) for the waveguide mode $\vec{H}_u$, and (E.12) for the longitudinal magnetic current, the coupling (E.10) is found to be

$$i_y^{upq\beta} = \begin{cases} e^{-\gamma_{uy}y'}\sqrt{\dfrac{\epsilon_n\epsilon_m\gamma_{uy}}{acjk\eta}}\dfrac{1}{k_{cuy}}\left[-\dfrac{m\pi}{a}\sin\theta\; I^y_{supq\beta}+\dfrac{n\pi}{c}\cos\theta\; I^y_{cupq\beta}\right] & \text{for TE modes,} \\ e^{-\gamma_{uy}y'}\sqrt{\dfrac{\epsilon_n\epsilon_m jk}{ac\gamma_{uy}\eta}}\dfrac{1}{k_{cuy}}\left[\dfrac{n\pi}{c}\sin\theta\; I^y_{supq\beta}+\dfrac{m\pi}{a}\cos\theta\; I^y_{cupq\beta}\right] & \text{for TM modes,} \end{cases} \tag{E.13}$$

where $I_s^y$ and $I_c^y$ are the integrals

$$I^y_{supq\beta} = \int_{s=-l/2}^{l/2}\int_{t=-w/2}^{w/2} \sin\left[\frac{m\pi}{a}\left(x_\beta(s,t)+\frac{a}{2}\right)\right]\cos\left[\frac{n\pi}{c}\left(z_\beta(s,t)+\frac{c}{2}\right)\right]\cdot \\ \sin\left[\frac{p\pi}{l}\left(s+\frac{l}{2}\right)\right]\cos\left[\frac{q\pi}{w}\left(t+\frac{w}{2}\right)\right]\mathrm{d}s\mathrm{d}t \tag{E.14}$$

and

$$I^y_{cupq\beta} = \int_{s=-l/2}^{l/2}\int_{t=-w/2}^{w/2} \cos\left[\frac{m\pi}{a}\left(x_\beta(s,t)+\frac{a}{2}\right)\right]\sin\left[\frac{n\pi}{c}\left(z_\beta(s,t)+\frac{c}{2}\right)\right]\cdot \\ \sin\left[\frac{p\pi}{l}\left(s+\frac{l}{2}\right)\right]\cos\left[\frac{q\pi}{w}\left(t+\frac{w}{2}\right)\right]\mathrm{d}s\mathrm{d}t. \tag{E.15}$$

Closed form expressions for the integrals (E.14) and (E.15) are found in appendix A. For slots in the upper wall, $y' = 0$, and for slots in the lower wall, $y' = b$. This means that the only difference in the coupling between a slot in the upper and lower wall is a factor $e^{-\gamma_{uy}b}$.

### E.1.3 Contribution to admittance from z-travelling modes

The contribution to the admittance from the $z$-travelling modes comes from the part of the Green's function in (E.2) that is not $\overleftrightarrow{G}{}^c_y$. By inserting this into the original expression (E.1) for the admittance and expanding the brackets, this is immediately found to be

$$y^2_{ij} = -\frac{1}{4}\sum_u \left(y^{uio}_{z1}y^{ujs}_{z2} + y^{uio}_{z3}y^{ujs}_{z4}\right), \tag{E.16}$$

where the quantities $y_{zi}^{upq\beta}$ are given by

$$y^{upq\beta}_{z1} = \frac{1}{\sinh(\gamma_{uz}c)}\left[i_z^{upq\beta+} - e^{-\gamma_{uz}c}\, i_z^{upq\beta-}\right], \tag{E.17}$$

$$y^{upq\beta}_{z2} = i_z^{upq\beta+}, \tag{E.18}$$

$$y^{upq\beta}_{z3} = \frac{1}{\sinh(\gamma_{uz}c)}\left[i_z^{upq\beta-} - e^{-\gamma_{uz}c}\, i_z^{upq\beta+}\right], \tag{E.19}$$

$$y^{upq\beta}_{z4} = i_z^{upq\beta-}, \tag{E.20}$$

where $i_z^{upq\beta\pm}$ is the coupling between mode $u$ travelling in the $\pm z$-direction and the basis function $pq$ in slot $\beta$. (In equation (E.16), the basis function indices $p$ and $q$ have been collected in the single indices $i$ and $j$.) This coupling is given by

$$i_z^{upq\beta\pm} = \iint_{S_\beta} \vec{H}_u^{\pm}(\vec{r}) \cdot \vec{m}_{pq}(\vec{r}) \mathrm{d}S \tag{E.21}$$

and is evaluated below.

### E.1.4 Coupling between basis functions in the upper or lower wall and z-travelling modes

We now evaluate the coupling integral (E.21). For TE modes, the $x$ and $z$-components of the $\vec{H}$-field are given by

$$\vec{H}_{mn}^{\mathrm{TE}\pm} \cdot \hat{x} = \pm \frac{m\pi}{k_{cuz} a} \sqrt{\frac{\gamma_u \epsilon_n \epsilon_m}{jk\eta ab}} \sin\left[\frac{m\pi}{a}\left(x + \frac{a}{2}\right)\right] \cos\left[\frac{n\pi y}{b}\right] e^{\mp\gamma_{uz} z}, \tag{E.22}$$

and

$$\vec{H}_{mn}^{\mathrm{TE}\pm} \cdot \hat{z} = \frac{k_{cuz}}{\gamma_u} \sqrt{\frac{\gamma_u \epsilon_n \epsilon_m}{jk\eta ab}} \cos\left[\frac{m\pi}{a}\left(x + \frac{a}{2}\right)\right] \cos\left[\frac{n\pi y}{b}\right] e^{\mp\gamma_{uz} z}. \tag{E.23}$$

For TM waves the two components are

$$\vec{H}_{mn}^{\mathrm{TM}\pm} \cdot \hat{x} = \pm \frac{n\pi}{k_{cuz} b} \sqrt{\frac{jk\epsilon_n \epsilon_m}{\gamma_{uz} \eta ab}} \sin\left[\frac{m\pi}{a}\left(x + \frac{a}{2}\right)\right] \cos\left[\frac{n\pi y}{b}\right] e^{\mp\gamma_{uz} z}, \tag{E.24}$$

and

$$\vec{H}_{mn}^{\mathrm{TM}\pm} \cdot \hat{z} = 0. \tag{E.25}$$

Inserting these expressions into equation (E.21) gives

$$i_z^{upq\beta\pm} = \begin{cases} \cos\left[\dfrac{n\pi y'}{b}\right] \sqrt{\dfrac{\gamma_{uz}\epsilon_n\epsilon_m}{jk\eta ab}} \left\{ \mp \dfrac{m\pi}{k_{cuz} a} \sin\theta I^z_{supq\beta\mp} + \cos\theta \dfrac{k_{cuz}}{\gamma_{uz}} I^z_{cupq\beta\mp} \right\} & \text{for TE modes, and} \\ \mp \cos\left[\dfrac{n\pi y'}{b}\right] \sin\theta \dfrac{n\pi}{k_{cuz} b} \sqrt{\dfrac{jk\epsilon_n\epsilon_m}{\gamma_{uz}\eta ab}} I^z_{supq\beta\mp} & \text{for TM modes,} \end{cases} \tag{E.26}$$

where the quantities $I^z_{sp\pm}$ and $I^z_{cp\pm}$ are given by the integrals

$$I^z_{supq\beta\pm} = \iint_{S_\beta} \sin\left[\frac{m\pi}{a}\left(x_\beta(s,t)+\frac{a}{2}\right)\right]\sin\left[\frac{p\pi}{l}\left(s+\frac{l}{2}\right)\right]\cos\left[\frac{q\pi}{w}\left(t+\frac{w}{2}\right)\right]e^{\pm\gamma_{uz}z}\mathrm{d}S, \tag{E.27}$$

$$I^z_{cupq\beta\pm} = \iint_{S_\beta} \cos\left[\frac{m\pi}{a}\left(x_\beta(s,t)+\frac{a}{2}\right)\right]\sin\left[\frac{p\pi}{l}\left(s+\frac{l}{2}\right)\right]\cos\left[\frac{q\pi}{w}\left(t+\frac{w}{2}\right)\right]e^{\pm\gamma_{uz}z}\mathrm{d}S, \tag{E.28}$$

and $y'$ is the $y$-coordinate for the slot, given by $y' = 0$ for slots in the upper wall, and $y' = b$ for slots in the lower wall.

These integrals can be evaluated analytically, and can be found in appendix A.

Just as for the coupling to $y$-travelling modes, the coupling between a transverse basis function and a $z$-travelling mode is obtained by interchanging $l$ and $w$, and increasing $\theta$ to $\theta + \pi/2$ in the expression (E.26) above.

This concludes the derivation of the self- and mutual admittances of compound slots in the upper broad wall in the infinite waveguide region. With the expressions (E.13) and (E.26) for the coupling between modes and basis functions, the contribution to the admittance from $y$- and $z$-travelling modes can be calculated from (E.9) and (E.16), respectively.

## E.2 Self- and mutual admittances of slots in the lower wall of a rectangular waveguide

The expressions for the admittances for slots in the lower wall of a rectangular waveguide are very similar to those derived in the previous section for slots in the upper wall. Again, the admittance is defined through the reaction integral (E.1), and the Green's function is still the Seki Green's funcion given by (E.2). The only difference is that the slots are now located at the bottom wall with $y = b$, which also means that the form of the cavity Green's function $\overleftrightarrow{G}^c_y$ valid for $y_s > y_o$ must be used. By equation (2.31) this is given by

$$\overleftrightarrow{G}^c_y(\vec{r},\vec{r}_s) = \frac{1}{4}\sum_u \frac{1}{\sinh(\gamma_{uy}b)}\left[\vec{H}^-_u(\vec{r}) - \vec{H}^+_u(\vec{r})\right]\left[e^{\gamma_{uy}b}\vec{H}^+_u(\vec{r}_s) - e^{-\gamma_{uy}b}\vec{H}^-_u(\vec{r}_s)\right]. \tag{E.29}$$

As for slots in the upper wall, the admittance is split up into two parts,

$$y_{ij} = y_{ij}^1 + y_{ij}^2 \tag{E.30}$$

representing contribution from the $y$-travelling modes and the $z$-travelling modes, respectively. These are treated in turn below.

### E.2.1 Contribution to admittance from y-travelling modes

The contribution $y_{ij}^1$ from modes travelling in the $y$-direction are found by inserting the cavity Green's function (E.29) into the original expression (E.1) for the admittance. By also noting from equations (E.6) and (E.7) for the $y$-propagating modes in the cavity that at the lower wall $y = b$ the two modes $\vec{H}_{mn}^-$ and $\vec{H}_{mn}^+$ are related by

$$\vec{H}_{mn}^- = -e^{2\gamma_{uy}b}\vec{H}_{mn}^+, \tag{E.31}$$

the contribution to the admittance from these modes is quickly found to be

$$y_{ij}^1 = \sum_u e^{2\gamma_{uy}b}\coth(\gamma_{uy}b)\iint_{S_o}\vec{H}_u^+(\vec{r}_o)\cdot\vec{m}_i^o(\vec{r}_o)\mathrm{d}S_o \times \iint_{S_s}\vec{H}_u^+(\vec{r}_s)\cdot\vec{m}_j^s(\vec{r}_s)\mathrm{d}S_s. \tag{E.32}$$

It is important to note that in the expression above, the two couplings between mode $u$ and the basis functions are for slots in the lower wall of the waveguide. However, since the $y$-mode coupling for a slot in the lower wall is just a factor $e^{-\gamma_{uy}b}$ compared to an identical slot in the upper wall, the contribution (E.32) to the admittance for a slot in the lower wall is identical to the corresponding $y$-mode contribution to the admittance for a corresponding slot in the upper wall, given by equation (E.9). In other words, the contribution to the admittance from $y$-travelling modes are identical for slots that are both in the upper wall and slots that are both in the lower wall of the waveguide.

### E.2.2 Contribution to admittance from z-travelling modes

Since the only difference in the Green's function for slots in the lower wall compared to slots in the upper wall is in the cavity part $\overleftrightarrow{G}_y^c$, the contribution to the admittance for

$z$-travelling modes is still given by the expression (E.16), but in this case the couplings $i_z^{upq\beta\pm}$ are evaluated for slots in the lower wall.

## E.3 Mutual admittance between two slots that are not overlapping longitudinally in the waveguide region

The mutual admittance between two slots in the waveguide region can be calculated by the method in the previous section. However, if the slots do not overlap longitudinally, it is easier and more efficient to calculate the admittance from the standard form (2.28) of the Green's function in an infinite waveguide.

If the two slots are denoted slot 1 and slot 2, and have their centers at $z$-coordinates $z_1$ and $z_2$ respectively, the mutual admittance becomes

$$\begin{aligned} -\langle \vec{m}_{pq}^{\,1} | \overleftrightarrow{G}_m^m | \vec{m}_{ij}^{\,2} \rangle &= -\iint_{S_1} \mathrm{d}S\ \vec{m}_{pq}^{\,1}(\vec{r}) \cdot \iint_{S_2} \overleftrightarrow{G}_m^m(\vec{r}, \vec{r}_s) \vec{m}_{ij}^{\,2}(\vec{r}_s) \mathrm{d}S_s = \\ &= \begin{cases} -\dfrac{1}{2} \displaystyle\sum_u i_z^{upq1+} i_z^{uij2-} & \text{for } z_1 > z_2 \\ -\dfrac{1}{2} \displaystyle\sum_u i_z^{upq1-} i_z^{uij2+} & \text{for } z_1 < z_2. \end{cases} \end{aligned} \tag{E.33}$$

Note that the above expression is valid regardless of whether the slots are in the upper or lower wall, and it can even be used to calculate the mutual admittance between two slots in different walls, as long as they do not overlap longitudinally. One only has to make sure that the correct expression for the couplings is used, depending on which wall the slot is located in. The case with two longitudinally overlapping slots in different walls is the last admittance left to discuss in the infinite waveguide region, and it is treated in the following section.

## E.4 Mutual admittance between longitudinally overlapping slots in opposite walls in the waveguide region

The mutual admittance between two slots, placed in opposite walls and possibly overlapping longitudinally, is now evaluated. The geometry is as shown in figure E.1, with one slot in the lower wall, and the other in the upper wall. Consider the case when the observation slot is in the lower wall at $y = b$ and the source slot is in the upper wall at $y = 0$.

For this geometry the Green's function is given by equations (E.2) and (E.3). By the same procedure as in section E.1 and E.2, the admittance is split up in two parts: the contribution $y_{ij}^1$ from $y$-travelling and $y_{ij}^2$ from $z$-travelling modes, respectively.

By inserting the $y$-part [Eq. (E.3)] of the Green's function into the definition (E.1) for the mutual admittance, the contribution from the $y$-travelling modes is found to be

$$y_{ij}^1 = \sum_u \frac{e^{\gamma_{uy} b}}{\sinh(\gamma_{uy} b)} \iint_{S_o} \vec{H}_u^+(\vec{r}_o) \cdot \vec{m}_i^o(\vec{r}_o) \mathrm{d}S_o \times \iint_{S_s} \vec{H}_u^+(\vec{r}_s) \cdot \vec{m}_j^s(\vec{r}_s) \mathrm{d}S_s, \tag{E.34}$$

where the first coupling integral is for the observation slot in the lower wall, and the second is for the source slot in the upper wall.

The contribution from $z$-travelling modes comes from the part of the Green's function that is not contained in the cavity part $\overleftrightarrow{G}_y^c$, and this is the same for slots that are in the upper wall, lower wall, or one slot in the upper and one in the lower. In all cases, the contribution from $z$-modes is given by equation (E.16), where in this case the observation slot is in the lower wall, and the source slot is in the upper wall.

The admittance is thus the sum of the expressions in (E.34) and (E.16). The mutual admittance when the source slot is in the lower wall and the observation slot is in the upper wall can be calculated from the the above expressions from reciprocity.

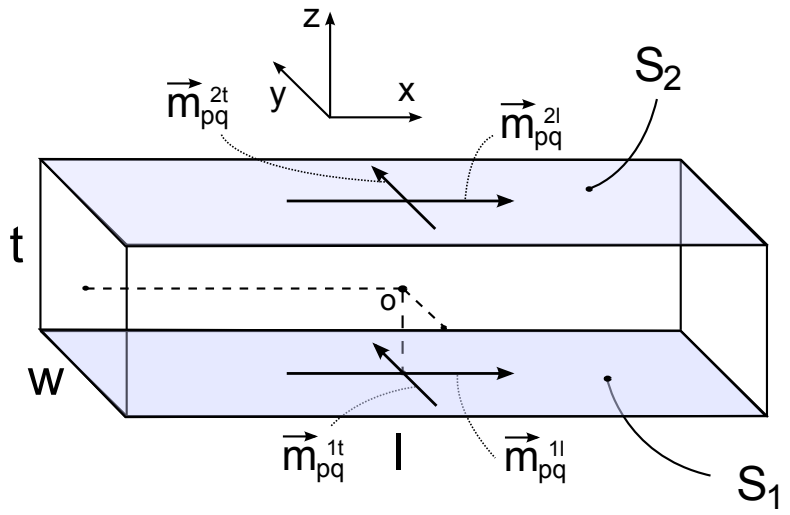


**Figure E.3:** Two slots $S_1$ and $S_2$ in the wall thickness (slot cavity) region and their corresponding longitudinal and transverse magnetic currents. Also note the orientation of the coordinate system, and that the origin is placed at the center of the slot cavity.

## E.5 Self and mutual admittances of slots in the slot cavity region

In this section the self and mutual admittances between slots in the slot cavity region (sometimes referred to as the wall thickness region) are evaluated. The wall thickness regions are the slot cavities that connect the different waveguides. We will consider a slot cavity of length $l$, width $w$ and thickness (height) $t$. A coordinate system with origin at the center of the cavity, and oriented as shown in figure E.3 is introduced. The surfaces $S_1$ and $S_2$ are the apertures connecting the slot cavity with the lower and upper waveguides, respectively, and it is thus on these surfaces the equivalent magnetic currents are located.

In the next subsection the self-admittance of the lower slot is evaluated (the self-admittance of the upper slot is identical to this due to symmetry), and thereafter the mutual admittance between the slots is evaluated.

When evaluating these, expressions for the $z$-travelling TE and TM modes will be needed, as well as the Green's function for the magnetic field inside the cavity. These are listed below for convenience.

The Green's function is of the form

$$\overleftrightarrow{G}{}_m^m(\vec{r},\vec{r}_s) = \frac{1}{4}\sum_u \frac{1}{\sinh(\gamma_{uz}t)}\left[\vec{H}_u^+(\vec{r})e^{\gamma_{uz}t/2} - \vec{H}_u^-(\vec{r})e^{-\gamma_{uz}t/2}\right]\times \left[\vec{H}_u^-(\vec{r}_s)e^{\gamma_{uz}t/2} - \vec{H}_u^+(\vec{r}_s)e^{-\gamma_{uz}t/2}\right] \tag{E.35}$$

for $z > z_s$, and

$$\overleftrightarrow{G}{}_m^m(\vec{r},\vec{r}_s) = \frac{1}{4}\sum_u \frac{1}{\sinh(\gamma_{uz}t)}\left[\vec{H}_u^-(\vec{r})e^{\gamma_{uz}t/2} - \vec{H}_u^+(\vec{r})e^{-\gamma_{uz}t/2}\right]\times \left[\vec{H}_u^+(\vec{r}_s)e^{\gamma_{uz}t/2} - \vec{H}_u^-(\vec{r}_s)e^{-\gamma_{uz}t/2}\right] \tag{E.36}$$

for $z < z_s$. The TE and TM modes are given by

$$\begin{aligned}
\vec{H}_{mn}^{\mathrm{TE}\pm}\cdot\hat{x} &= \pm\frac{m\pi}{lk_{cu}}\sqrt{\frac{\gamma_{uz}\epsilon_m\epsilon_n}{wljk\eta}}e^{\mp\gamma_{uz}z}\sin\left[\frac{m\pi}{l}\left(x+\frac{l}{2}\right)\right]\cos\left[\frac{n\pi}{w}\left(y+\frac{w}{2}\right)\right] \\
\vec{H}_{mn}^{\mathrm{TM}\pm}\cdot\hat{x} &= \pm\frac{n\pi}{wk_{cu}}\sqrt{\frac{jk\epsilon_m\epsilon_n}{wl\gamma_{uz}\eta}}e^{\mp\gamma_{uz}z}\sin\left[\frac{m\pi}{l}\left(x+\frac{l}{2}\right)\right]\cos\left[\frac{n\pi}{w}\left(y+\frac{w}{2}\right)\right] \\
\vec{H}_{mn}^{\mathrm{TE}\pm}\cdot\hat{y} &= \pm\frac{n\pi}{wk_{cu}}\sqrt{\frac{\gamma_{uz}\epsilon_m\epsilon_n}{wljk\eta}}e^{\mp\gamma_{uz}z}\cos\left[\frac{m\pi}{l}\left(x+\frac{l}{2}\right)\right]\sin\left[\frac{n\pi}{w}\left(y+\frac{w}{2}\right)\right] \\
\vec{H}_{mn}^{\mathrm{TM}\pm}\cdot\hat{y} &= \mp\frac{m\pi}{lk_{cu}}\sqrt{\frac{jk\epsilon_m\epsilon_n}{wl\gamma_{uz}\eta}}e^{\mp\gamma_{uz}z}\cos\left[\frac{m\pi}{l}\left(x+\frac{l}{2}\right)\right]\sin\left[\frac{n\pi}{w}\left(y+\frac{w}{2}\right)\right].
\end{aligned} \tag{E.37}$$

### E.5.1 Self-admittance of an aperture in the wall thickness region

We now calculate the self-admittance $-\langle\vec{m}_i^1|\overleftrightarrow{G}{}_m^m|\vec{m}_j^1\rangle$ of the lower aperture in the slot cavity. This admittance consists of four distinct parts: the admittance between the longitudinally directed basis functions, the admittance between the longitudinal and transverse basis functions, the admittance between transverse and longitudinal basis functions and finally the admittance between the transverse basis functions. Specifically, these are given by the reaction integrals $-\langle\vec{m}_{pq}^{1l}|\overleftrightarrow{G}{}_m^m|\vec{m}_{uv}^{1l}\rangle$, $-\langle\vec{m}_{pq}^{1l}|\overleftrightarrow{G}{}_m^m|\vec{m}_{uv}^{1t}\rangle$, $-\langle\vec{m}_{pq}^{1t}|\overleftrightarrow{G}{}_m^m|\vec{m}_{uv}^{1l}\rangle$ and $-\langle\vec{m}_{pq}^{1t}|\overleftrightarrow{G}{}_m^m|\vec{m}_{uv}^{1t}\rangle$, and they must all be evaluated. They are treated in turn below.

### Admittance between longitudinal components

The admittance between the longitudinal components in the lower slot is

$$-\langle \vec{m}_{pq}^{1l} | \overleftrightarrow{G}_{m}^{m} | \vec{m}_{uv}^{1l} \rangle = -\frac{1}{4} \sum_{u} \frac{1}{\sinh(\gamma_{uz} t)} \iint_{S_1} \left[ \vec{H}_u^+(\vec{r}) e^{\gamma_{uz} t/2} - \vec{H}_u^-(\vec{r}) e^{-\gamma_{uz} t/2} \right] \cdot \vec{m}_{pq}^{1l}(\vec{r}) \mathrm{d}S \cdot \iint_{S_1} \left[ \vec{H}_u^-(\vec{r}_s) e^{\gamma_{uz} t/2} - \vec{H}_u^+(\vec{r}_s) e^{-\gamma_{uz} t/2} \right] \cdot \vec{m}_{uv}^{1l}(\vec{r}_s) \mathrm{d}S_s, \tag{E.38}$$

where the expression (E.36) for the Green's function in the slot cavity has been used. The sum is over all TE and TM modes. Inserting the expressions (E.37) for the modes in the cavity, and (3.30) for the basis functions, readily gives for the admittance

$$-\langle \vec{m}_{pq}^{1l} | \overleftrightarrow{G}_{m}^{m} | \vec{m}_{uv}^{1l} \rangle = \coth(\gamma_{pq} t) \left[ \left( \frac{p\pi}{l} \right)^2 \frac{\gamma_{pq}}{jk} + \left( \frac{q\pi}{w} \right)^2 \frac{jk}{\gamma_{pq}} \right] \frac{\epsilon_q l}{2\eta w k_{cu}^2} \left[ \Delta_{qq}^{w} \right]^2 \delta_{pu} \delta_{qv}, \tag{E.39}$$

where $\delta_{mn}$ is the Kronecker delta, the symbol $\Delta_{mn}^{a}$ is defined by

$$\Delta_{mn}^{a} = \begin{cases} 0 & \text{for } m \neq n \\ a & \text{for } m = n = 0 \\ \dfrac{a}{2} & \text{for } m = n > 0 \end{cases} \tag{E.40}$$

and $\gamma_{pq} = \sqrt{(p\pi/l)^2 + (q\pi/w)^2 - k^2}$ is the propagation constant. Note that the two Kronecker deltas in equation (E.39) imply that the admittance between different basis functions is identically zero. The only non-zero terms are the ones with $(p, q) = (u, v)$, that is, this admittance matrix is diagonal.

### Admittance between transverse components

Since the transverse basis functions are identical to the longitudinal basis functions of a slot of length $w$ and width $l$ that is rotated an additional 90°, the admittance $-\langle \vec{m}_{pq}^{1t} | \overleftrightarrow{G}_{m}^{m} | \vec{m}_{uv}^{1t} \rangle$ between the transverse basis functions in the lower slot is found by interchanging $l$ and $w$

in the expression (E.39) for the admittance between the longitudinal components:

$$-\langle \vec{m}_{pq}^{1t} | \overleftrightarrow{G}_{m}^{\ m} | \vec{m}_{uv}^{1t} \rangle = \coth(\gamma_{pq} t) \left[ \left( \frac{p\pi}{w} \right)^2 \frac{\gamma_{pq}}{jk} + \left( \frac{q\pi}{l} \right)^2 \frac{jk}{\gamma_{pq}} \right] \frac{\epsilon_q w}{2\eta l k_{cu}^2} \left[ \Delta_{qq}^{l} \right]^2 \delta_{pu} \delta_{qv}, \quad \text{(E.41)}$$

where $\gamma_{pq} = \sqrt{(p\pi/w)^2 + (q\pi/l)^2 - k^2}$.

### Admittance between longitudinal and transverse components

The admittance between transverse and longitudinal basis functions in the lower aperture is given by

$$-\langle \vec{m}_{pq}^{1l} | \overleftrightarrow{G}_{m}^{\ m} | \vec{m}_{uv}^{1t} \rangle = -\frac{1}{4} \sum_{u} \frac{1}{\sinh(\gamma_{uz} t)} \iint_{S_1} \left[ \vec{H}_u^+(\vec{r}) e^{\gamma_{uz} t/2} - \vec{H}_u^-(\vec{r}) e^{-\gamma_{uz} t/2} \right] \cdot \vec{m}_{pq}^{1l}(\vec{r}) \mathrm{d}S \cdot \iint_{S_1} \left[ \vec{H}_u^-(\vec{r}_s) e^{\gamma_{uz} t/2} - \vec{H}_u^+(\vec{r}_s) e^{-\gamma_{uz} t/2} \right] \cdot \vec{m}_{uv}^{1t}(\vec{r}_s) \mathrm{d}S_s. \quad \text{(E.42)}$$

Using the expressions (E.37) and (3.30) for the modes and basis functions, respectively, it is easily found

$$-\langle \vec{m}_{pq}^{1l} | \overleftrightarrow{G}_{m}^{\ m} | \vec{m}_{uv}^{1t} \rangle = \left[ \frac{\gamma_{pq}}{jk} - \frac{jk}{\gamma_{pq}} \right] \coth(\gamma_{pq} t) pq \frac{\pi^2}{w k_{cu}^2} \frac{\Delta_{pv}^{l} \Delta_{qu}^{w}}{\eta l} (-1)^p, \quad \text{(E.43)}$$

where $\gamma_{pq} = \sqrt{(p\pi/l)^2 + (q\pi/w)^2 - k^2}$.

### Admittance between transverse and longitudinal components

The last reaction integral in the self admittance of a slot in the wall thickness region is $\langle \vec{m}_{pq}^{1t} | \overleftrightarrow{G}_{m}^{\ m} | \vec{m}_{uv}^{1l} \rangle$. Due to reciprocity, this is given by

$$\langle \vec{m}_{pq}^{1t} | \overleftrightarrow{G}_{m}^{\ m} | \vec{m}_{uv}^{1l} \rangle = \langle \vec{m}_{uv}^{1l} | \overleftrightarrow{G}_{m}^{\ m} | \vec{m}_{pq}^{1t} \rangle, \quad \text{(E.44)}$$

which was calculated in the section just above. These two matrices are thus each other's transposes.

### E.5.2 Mutual admittance between apertures in the slot cavity region

In the previous section the self admittance of a slot in the wall thickness region was calculated, and in this section the mutual admittance between the slots is evaluated. The mutual admittance will here be evaluated from slot 2 to slot 1, i.e. the admittance is calculated when the basis functions in the lower slot are weighed with the field from the basis functions in the upper slot. The admittance calculated the other way around can be found from reciprocity, but due to symmetry this will be identical to the one calculated below.

The mutual admittance $-\langle \vec{m}_i^1 | \overleftrightarrow{G}_m^m | \vec{m}_j^2 \rangle$ takes on four distinct forms, depending on whether the basis functions are longitudinally or transversely directed. These are treated in turn below.

#### Mutual admittance between longitudinally directed basis functions

Using the expression (E.36) for the Green's function, the mutual admittance between longitudinally directed basis functions is

$$-\langle \vec{m}_{pq}^{1l} | \overleftrightarrow{G}_m^m | \vec{m}_{uv}^{2l} \rangle = -\frac{1}{4} \sum_u \frac{1}{\sinh(\gamma_{uz} t)} \iint_{S_1} \left[ \vec{H}_u^-(\vec{r}) e^{\gamma_{uz} t/2} - \vec{H}_u^+(\vec{r}) e^{-\gamma_{uz} t/2} \right] \cdot \vec{m}_{pq}^{1l}(\vec{r}) \mathrm{d}S \cdot \iint_{S_2} \left[ \vec{H}_u^+(\vec{r}_s) e^{\gamma_{uz} t/2} - \vec{H}_u^-(\vec{r}_s) e^{-\gamma_{uz} t/2} \right] \cdot \vec{m}_{uv}^{2l}(\vec{r}_s) \mathrm{d}S_s. \tag{E.45}$$

Substituting the expressions (E.37) for the waveguide modes and (3.30) for the basis functions into the above equation gives

$$-\langle \vec{m}_{pq}^{1l} | \overleftrightarrow{G}_m^m | \vec{m}_{uv}^{2l} \rangle = \frac{1}{\sinh(\gamma_{pq} t)} \left[ \left( \frac{p\pi}{l} \right)^2 \frac{\gamma_{pq}}{jk} + \left( \frac{q\pi}{w} \right)^2 \frac{jk}{\gamma_{pq}} \right] \frac{\epsilon_q l}{2\eta w k_{cu}^2} \left[ \Delta_{qq}^w \right]^2 \delta_{pu} \delta_{qv} \tag{E.46}$$

### Mutual admittance between longitudinal and transverse basis functions

The admittance $-\langle \vec{m}_{pq}^{1l} | \overleftrightarrow{G}_{m}^{m} | \vec{m}_{uv}^{2t} \rangle$ is found by the same procedure as above, the only difference being that $\vec{m}_{uv}^{2l}$ is replaced by $\vec{m}_{uv}^{2t}$. The result is

$$-\langle \vec{m}_{pq}^{1l} | \overleftrightarrow{G}_{m}^{m} | \vec{m}_{uv}^{2t} \rangle = \left[ \frac{\gamma_{pq}}{jk} - \frac{jk}{\gamma_{pq}} \right] \frac{1}{\sinh(\gamma_{pq} t)} pq \frac{\pi^2}{w k_{cu}^2} \frac{\Delta_{pv}^{l} \Delta_{qu}^{w}}{\eta l} (-1)^p, \tag{E.47}$$

where $\gamma_{pq} = \sqrt{(p\pi/l)^2 + (q\pi/w)^2 - k^2}$.

### Mutual admittance between transverse and longitudinal basis functions

The admittance $-\langle \vec{m}_{pq}^{1t} | \overleftrightarrow{G}_{m}^{m} | \vec{m}_{uv}^{2l} \rangle$ is identical to $-\langle \vec{m}_{pq}^{2t} | \overleftrightarrow{G}_{m}^{m} | \vec{m}_{uv}^{1l} \rangle$ due to the symmetrical geometry, and this is identical to $-\langle \vec{m}_{uv}^{1l} | \overleftrightarrow{G}_{m}^{m} | \vec{m}_{pq}^{2t} \rangle$ due to reciprocity. This is exactly what was calculated in the previous section and given by (E.47). So

$$-\langle \vec{m}_{pq}^{1t} | \overleftrightarrow{G}_{m}^{m} | \vec{m}_{uv}^{2l} \rangle = -\langle \vec{m}_{uv}^{1l} | \overleftrightarrow{G}_{m}^{m} | \vec{m}_{pq}^{2t} \rangle. \tag{E.48}$$

In terms of matrices, this means that these two admittance matrices are each other's transposes.

### Mutual admittance between transverse basis functions

The mutual admittance between transverse basis functions is found from

$$-\langle \vec{m}_{pq}^{1t} | \overleftrightarrow{G}_{m}^{m} | \vec{m}_{uv}^{2t} \rangle = -\frac{1}{4} \sum_{u} \frac{1}{\sinh(\gamma_{uz} t)} \iint_{S_1} \left[ \vec{H}_{u}^{-}(\vec{r}) e^{\gamma_{uz} t/2} - \vec{H}_{u}^{+}(\vec{r}) e^{-\gamma_{uz} t/2} \right] \cdot \vec{m}_{pq}^{1t}(\vec{r}) \mathrm{d}S \cdot \iint_{S_2} \left[ \vec{H}_{u}^{+}(\vec{r}_s) e^{\gamma_{uz} t/2} - \vec{H}_{u}^{-}(\vec{r}_s) e^{-\gamma_{uz} t/2} \right] \cdot \vec{m}_{uv}^{2t}(\vec{r}_s) \mathrm{d}S_s. \tag{E.49}$$

When the expressions (E.37) and (3.30) for the modes and basis functions are substituted

into this expression, it reduces to

$$-\langle \vec{m}_{pq}^{1t} | \overleftrightarrow{G}_{m}^{m} | \vec{m}_{uv}^{2t} \rangle = \frac{1}{\sinh(\gamma_{pq} t)} \left[ \left( \frac{p\pi}{w} \right)^2 \frac{\gamma_{pq}}{jk} + \left( \frac{q\pi}{l} \right)^2 \frac{jk}{\gamma_{pq}} \right] \frac{\epsilon_q w}{2\eta l k_{cu}^2} \left[ \Delta_{qq}^{l} \right]^2 \delta_{pu} \delta_{qv}, \quad \text{(E.50)}$$

where $\gamma_{pq} = \sqrt{(p\pi/w)^2 + (q\pi/l)^2 - k^2}$ and $k_{cu}^2 = (p\pi/w)^2 + (q\pi/l)^2$.

This concludes the discussion on the admittances in the waveguide and wall thickness regions.

## E.6 Summary

This appendix dealt solely with evaluating the self and mutual admittances of slots in the infinite waveguide region and slot cavity region, as well as the coupling between basis functions and waveguide modes. The admittances are matrices, where each element is a reaction integral corresponding to a specific basis function in a slot weighed with the magnetic field generated by another basis function in (possibly) another slot, and the position of the elements in this matrix depends on in which order the basis function are enumerated. Four different kinds of reaction integrals occur in the admittance matrices: admittances between longitudinal components, admittances between transverse and longitudinal components, admittances between longitudinal and transverse components and finally admittances between transverse components.

# Bibliography


[1] A F. Stevenson. Theory of slots in rectangular waveguides. *Journal of Applied Physics*, 19(1):24–38, Jan 1948.

[2] AA Oliner. The impedance properties of narrow radiating slots in the broad face of rectangular waveguide: Part i–theory. *Antennas and Propagation, IRE Transactions on*, 5(1):4–11, January 1957.

[3] T.V. Khac. *A Study of Some Slot Discontinuities in Rectangular Waveguides*. Monash University, 1974.

[4] T. Vu Khac and C.T. Carson. Coupling by slots in rectangular waveguides with arbitrary wall thickness. *Electronics Letters*, 8(18):456–458, September 1972.

[5] G. Stern and R. Elliott. Resonant length of longitudinal slots and validity of circuit representation: Theory and experiment. *IEEE Transactions on Antennas and Propagation*, 33(11):1264–1271, 1985.

[6] L. Josefsson. Analysis of longitudinal slots in rectangular waveguides. *IEEE Transactions on Antennas and Propagation*, 35(12):1351–1357, 1987.

[7] S.R. Rengarajan. Analysis of a centered-inclined waveguide slot coupler. *Microwave Theory and Techniques, IEEE Transactions on*, 37(5):884–889, May 1989.

[8] Lars Manholm. *Analysis of slotted waveguide antennas*. Chalmers University of Technology, 1998.

[9] Lars Manholm, J. Hirokawa, and Per-Simon Kildal. Analysis using the virtual cavity method of a waveguide coupling junction with overlapping slots. *IEICE International Symposium on Antennas and Propagation, Chiba, Japan, Sept., 1996.*, 1996.

[10] J. Hirokawa. *A Study of Slotted Waveguide Array Antennas*. PhD dissertation, Tokyo Institute of Technology, 1993.

[11] L. Manholm J. Hirokawa and P.-S. Kildal. Analysis of an untilted wire-excited slot in the narrow wall of a rectangular waveguide by including the actual external structure. *IEEE Transactions on Antennas and Propagation*, 45(1):1038–1044, June 1997.

[12] Johan Wettergren. FEED_WG2, S-matrisberäkning för kopplingsvågledare i två lager. *D-G-PRC-1082826-RSE, Proprietary document of RUAG Space AB*.

[13] C. Peterson and S.R. Rengarajan. A rigorous analysis of weakly excited broadwall slots. In *Antennas and Propagation Society International Symposium, 1994. AP-S. Digest*, volume 1, pages 522–525 vol.1, June 1994.

[14] C.L. Peterson. *A Rigorous Analysis of Rectangular Apertures in Rectangular Waveguides*. University of California, Los Angeles, 1995.

[15] Roger F. Harrington. *Field Computation by Moment Methods*. Wiley-IEEE Press, 1993.

[16] John David Jackson. *Classical electrodynamics*. Wiley, New York, NY, 3rd ed. edition, 1999.

[17] C.A. Balanis. *Advanced Engineering Electromagnetics*. Wiley, 1989.

[18] D.M. Pozar. *Microwave Engineering*. Wiley, 2004.

[19] D.K. Cheng. *Fundamentals of Engineering Electromagnetics*. Addison-Wesley series in electrical engineering. Addison-Wesley Publishing Company, 1993.

[20] Leopold B. Felsen, Nathan Marcuvitz, and IEEE Xplore (e-book collection). *Radiation and scattering of waves*. IEEE Press, Piscataway, NJ, 1994.

[21] R.E. Collin. *Foundations For Microwave Engineering, 2nd ed.* Wiley India Pvt. Limited, 2007.

[22] Robert E. Collin, Institute of Electrical, and Electronics Engineers. *Field theory of guided waves*. IEEE, New York; Oxford, 1991.

[23] Hajime Seki. Analysis of waveguide directional filters by the moment method (invited article). *International Journal of Microwave and Millimeter-Wave Computer-Aided Engineering*, 3(3):183–191, 1993.